

**Analysis of Distress Along U.S. 331, Montgomery, AL
Between Mile Markers 88.480 and 91.070**

by

Richard Benjamin Jannett

A thesis submitted to the Graduate Faculty of
Auburn University
in partial fulfillment of the
requirements for the Degree of
Master of Science

Auburn, Alabama
May 5, 2013

Keywords: Pavement distress, sulfate, ettringite, lime

Copyright 2013 by Richard Benjamin Jannett

Approved by

David J. Elton, Chair, Professor of Civil Engineering
J. Brian Anderson, Associate Professor of Civil Engineering
David H. Timm, Brasfield & Gorrie Professor of Civil Engineering

Abstract

This report investigates the cause of asphalt concrete pavement distress along U.S. 331 between mile markers 88.480 and 91.070. The distress consisted of standalone bumpy sections of the asphalt concrete pavement, all less than about 50 feet in length, and bumps where the road crosses culverts or abuts bridges. At culverts and bridges, the bumpy sections were less than ten feet long. Because ALDOT personnel were not concerned about the causes of bumps at the bridges and culverts, those bumps were not investigated. The roadway was constructed on lime treated, clayey soils.

Swelling clays and ettringite formation were investigated as causes of the standalone distress. While swelling subgrade soils were present, the shape of the distressed surface did not coincide with the swelling soil distress. Swelling soil distress results in much longer wavelength distress over much longer distances than observed.

Ettringite formation was investigated as a cause of the standalone distress. Ettringite formation is accompanied by an increase in soil volume, leading to surface heave. This mineral forms in sulfate rich lime treated soils. Lime was added to the soils as part of the construction practice. High sulfate concentrations were found to exist in the soils.

The investigation had office, laboratory, and field components. Soil and drainage maps and construction records were examined. Field grab samples (all clayey soils) from U.S. 331 shoulders were evaluated for plasticity, mineral composition, and swell potential. Samples from under the asphalt concrete were taken by Alabama Department of Transportation personnel and

evaluated for organic content, plasticity and mineral composition.

The pavement distress is most likely due to ettringite formation. The research implementation recommendation is to identify sulfate rich soils before construction of lime treated soil, and allow time for ettringite to form before placing asphalt concrete. Chapter 5 provides detailed recommendations.

Acknowledgments

I would like to thank my advisor, Dr. David Elton, for guidance on this project and what I have learned about engineering and other aspects of life. I would also like to thank Dr. Anderson and Dr. Timm for serving on my thesis committee and for their input and time invested in this project.

The following individuals are thanked for their help and support of this project:

Francisco Arriaga, Lindy Blackburn, Rob Bubb, Buddy Cox, Larry Crowley, Kaye Davis, Hannah Doering, Seleena Foster, Jason Fox, Alice Fraasa, Zane Hartzog, Don Hoggle, Leonard Hope Jr., Ron Hope, Suzette B. Jannett, Thomas Cottongim Jannett, Grant Julian, Clifford Lange, Charles M. Lukehart, Jeff McCollum, Greg Mercer, Eric Miller, Jason Moore, Jonathan Newman, Buzz Powell, Anand Puppala, Tyson Rupnow, Dion Sanders, James Saunders, Sherry Smith, Samuel Wheeler, Richard Willis, Lorraine Wolf, Seth Wood, and Richard Zang.

Table of Contents

Abstract	ii
Acknowledgments.....	iv
List of Tables	xvi
List of Figures	xvii
Chapter I: Introduction.....	1
a. Overview.....	1
b. Objective.....	1
c. Scope of Work	1
Chapter II: Literature Review	2
a. Pavement Distresses.....	2
i. Introduction.....	2
ii. Types of Distresses	2
1. Asphalt Concrete.....	2
a. Fatigue Cracking	2
b. Block Cracking.....	3
c. Joint Reflection Cracking from Concrete Slab	4

d.	Lane/Shoulder Elevation Differential	5
e.	Longitudinal and Transverse Cracking	6
f.	Pumping and Water Bleeding	7
g.	Rutting	8
h.	Swell	9
i.	Bleeding	9
j.	Corrugation	10
k.	Depression	11
l.	Patch Deterioration	12
m.	Polished Aggregate	13
n.	Potholes	14
o.	Raveling and Weathering	15
p.	Slippage Cracking	16
2.	Portland Cement Concrete	16
a.	Blowup	16
b.	Corner Break	17
c.	Faulting of Transverse Joints and Cracks	18
d.	Joint Load Transfer System Associated Deterioration	19
e.	Lane/Shoulder Elevation Differential	20
f.	Longitudinal Cracks	20

g.	Longitudinal Joint Faulting	20
h.	Pumping and Water Bleeding	20
i.	Spalling.....	21
j.	Swell.....	22
k.	Transverse and Diagonal Cracks.....	22
l.	Edge Punchout.....	23
m.	Localized Distress	24
b.	Roughness Evaluation Methods.....	25
i.	Introduction.....	25
ii.	Profilers.....	25
1.	Profilograph	25
2.	Dipstick Profiler.....	26
3.	Longitudinal Surveys	27
4.	Rolling Straightedge Profilometer	28
5.	Surface Dynamics Profilometer	28
6.	Siometer	29
7.	Mays Ridemeter	29
iii.	International Roughness Index (IRI)	30
c.	Soil Heave.....	31
i.	Expansive Clays.....	31

1.	Introduction.....	31
2.	Affected Soil types.....	31
3.	Cause.....	32
ii.	Ettringite Formation and Sulfates	33
1.	Introduction.....	33
2.	Problems Associated with Ettringite Formation	33
3.	Soil Conditions conducive to ettringite formation.....	34
4.	Sources of Sulfate	36
5.	Distribution of Sulfates	37
6.	Testing for Sulfate-Rich Soils.....	37
7.	Ettringite Formation Mechanism	38
d.	Soil Stabilization Techniques	40
i.	Treatment of Expansive Clays	40
1.	Introduction.....	40
2.	Lime Stabilization.....	40
a.	Lime Stabilization Mechanism.....	40
b.	Lime-Soil Interactions.....	41
c.	Curing Conditions	42
d.	Swell Potential vs. Plasticity Index.....	43
3.	Mechanical Stabilization.....	48

a.	Compaction	48
b.	Geosynthetics	49
4.	Cement Stabilization.....	49
ii.	Treatment of Sulfate Rich Soil	50
e.	Clay Chemistry	52
i.	Introduction.....	52
ii.	Significance of Clay Chemistry	52
iii.	Mineral Structure	52
iv.	Mineral Types	54
1.	Kaolinite.....	55
2.	Halloysite	55
3.	Illite	56
4.	Montmorillonite (Smectite)	57
5.	Chlorite	58
f.	X-Ray Diffraction	58
i.	Introduction.....	58
ii.	Instrumentation	59
iii.	Identification of ettringite mineral	60
g.	Electromagnetometer	61
i.	Introduction.....	61

ii.	Explanation of how Electromagnetometers work.....	61
iii.	Instrumentation used in this study	62
iv.	Sulfate determination	62
Chapter III:	Field Study of US 331	63
a.	Introduction.....	63
b.	Possible causes of distress	63
i.	Sulfate induced swell	63
ii.	Swelling clays	63
iii.	Logging truck traffic	63
iv.	Poor drainage	64
v.	Poor compaction	64
vi.	Lime Reactivity Issues	64
vii.	Construction procedures	64
c.	Locations of distressed areas	65
d.	Description of Problem	67
e.	Data from ALDOT	67
i.	Introduction.....	67
ii.	Background	67
iii.	Resources	68
1.	Construction Records.....	68

2.	Soil Testing Data.....	68
3.	Plan and Profile drawings	68
f.	Experimental Approach	68
i.	Overview.....	68
ii.	Soil Sampling.....	69
1.	Introduction.....	69
2.	Sampling Strategy.....	69
3.	Surface Samples.....	69
a.	Map of Sample Locations	70
b.	Sample Identification key.....	70
4.	Subsurface Sampling	70
b.	Borings	71
iii.	Soil Testing.....	74
1.	Introduction.....	74
2.	Lab Study	75
a.	Visual Inspection.....	75
b.	Standard Proctor Tests (ASTM 2005).....	75
c.	Loss on Ignition (AASHTO 1986).....	76
d.	Clay Mineral Type	77
e.	X-Ray Diffraction	78

f.	Swell Tests (ASTM 2008).....	79
g.	Atterberg Limits	80
h.	Inductively Coupled Argon Plasma (ICAP).....	81
3.	Field Study	82
a.	International Roughness Index (IRI) Testing.....	82
b.	Electromagnetic Survey	83
c.	Drainage Observations	84
d.	Visual Inspection.....	84
iv.	Analysis of Soil Testing Data	84
1.	Lab Study	84
a.	Visual Inspection.....	84
b.	Loss on Ignition.....	85
c.	X-Ray Diffraction	85
d.	Swell Tests	85
e.	Atterberg Limits	85
2.	Field Study	85
a.	Inductively Coupled Argon Plasma (ICAP).....	85
b.	International Roughness Index (IRI) Testing.....	85
c.	Electromagnetic Survey	86
d.	IRI and Electrical Conductivity vs. Distance	86

v.	Analysis of ALDOT Data	87
1.	Plan and Profile drawings	87
2.	Construction Records.....	88
3.	Soil Testing Data.....	88
4.	Borings	89
g.	Evaluation of Causes of Pavement Distress in US 331	89
i.	Drainage Issues	89
ii.	Swelling Soils	89
1.	Surface soils	90
2.	Deeper soils.....	90
iii.	Ettringite Formation.....	90
Chapter IV:	Conclusion	91
Chapter V:	Recommendations	92
a.	Introduction.....	92
b.	Site preparation considerations	92
i.	Check for sulfate rich soils	92
ii.	Treat sulfate rich soils.....	92
iii.	Remove organic matter from roadbed.	93
Chapter VI:	Suggestions for Further Research	94
Chapter VII:	References	95

Appendix A: GEOLOGIC, SOILS, AND TOPOGRAPHIC MAPS OF DISTRESSED AREAS	A-1
A.1 Geologic map of U.S. 331.....	A-2
A.2 Soils Map Of U.S. 331 Showing Distressed Areas A-H.....	A-3
A.3 Topographic Map of U.S. 331 between mile markers 88.5 and 91	A-4
Appendix B: SOIL CHARACTERIZATION AND CLASSIFICATION.....	B-1
B.1 Atterberg Limits.....	B-1
B.2 Clay Mineral Type	B-3
B.3 Soil Classification	B-5
Appendix C: STANDARD PROCTOR TESTING	C-1
C.1 Introduction.....	C-1
C.1.1 Standard Proctor Curve, Sample A-2-2	C-1
C.1.2 Standard Proctor curve, Sample B-1.....	C-2
C.1.3 Standard Proctor Curve, Sample B-4.....	C-3
C.1.4 Standard Proctor Curve, Sample B-6.....	C-4
C.1.5 Standard Proctor Curve, Sample E-6	C-5
C.1.6 Standard Proctor Curve, Sample G-3.....	C-6
Appendix D: SWELL TESTING.....	D-1
D.1 Introduction.....	D-1
D.1.1 Sample A-2-2, swell = 10.2%	D-1

D.1.2	Sample B-1, swell = 3.3%	D-2
D.1.3	Sample B-4, swell = 3.7%	D-3
D.1.4	Sample B-6, swell = 2.4%	D-4
D.1.5	Sample E-6, swell = 6.7%	D-5
D.1.6	Sample G-3, swell = 3.0%	D-6
Appendix E: STATISTICAL COMPARISON OF PROFILOGRAPH AND ELECTRICAL CONDUCTIVITY DATA		E-1

List of Tables

Table 1: Risk associated with sulfate concentration in sulfate-bearing clays (Little 2009).	35
Table2: Percent swell of three soil types in differing lime and soluble sulfate conditions (Puppala 2005).....	36
Table3: Boring Locations	72
Table 4: Percent loss of boring samples	77
Table 5: Clay Mineral types for one foot deep samples	78
Table 6: Clay Mineral types for two foot deep samples, n/a – not available.....	78
Table 7: Atterberg limits for one foot deep samples.....	81
Table 8: Atterberg limits for two foot deep samples, n/a – not available.....	81
Table 9: Distressed locations determined by visual inspection	84
Table 10: Atterberg limits for one foot deep samples, n/a – not available.	B-1
Table 11: Atterberg limits for two foot deep samples, n/a – not available.....	B-2
Table 12: Clay Mineral types for one foot deep samples, n/a – not available.....	B-4
Table 13: Clay Mineral types for two foot deep samples, n/a – not available.....	B-4
Table 14: USCS soil classification for one foot deep samples, n/a – not available.....	B-5
Table 15: USCS soil classification for two foot deep samples, n/a – not available.	B-5

List of Figures

Figure 1: Fatigue cracking caused by frost action (Hoffman and Muench 2011)	3
Figure 2: Block cracking (Hoffman and Muench 2011).....	4
Figure 3: Joint reflection cracking (Hoffman and Muench 2011)	5
Figure4: Lane/Shoulder Elevation Differential (FHWA 2003).....	6
Figure5: Longitudinal crack as a result of poor joint construction (Hoffman and Muench 2011).	7
Figure 6: Pumping as a result of vehicular loading (Hoffman and Muench 2011)	8
Figure 7: Rutting with fatigue cracking (Hoffman and Muench 2011)	8
Figure 8: Swell due to frost heave (Hoffman and Muench 2011)	9
Figure 9: Bleeding in the wheelpaths (Hoffman and Muench 2011).....	10
Figure 10: Corrugation (Halifax Regional Municipality 2012).....	11
Figure 11: Depression (Hoffman and Muench 2011).....	12
Figure 12: High severity patching (FHWA 2003)	13
Figure 13: Polished aggregate (Hoffman and Muench 2011).....	13
Figure 14: Pothole as a result of fatigue cracking (Hoffman and Muench 2011).....	14
Figure 15: Raveling due to segregation (Hoffman and Muench 2011)	15
Figure 16: Slippage cracking (Hoffman and Muench 2011)	16
Figure 17: Blowup on SR 195 in eastern Washington (Hoffman and Muench 2011).....	17
Figure 18: Corner break (Hoffman and Muench 2011).....	18
Figure 19: Faulting of a transverse joint (Hoffman and Muench 2011).....	19

Figure 20: Dowel corrosion causing joint load transfer system failure (Hoffman and Muench 2011)	19
Figure 21: Crack spalling (Hoffman and Muench 2011).....	22
Figure 22: High severity transverse cracking (FHWA 2003).....	23
Figure 23: Edge punchout (Hoffman and Muench 2011).....	24
Figure 24: Profilograph (Sayers and Karamihas 1998)	25
Figure 25: Dipstick Profiler (Sayers and Karamihas 1998).....	26
Figure 26: Rod and Level used for longitudinal surveys (Sayers and Karamihas 1998)	27
Figure 27: Rolling Straightedge Profilometer (Sayers and Karamihas 1998).....	28
Figure 28: Vehicle equipped with the Mays Ride Meter (Sayers and Karamihas 1998)	30
Figure 29: Typical IRI values for roadways (Sayers and Karamihas 1998).....	31
Figure 30: Schematic of double diffuse layer size as it varies with water content.....	33
Figure 31: Heave caused by ettringite formation (Harris 2004).....	34
Figure 32: The EM 38 Magnetometer (Natarajan 2004).....	38
Figure 33: Typical relationship between swell and plasticity index (Little 1995).....	43
Figure 34: Lime slurry mixed with a jet mixer (Little 1995).....	45
Figure 35: Pipe spreader bar used for spreading dry hydrated lime (Little 1995).....	46
Figure 36: Typical machinery used for lime slurry pressure injection (Little 1995).....	47
Figure 37: Typical grid patterns for single, double, and triple injection (Little 1995).....	48
Figure 38: Effect of mellowing period on sulfate content (Little 2009).....	51
Figure 39: (a) Single silica tetrahedron. (b) Isometric representation of silica tetrahedral sheet. (c) Symbolic representation of silica tetrahedral sheet. (d) Top view of silica tetrahedral sheet (Ranjan 1991).....	53
Figure 40: (a) Single aluminum octahedron. (b) Isometric representation of the aluminum octahedral sheet. (c) Symbolic representation of the aluminum octahedral sheet. (d) Top view of the aluminum octahedral sheet (Ranjan 1991).....	54

Figure 41: Schematic of the kaolinite structure (Ranjan 1991).	55
Figure 42: Representation of the illite structure (Ranjan 1991)	56
Figure 43: Diagram of the montmorillonite structure (Ranjan 1991).	57
Figure 44: Bragg Brentano 2-Theta : Theta goniometer setup (Scintag 1999).	59
Figure 45: Bragg Brentano Theta : Theta goniometer setup (Scintag 1999).	60
Figure 46: Areas of Distress along U.S. 331 (USDA 1926) and (Google, U.S. Geological Survey 2012).	66
Figure 47: Key for soil samples taken at each of the six U.S. 331 cross-sectional locations shown above (1-6) at each of the eight distressed locations.	70
Figure 48: A continuous drilling sample in the plastic tube.	73
Figure 49: Drill rig used for sampling.	73
Figure 50: Inserting tubes into hollow stem auger.	74
Figure 51: Gypsum crystals found in Boring 4-A.	75
Figure 52: Standard Proctor Curve for sample A-2-2.	76
Figure 53: Relationship between Atterberg limits and mineral type (Casagrande 1948, Mitchell 1976).	77
Figure 54: X-Ray diffraction results from sample 1-A, showing presence of ettringite and gypsum.	79
Figure 55: Swell test, Sample B-6. Peak swell =2.4%	80
Figure 56: IRI data from northbound U.S. 331, right lane.	82
Figure 57: Electrical Conductivity vs. Linear Distance	83
Figure 58: IRI and electrical conductivity vs. distance. The February 10, 2012 electrical conductivity test is represented by the solid line and the February 24, 2012 IRI test is represented by the dashed line. Note: Distress at locations 9504, 10032, and 12672 ft. due to poor compaction near culverts, are removed from this plot for clarity.	87
Figure 59: Geologic Map of U.S. 331 (Geological Survey of Alabama 1988)	A-2

Figure 60: Soils map of U.S. 331 distressed areas, A-H (USDA 1926); (Google, U.S. Geological Survey 2012).	A-3
Figure 61: Topographic map of U.S.331 between mile markers 88.5 and 91 (U.S. Geological Survey 1958).	A-4
Figure 62: Relationship between Atterberg limits and mineral type (Casagrande 1948).	B-3
Figure 63: Standard Proctor curve, Sample A-2-2.	C-1
Figure 64: Standard Proctor curve, sample B-1	C-2
Figure 65: Standard Proctor curve, sample B-4.	C-3
Figure 66: Standard Proctor curve, sample B-6.	C-4
Figure 67: Standard Proctor curve, sample E-6	C-5
Figure 68: Standard Proctor curve, sample G-3.	C-6
Figure 69: Swell test, Sample A-2-2. Peak swell =10.2%	D-1
Figure 70: Swell test, Sample B-1. Peak swell =3.3%	D-2
Figure 71: Swell test, Sample B-4. Peak swell =3.7%	D-3
Figure 72: Swell test, Sample B-6. Peak swell =2.4%	D-4
Figure 73: Swell test, Sample E-6. Peak swell =6.7%	D-5
Figure 74: Swell test, Sample G-3. Peak swell =3.0%	D-6
Figure 75: IRI vs. Electrical Conductivity	E-1
Figure 76: IRI and electrical conductivity vs. distance. The February 10, 2012 electrical conductivity test is represented by the solid line and the February 24, 2012 IRI test is represented by the dashed line.	E-2

Chapter I: Introduction

a. Overview

This thesis investigates the cause of pavement distress along U.S. 331 between mile markers 88.480 and 91.070 so that future projects can avoid similar distress. The pavement distress consists of intermittent bumpy sections that are approximately 50 feet in length with International Roughness Index values greater than 100 with some reaching values of over 180. These bumps are likely due to expansion associated with ettringite formation. Bumps due to ettringite formation are occasionally found in Texas roadway projects. Ettringite may form when high sulfate content soils, like those along this stretch of roadway, are lime treated. The soils at this location contain sulfates and ettringite. The sulfates were located with an electromagnetic survey. Ettringite was determined with X-ray diffraction on soil samples.

b. Objective

Determine possible causes for the pavement distress on US 331 in south Montgomery County.

c. Scope of Work

A program of field and laboratory testing was performed to identify the cause of distress. Qualitative and quantitative data was gathered from field reconnaissance. Disturbed and undisturbed specimens were collected from targeted distressed and non-distressed zones for in-depth laboratory investigation. Testing included Atterberg limits, swell, loss on ignition, inductively coupled argon plasma (ICAP), X-ray diffraction (XRD), standard Proctor, International Roughness Index (IRI), and electromagnetic survey. The results identify factors that are contributing to the distress of the U.S. 331 roadway.

Chapter II: Literature Review

a. Pavement Distresses

i. Introduction

The purpose of this section is to provide an overview of the types of distress that occur in both asphalt concrete and Portland cement concrete pavements. This overview includes a description, cause, and prevention for each of the distress types.

ii. Types of Distresses

1. Asphalt Concrete

This section provides an overview of the types of distresses that are common in asphalt concrete pavements. The overview includes a description, cause, and repair for each type of distress.

a. Fatigue Cracking

Fatigue cracking is commonly found on high traffic roadways subjected to repeated traffic loadings. Often referred to as “alligator cracking,” fatigue cracking has the appearance of an alligator’s skin with multiple interconnected cracks present in the wheel paths of the roadway. Fatigue cracking is caused by repeated traffic loadings resulting in a fatigue failure of the asphalt. The crack starts at the bottom of an asphalt layer because the tensile stresses are greatest at that location. After the crack forms, it continues to propagate towards the surface with repeated loadings and eventually forms a visible surface crack (Huang 2004). Pavements constructed over base courses that are not properly compacted often exhibit fatigue cracking (Yoder and Witczak 1975).

Severity of fatigue cracking can either be low, moderate, or high. Fatigue cracking is often repaired by sealing to prevent water intrusion. Low severity fatigue cracking has little if

any interconnected cracks and no evidence of pumping, spalling, or sealing. Moderate severity fatigue cracking forms a complete pattern and may be slightly spalled or partially sealed, but does not show evidence of pumping. High severity fatigue cracks form a complete pattern and exhibit moderate to severe spalling and may have evidence of pumping (FHWA 2003).



Figure 1: Fatigue cracking caused by frost action (Hoffman and Muench 2011)

There are two types of repairs for fatigue cracking based on the severity of the distress. For localized fatigue cracking, the distressed pavement should be removed and the underlying soils should be removed and replaced with a more suitable materials followed by recompaction and an asphalt patch. For large areas of fatigue cracking, problematic soils should be replaced and an asphalt overlay of adequate thickness to provide full structural support for the traffic loading should be applied over the entire pavement surface. Adequate drainage should be ensured so that the structural support of the base, subbase, and subgrade remains intact (Hoffman and Muench 2011).

b. Block Cracking

Block cracking typically occurs over the entire surface of a roadway as cracks form in a grid like pattern. Each “block” varies in size from 1 to 100 square feet. Block cracking is caused by the temperature differential throughout the depth of the asphalt layer due to daily temperature cycling. The change in temperature affects the top of the asphalt layer first, causing a volume change that is not experienced in the bottom of the asphalt layer. This differential

volume change causes cyclic stresses to form in the asphalt layer which leads to a crack (Huang 2004).

Severity of block cracking can either be low, moderate, or high based on crack width and condition of adjacent cracks. Low severity block cracking has cracks that average less than 6mm in width or cracks that exhibit sealant that is in good enough condition that the crack width cannot be measured. Moderate severity block cracking has cracks that average between 6 mm and 19 mm in width and also includes cracks under 19 mm wide that have low severity adjacent cracks. High severity block cracking has cracks that average over 19 mm wide and also includes cracks under 19 mm wide that have moderate to high severity adjacent cracking (FHWA 2003).



Figure 2: Block cracking (Hoffman and Muench 2011)

Repair is dependent upon the severity of the cracking. Cracks less than half an inch wide should be sealed with asphalt to prevent moisture from reaching the subgrade as well as the deterioration of the crack edges. Pavements with cracks greater than half an inch wide should be removed and replaced with a new asphalt surface (Hoffman and Muench 2011).

c. Joint Reflection Cracking from Concrete Slab

Joint reflection cracking occurs when an asphalt pavement is constructed over an existing concrete pavement. This type of cracking only refers to reflection cracks caused by planned joints in the concrete pavement such as thermal expansion joints, widening joints, or any other planned joint. The cracks appear in the asphalt layer directly above the concrete joints. Joint

reflection cracking is caused by stresses created by the movement of the underlying concrete slabs (Huang 2004).

Severity of joint reflection cracking can either be low, moderate, or high based on crack width and condition of adjacent cracks. Low severity joint reflection cracking has cracks that average less than 6mm in width or cracks that exhibit sealant that is in good enough condition that the crack width cannot be measured. Moderate severity joint reflection cracking has cracks that average between 6 mm and 19 mm in width and also includes cracks under 19 mm wide that have low severity random adjacent cracks. High severity joint reflection cracking has cracks that average over 19 mm wide and also includes cracks under 19 mm wide that have moderate to high severity random adjacent cracking (FHWA 2003).



Figure 3: Joint reflection cracking (Hoffman and Muench 2011)

Repair is dependent upon the severity of the cracking. Cracks less than half an inch wide should be sealed to prevent moisture from reaching the subgrade as well as the deterioration of the crack edges. Pavements with cracks greater than half an inch wide should be removed and replaced with a new asphalt overlay (Hoffman and Muench 2011).

d. Lane/Shoulder Elevation Differential

Lane/shoulder elevation differential occurs at locations where the wearing surface and the shoulder are at different elevations. This distress can occur for many reasons including, but not limited to consolidation, pumping, heave, or loss of material caused by vehicular loading on a

granular shoulder (Huang 2004). Lane/shoulder elevation differential can also be caused by settlement due to differences in pavement materials in the lane and shoulder (FHWA 2003).



Figure4: Lane/Shoulder Elevation Differential (FHWA 2003)

Diamond grinding the pavement to a uniform elevation is a remediation for elevation differentials over 3mm (Hoffman and Muench 2011).

e. Longitudinal and Transverse Cracking

Longitudinal cracks occur parallel to the centerline while transverse cracks occur perpendicular to the centerline (Huang 2004). Longitudinal cracking is categorized by location as either wheelpath longitudinal cracking or nonwheelpath longitudinal cracking. Wheelpath longitudinal cracking that meanders or has adjacent cracks is classified as fatigue cracking (FHWA 2003). This type of cracking is often caused by asphalt shrinkage or hardening, non-joint reflective cracking from an underlying concrete pavement, or inadequate lane joint construction. These cracks are not attributed to traffic loading (Huang 2004).

Severity of longitudinal and transverse cracking can either be low, moderate, or high based on crack width and condition of adjacent cracks. Low severity longitudinal and transverse cracking has cracks that average less than 6mm in width or cracks that exhibit sealant that is in good enough condition that the crack width cannot be measured. Moderate severity longitudinal and transverse cracking has cracks that average between 6 mm and 19 mm in width and also includes cracks under 19 mm wide that have low severity random adjacent cracks. High severity

longitudinal and transverse cracking has cracks that average over 19 mm wide and also includes cracks under 19 mm wide that have moderate to high severity random adjacent cracking (FHWA 2003).



Figure5: Longitudinal crack as a result of poor joint construction (Hoffman and Muench 2011)

Repair is dependent upon the severity of the cracking. Cracks less than half an inch wide should be sealed to prevent moisture from reaching the subgrade as well as the deterioration of the crack edges. Pavements with cracks greater than half an inch wide should be removed and replaced with a new asphalt overlay (Hoffman and Muench 2011).

f. Pumping and Water Bleeding

These types of distresses are evidenced by the surface accumulation of fine material or staining of the pavement near cracks. Pumping occurs when water and soil under a roadway is forced upward through cracks due to vehicular loading. Water bleeding is the slow seepage of water through pavement cracks. Both pumping and water bleeding cause a loss of material from underneath the roadway surface, resulting in a void and loss of structural support (Huang 2004). The severity level and amount of pumping and water bleeding varies with changing moisture

conditions (FHWA 2003).



Figure 6: Pumping as a result of vehicular loading (Hoffman and Muench 2011)

To prevent pumping and water bleeding, adequate drainage and soil strength should be ensured (Hoffman and Muench 2011).

g. Rutting

Rutting appears as a longitudinal indentation occurring in the wheelpaths. Rutting is a load induced distress that occurs most often on poorly compacted asphalt and soil layers or areas subject to high temperatures (Huang 2004). Rutting can lead to a progressive pavement failure including cracking and complete pavement disintegration (Parker and Brown 1993). Fatigue cracking is often present in conjunction with rutting (Hoffman and Muench 2011). Ruts may also fill with water and can cause hydroplaning (Yoder and Witczak 1975).



Figure 7: Rutting with fatigue cracking (Hoffman and Muench 2011)

Ruts greater than 1/3" deep should be leveled using a grinder and overlaid with a new

asphalt surface course (Hoffman and Muench 2011).

h. Swell

Swell is identified by a bulge on the roadway surface. Swell can result from swelling clays, frost action in the subgrade, blowup of an underlying concrete pavement or ettringite formation. These bulges may cause oil to spill from vehicles, resulting in oil spots on the asphalt surface in areas of swell (Huang 2004).



Figure 8: Swell due to frost heave (Hoffman and Muench 2011)

Swelling clays can be remediated by the use of lime treatment. Heave due to frost action can be remediated by either stabilizing the affected soil or replacing it with a more suitable material (Hoffman and Muench 2011). Adequate drainage limits the amount of water available and reduces the amount of swell. Ettringite may form in the subgrade layers causing heave (Little 2009).

i. Bleeding

Bleeding is a film of asphalt that forms on the surface of an asphalt pavement frequently found in the wheelpaths (FHWA 2003). It is evidenced by a sticky shiny surface. Bleeding causes a reduction in skid resistance in wet conditions (Huang 2004). This distress is caused by

the asphalt mix having too high of a binder content or too low of an air void content (Huang 2004). Bleeding can also occur if an asphalt binder that is too soft for the climate is used (Yoder and Witczak 1975).



Figure 9: Bleeding in the wheelpaths (Hoffman and Muench 2011)

The repairs for bleeding focus on removing the asphalt surface film but do not correct the problem that initially caused bleeding. If the bleeding is minor, the excess binder can be removed by blotting it with coarse sand. If the bleeding is major, the excess binder can be removed with a motor grader or a heater planer (Hoffman and Muench 2011).

j. Corrugation

Corrugation appears as ripples across the surface of an asphalt pavement (Huang 2004). This distress is most commonly found on hills, curves, intersections or other places that vehicles commonly accelerate (FHWA 2003). Corrugation is the result of shear forces within an asphalt layer or between the asphalt layer and the underlying soil layer caused by acceleration and deceleration of vehicles (Huang 2004).



Figure 10: Corrugation (Halifax Regional Municipality 2012)

To repair a corrugated pavement, the damaged section should be removed and overlaid with a new asphalt surface course (Hoffman and Muench 2011).

k. Depression

Depressions exist when one part of the pavement surface is at a lower elevation than the surrounding pavement. This distress is caused by local base, sub-base, or subgrade settlement or exists as a construction flaw (Huang 2004).



Figure 11: Depression (Hoffman and Muench 2011)

Depressions should be repaired by removing the affected pavement and soils and replacing with adequate soils along with an asphalt patch (Hoffman and Muench 2011).

I. Patch Deterioration

Patch deterioration is the degradation of an asphalt patch where a portion of the original asphalt was replaced with new asphalt (Huang 2004). Patch deterioration severity can be categorized as either low, moderate, or high. Low severity patch deterioration includes any low severity distress including ruts depths less than 6 mm and no evidence of pumping. Moderate severity patch deterioration includes any moderate severity distress including rut depths from 6 mm to 12 mm and no evidence of pumping. High severity patch deterioration includes any high severity distress including rut depths greater than 12 mm, additional patching over the original patch, or evidence of pumping (FHWA 2003). This type of distress is caused by traffic loading or poor material and construction practices (Huang 2004).



Figure 12: High severity patching (FHWA 2003)

Patch deterioration can be repaired by removing the deteriorated patch and applying another patch.

m. Polished Aggregate

Aggregate at the surface of the asphalt that has become very smooth is known as polished aggregate (Huang 2004). Exposure of coarse aggregate due to wearing away of the surface binder is also known as polished aggregate (FHWA 2003). This type of distress is caused by vehicular loading and friction between tires and aggregate which causes it to occur most often in the wheel path (Huang 2004).



Figure 13: Polished aggregate (Hoffman and Muench 2011)

To increase the skid resistance on a polished aggregate surface, a skid resistant slurry seal or another asphalt overlay should be applied (Hoffman and Muench 2011).

n. Potholes

A pothole is a very localized deep depression on the asphalt surface (Huang 2004). The minimum plan dimension for potholes is 150 mm (FHWA 2003). Broken pavement from fatigue cracking, local disintegration, saturated soils, and freeze-thaw action can all contribute to the formation of potholes (Huang 2004). Pothole severity may be either described as low, moderate, or high based on depth. Low severity potholes have a depth of less than 25 mm. Moderate severity potholes have a depth of 25 mm to 50 mm. High severity potholes have a depth greater than 50 mm (FHWA 2004).



Figure 14: Pothole as a result of fatigue cracking (Hoffman and Muench 2011)

Potholes should be repaired by applying the proper patch. To prevent potholes that occur from fatigue cracking, adequate drainage should be ensured (Hoffman and Muench 2011).

o. Raveling and Weathering

A pavement that has experienced raveling and weathering appears as a disintegrated pavement surface with dislodged aggregate particles (Hoffman and Muench 2011). Raveling ranges from a loss of fine aggregate all the way to a loss of coarse aggregate and obvious surface pitting (FHWA 2003). Raveling and weathering can be caused either by a loss of bond between the aggregate particles and binder or by mechanical dislodgement. This loss of bond can be a result of a dust coating on the aggregate, aggregate segregation, or inadequate compaction. Mechanical dislodgement is often the result of vehicles such as snow plows or vehicles having studded tires that cause damage to the pavement (Hoffman and Muench 2011).



Figure 15: Raveling due to segregation (Hoffman and Muench 2011)

Small areas that experience raveling may be repaired by removing the affected pavement and replacing with an asphalt patch. Large raveled areas can be repaired by removing the affected pavement and replacing the asphalt (Hoffman and Muench 2011).

p. Slippage Cracking

Slippage cracks appear as crescent shaped cracks oriented with the two points of the crescent facing against the flow of traffic. Slippage cracks are caused by a weak asphalt surface layer or a poor tack coat resulting in a weak bond between asphalt layers. This situation allows lateral movement of the surface course causing it to crack (Huang 2004).



Figure 16: Slippage cracking (Hoffman and Muench 2011)

Damaged pavement as a result of slippage cracking can be removed and replaced with an asphalt patch (Hoffman and Muench 2011).

2. Portland Cement Concrete

This section provides an overview of the types of distresses that are common in Portland cement concrete pavements. The overview includes a description, cause, and repair for each type of distress.

a. Blowup

Blowups occur at transverse joints where the concrete slabs have moved upward (Huang 2004). Blowups are often accompanied by the shattering of concrete in the affected area (FHWA

2003). The upward movement is caused by a joint that provides insufficient capacity for the volume change of a slab due to heat expansion. Slab expansion causes stresses to build up in the slabs until the stresses become too great and a blowup occurs. Often, the capacity of the joint is reduced by foreign, incompressible materials entering the joint space (Huang 2004).



Figure 17: Blowup on SR 195 in eastern Washington (Hoffman and Muench 2011)

Blowups should be repaired using a full-depth patch (Hoffman and Muench 2011).

Blowups can be avoided by using pressure relief joints or cleaning foreign material from the joint (Yoder and Witczak 1975).

b. Corner Break

A corner break is a crack that extends vertically throughout the entire slab thickness and intersects the slab joints less than 6 ft. from the corner (Huang 2004). Corner breaks occur at approximately a 45 degree angle relative to the direction of traffic (FHWA 2003). Severity of a corner break can be low, moderate, or high depending on spalling, faulting, excess cracking, and patching. A low severity corner break is spalled for no more than ten percent of its length and does not exhibit faulting, excess cracking of the corner piece, loss of material, or patching. A moderate severity corner break may have low severity spalling for greater than ten percent of the crack length, faulting less than 13 mm, and no excess cracking of the corner piece. High severity

corner breaks are characterized by high severity spalling for greater than ten percent of the crack length, faulting at 13 mm or less, excess cracking of the corner piece, or patching material (FHWA 2003). Factors that cause corner breaks include traffic loading, loss of support, poor load transfer, and warping stresses (Huang 2004).



Figure 18: Corner break (Hoffman and Muench 2011)

A corner break should be repaired using a full-depth patch (Hoffman and Muench 2011).

c. Faulting of Transverse Joints and Cracks

Faulting of a transverse joint is an elevation difference between two slabs at the joint. Crack faulting results in an elevation difference across a crack (Huang 2004). Faulting can either be categorized as positive or negative faulting. If the approach slab is higher than the departure slab, the faulting is known as positive and if the approach slab is lower than the departure slab, the faulting is known as negative (FHWA 2003). Faulting is caused by pumping due to heavy loadings which results in a buildup of loose material under the trailing slab causing an elevation difference. The elevation difference can also be caused by a depression of the leading slab (Huang 2004).



Figure 19: Faulting of a transverse joint (Hoffman and Muench 2011)

Faulting can be remediated by milling the pavement at the fault to restore ride quality (Hoffman and Muench 2011).

d. Joint Load Transfer System Associated Deterioration

Joint load transfer system associated deterioration is a transverse crack that occurs at the end of the load transfer dowels. This type of distress occurs when dowels are heavily corroded or misaligned. This distress may also occur when the dowel diameter is too small for the traffic loading (Huang 2004).



Figure 20: Dowel corrosion causing joint load transfer system failure (Hoffman and Muench 2011)

Deterioration due to joint load transfer system failure can be prevented by using properly sized and aligned dowels (Huang 2004).

Deterioration of a joint load transfer system should be repaired by removing and replacing the dowels in conjunction with a full-depth patch (Hoffman and Muench 2011).

e. Lane/Shoulder Elevation Differential

This distress is the same as previously described for asphalt concrete pavements, Chapter II, a, ii, 1, d.

f. Longitudinal Cracks

Longitudinal cracks occur parallel to the centerline of the roadway. These cracks are caused by improper joint construction or a combination of heavy traffic loading, loss of foundation support, and warping stresses caused by daily heat cycling (Huang 2004).

To remediate longitudinal cracking, the cracks should be sealed to prevent intrusion of water and other foreign material that can lead to further pavement deterioration. Pavement with cracks larger than half an inch should be removed and replaced with a new concrete overlay (Hoffman and Muench 2011).

g. Longitudinal Joint Faulting

Longitudinal joint faulting is an elevation difference over a longitudinal joint. Longitudinal joint faulting can be caused by consolidation, pumping, or heave (Huang 2004).

Faulting can be remediated by milling the pavement at the fault to restore ride quality (Hoffman and Muench 2011).

h. Pumping and Water Bleeding

This type of distress may be evidenced by the accumulation of fine material or staining of the pavement near cracks. The ejection of water under traffic loading after a rainstorm is also evidence of pumping (Huang 2004). The severity level and amount of pumping and water bleeding varies with changing moisture conditions (FHWA 2003). Pumping is caused by the

slab deflecting under a load and forcing water out of a joint or crack. The water that is forced through the crack carries fine particles from under the slab causing a progressive loss of support. Water bleeding is the seepage of water through a joint or crack (Huang 2004). As the subgrade support is removed by pumping, transverse cracks may also form 5 or 6 feet ahead of the joint (Yoder and Witczak 1975).

To prevent pumping and water bleeding, adequate subgrade drainage should be ensured. Affected areas should be removed and replaced with a full depth patch and load transfer issues should also be addressed (Hoffman and Muench 2011).

i. Spalling

Two classifications of spalling exist, spalling that occurs along transverse and longitudinal joints or cracks and spalling that occurs at corners. Characteristics of joint or crack spalling include cracks, breaks, or chips within two feet of the joint or crack. A corner spall is the chipping of the slab within two feet of the corner. Neither type of spalling extends vertically through the slab (Huang 2004). Severity of spalling can be described as low, moderate, or high depending upon the width of the spall, loss of material, and patching. A low severity spall has loss of material and is less than 75mm measured to the face of the joint or a spall that has no loss of material or patching. A moderate severity spall is between 75 mm and 150 mm wide and exhibits loss of material. A high severity spall is greater than 150 mm wide and has loss of material or may be broken into two pieces or contain patch material (FHWA 2003). Joint or crack spalling can be caused by a variety of factors including the infiltration of incompressible materials into the joint or crack, heavy traffic loading, weak concrete, or poor load transfer devices. Corner spalls are often caused by freeze-thaw or “D” cracking (Huang 2004).



Figure 21: Crack spalling (Hoffman and Muench 2011)

Spalling can be repaired with either a partial depth patch or full depth patch depending on the severity (Hoffman and Muench 2011).

j. Swell

This distress is the same as previously described for asphalt concrete pavements, Chapter II, a, ii, 1, h.

k. Transverse and Diagonal Cracks

A transverse crack occurs perpendicular to the centerline of the roadway while a diagonal crack occurs at an angle relative to the centerline of the roadway. Hairline cracks less than six feet in length are not placed in this distress category (Huang 2004). Severity of transverse cracking is either low, moderate, or high based on crack width, faulting, and spalling. Low severity cracks are less than 3mm wide with no spalling or faulting. Moderate severity cracks are between 3 mm and 6 mm wide or may have spalling up to 75 mm or faulting up to 6 mm. High severity cracks are greater than 6 mm wide or may have spalling 75 mm or greater or faulting greater than 6 mm (FHWA 2003). Transverse and diagonal cracks are typically caused by heavy traffic loading along with stresses caused by temperature gradients, moisture gradients, and drying shrinkage (Huang 2004).



Figure 22: High severity transverse cracking (FHWA 2003)

This type of cracking should be sealed to prevent further pavement deterioration caused by intrusion of water and other foreign material. Pavement with cracks larger than half an inch should be removed and replaced with a new overlay (Hoffman and Muench 2011).

I. Edge Punchout

Edge punchout occurs in continuously reinforced concrete pavements when a section of pavement that is not at the corner pushes into the subgrade and is at a lower elevation than the surrounding pavements (Huang 2004). The severity of edge punchouts can be low, moderate, or high depending upon spalling, faulting, or movement under traffic. A low severity edge punchout has tight cracks and less than 75 mm of spalling, or less than 6 mm of faulting. Y-cracking is not a low severity edge punchout. A moderate severity edge punchout has between 75 mm and 150 mm of spalling or between 6 mm and 13 mm of faulting. A high severity edge punchout has greater than 150 mm of spalling, greater than 13 mm of faulting, moves under traffic loading, is broken into two or more pieces, or has been patched (FHWA 2003). Edge punchout is a result of a loss of aggregate interlock at a crack in combination with repetitive heavy truck loadings (Huang 2004).



Figure 23: Edge punchout (Hoffman and Muench 2011)

Punchout should be repaired using a full-depth patch (Hoffman and Muench 2011).

m. Localized Distress

Localized distress is where the concrete slab breaks up or spalls in a very localized area, often in the wheelpaths. Localized distress is caused by inadequate concrete consolidation (Huang 2004).

Remediation for localized distress should either be a full-depth patch or a partial-depth patch based on the depth of the distress (Hoffman and Muench 2011).

b. Roughness Evaluation Methods

i. Introduction

This section provides a description of nine methods used to evaluate pavement roughness. It is important to quantify pavement roughness so that changes in roughness can be observed with respect to changing variables.

ii. Profilers

The seven roughness evaluation methods that will be discussed are the Profilograph, Dipstick Profiler, Longitudinal Surveys, Rolling Straightedge Profilometer, Surface Dynamics Profilometer, Siometer, and Mays Ridemeter.

1. Profilograph

A profilograph is a multi-wheel low-speed rolling device. One wheel is in the center of the device and the rest of the wheels are towards the ends. The deviation of the central wheel compared to the average position of the other wheels is recorded as well as the longitudinal distance the machine has traveled. Profilograph data is displayed using the International Roughness Index (IRI) as shown in section iii. (Sayers and Karamihas 1998).

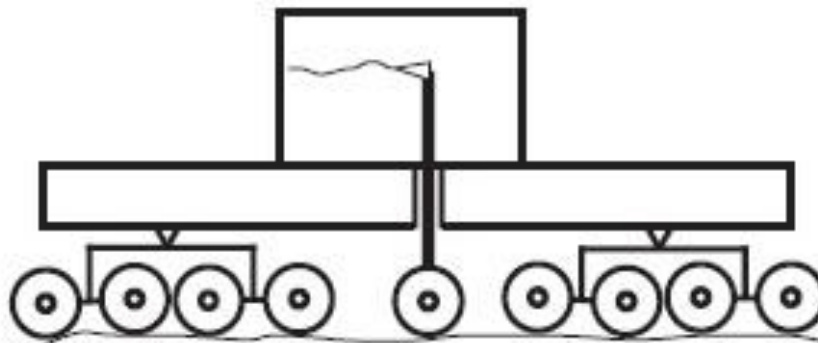


Figure 24: Profilograph (Sayers and Karamihas 1998)

2. Dipstick Profiler

The Dipstick Profiler looks like an upside down “T” with a support at each end of the crossbar. The supports are spaced 305 mm apart and the elevation differential between these two supports is measured by a precision inclinometer. The data is recorded by an on-board computer. This device is used by positioning the crossbar of the upside down “T” along the desired profile line. The machine will beep when stable indicating that a reading has been recorded. After this reading has been taken, the machine should be pivoted 180 degrees about the leading support and when both supports are stable; the machine will record a reading and beep again. The machine should be “walked” in this manner until the desired profile length is achieved. The dipstick profiler provides a true roadway profile (Sayers and Karamihas 1998).

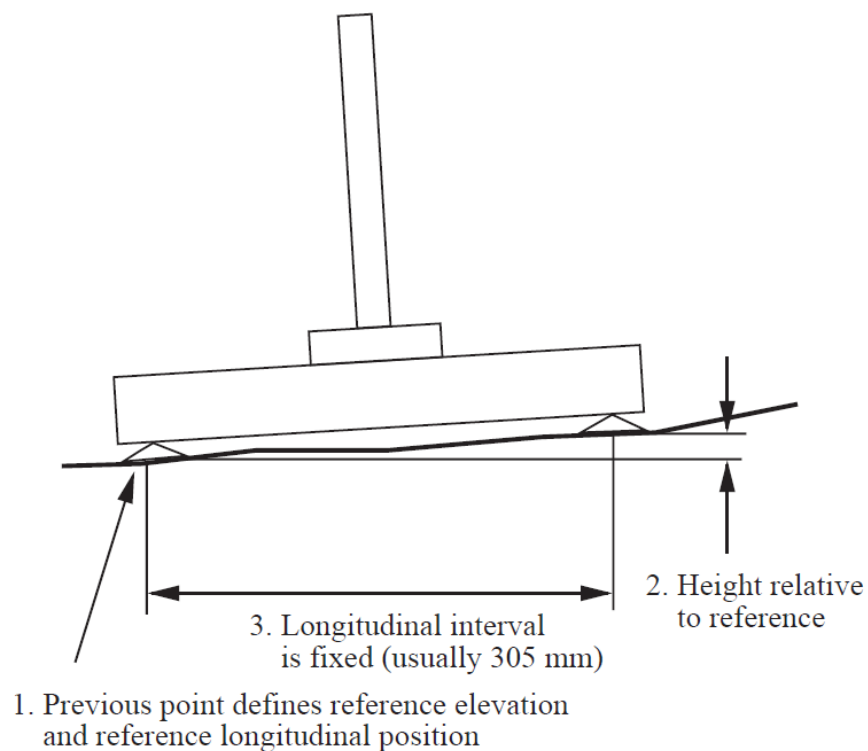


Figure 25: Dipstick Profiler (Sayers and Karamihas 1998)

3. Longitudinal Surveys

Longitudinal surveys are performed using a rod, level, and tape. The rod and level are used in conjunction to provide an elevation relative to a reference elevation. The tape is used to provide the horizontal distance of the elevation measurements relative to a reference point. The elevations and horizontal distance measurements are used in conjunction to provide a profile which in turn can be used to determine roughness. This method is seldom used for roughness evaluation because elevation measurements must be taken at very close intervals (1 ft.) and must be very accurate (within 0.5 mm) to provide sufficient data. Longitudinal surveys provide a true roadway profile. This is known as a static method because measurements are made with instruments that are not moving (Sayers and Karamihas 1998).

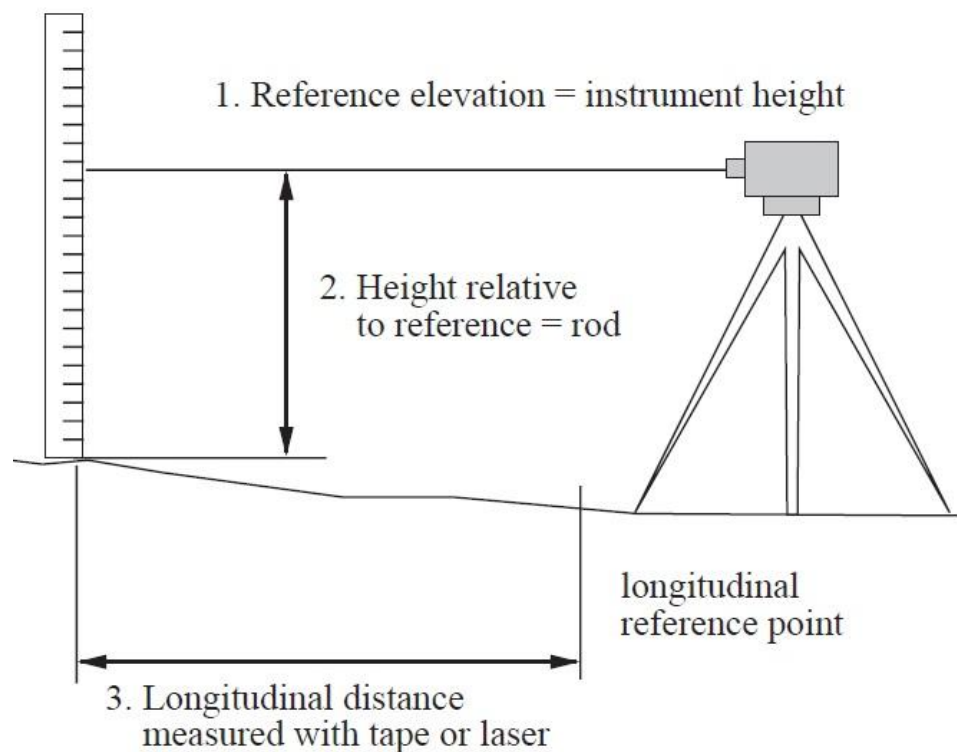


Figure 26: Rod and Level used for longitudinal surveys (Sayers and Karamihas 1998)

4. Rolling Straightedge Profilometer

A rolling straightedge profilometer is a straightedge that is supported at each end with a fixed wheel and also has a wheel at the midpoint that is allowed to move vertically. A rolling straightedge profilometer is similar to a profilograph. When the device is rolled along the pavement surface, the deviation of the center wheel relative to the fixed wheels is recorded along with a longitudinal distance that the machine has moved. Rolling straightedge profilometers do not provide an absolute profile, but the deviation of the central wheel with respect to the fixed wheels correlates to pavement roughness (Sayers and Karamihas 1998).

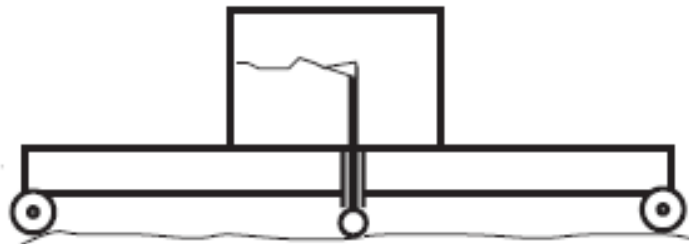


Figure 27: Rolling Straightedge Profilometer (Sayers and Karamihas 1998)

5. Surface Dynamics Profilometer

The Surface Dynamics profilometer is a vehicle mounted device consisting of five major components: a pair of road-following wheels, a pair of potentiometers, a pair of accelerometers, and analog-to-digital and digital processing subsystems. Each of the road-following wheels is mounted under the vehicle so that they follow the wheelpaths. A 300 lb. spring force keeps the road-following wheels on the pavement surface. The potentiometers are mounted directly above the road-following wheels and the accelerometers are mounted directly above the potentiometers. The computer takes input data from the road-following wheels, the potentiometers, and the accelerometers and creates a road profile for each wheelpath (Nair, Hudson, and Lee 1985).

6. Siometer

The SIometer is a device used to measure roughness that uses an accelerometer, a computer, and software. The basic principle of the SIometer is to predict a roadway profile by measuring the vertical acceleration and speed of the vehicle. Before testing, a dynamic calibration is performed to obtain typical vertical acceleration values for the vehicle at 50 mph over a “typical” class of roadway. When the SIometer is used, these typical values are discarded by the computer and a roadway profile is produced (Hankins 1985). The SIometer provides an estimate of the true roadway profile (Nair, Hudson, and Lee 1995).

7. Mays Ridemeter

The Mays Ride Meter is a response-type system that measures the vehicle response as it traverses a roadway based on the suspension travel. A vehicle is outfitted with a transducer to measure suspension travel as well as a device used to record suspension data. As the vehicle moves down the road, the system records accumulated suspension strokes. This is displayed as an index value with the units of inches per mile with inches being the total inches of suspension travel and miles being the longitudinal distance traversed. A higher value obtained correlates to a rougher pavement surface. The Mays Ride Meter does not produce repeatable results because the suspension characteristics of the vehicle change over time and different vehicles have different suspension characteristics (Sayers and Karamihas 1998).

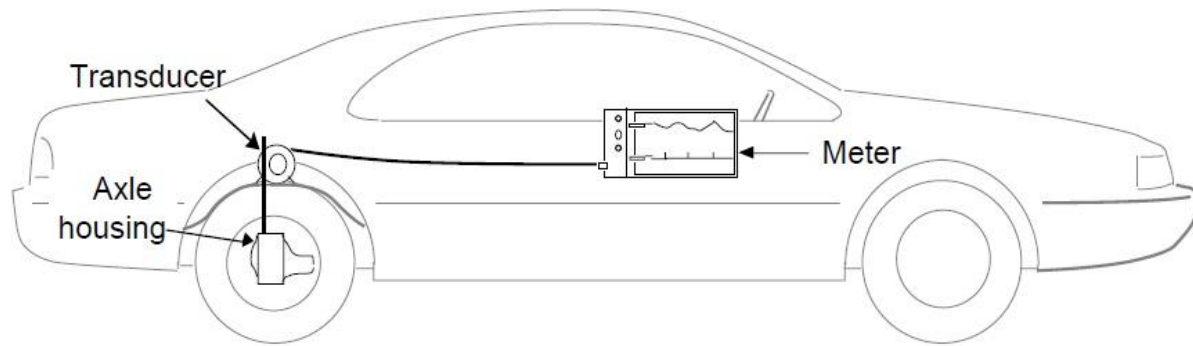


Figure 28: Vehicle equipped with the Mays Ride Meter (Sayers and Karamihas 1998)

iii. International Roughness Index (IRI)

The International Roughness Index (IRI) is an index value that is correlated to pavement roughness. The IRI value is in the units of inches per mile with the inches being the vertical deviation and the miles being the horizontal distance along the profile. A high IRI value correlates to a rougher pavement than a low value. Since the IRI is considered to be a property of the true pavement profile, it can be measured with a variety of valid profilers. Vehicles outfitted with an onboard computer as well as a system of lasers and accelerometers are common for determining IRI values. While other indices cannot produce the same values with different vehicles or sometimes even the same vehicle, the IRI is a very repeatable and consistent test (Sayers and Karamihas 1998). The repeatability and consistency of this test means that it can be used to see how pavement roughness varies with time when multiple tests are run.

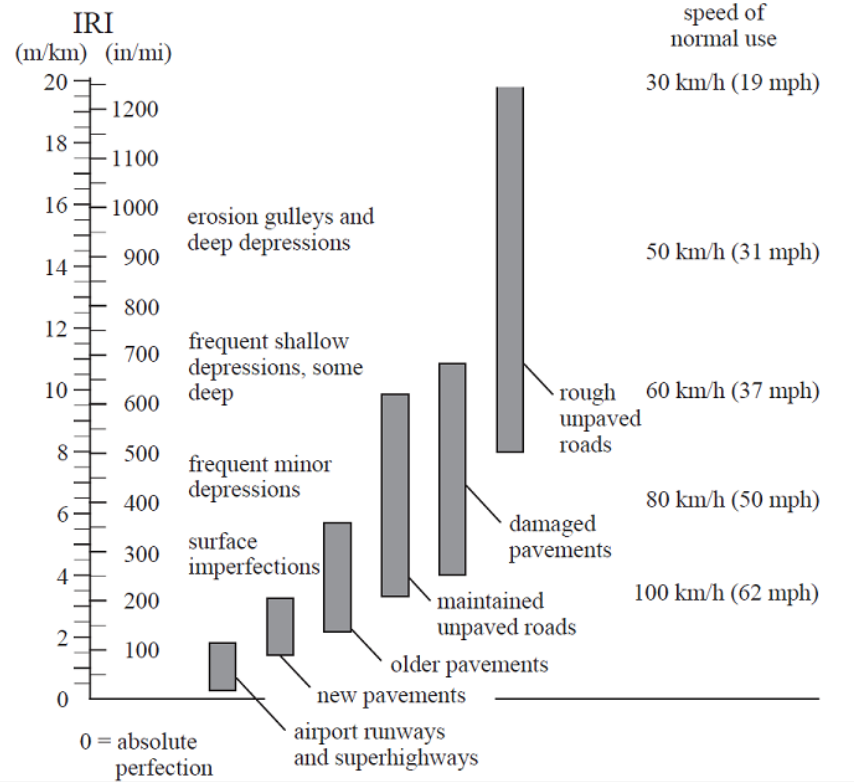


Figure 29: Typical IRI values for roadways (Sayers and Karamihis 1998)

c. Soil Heave

i. Expansive Clays

1. Introduction

This section provides an overview of expansive clays. This overview includes the types of soils affected and causes associated with swelling soil. It is important to understand the nature of swelling soil as it can cause pavement distresses.

2. Affected Soil types

Swelling is a phenomenon typically observed in fine grained highly plastic clay soils. Steatite is the common name for clay minerals that experience volume change due to a change in water content. Montmorillonite is the most commonly found mineral in the smectite family (McCarthy 2007).

3. Cause

The mechanism of swell occurs when positively charged water molecules interact with negatively charged clay soil particles. This interaction results in a cation exchange and an attraction between the water molecules and the soil particles. This attraction of water molecules causes them to accumulate around the clay particle, resulting in a double diffuse layer surrounding the clay particle (Wersin et. al 2004). This double diffuse layer causes more water to be present in the pore spaces between clay particles resulting in an increase in pore pressure. If this pore pressure increase is greater than the surcharge pressure on the clay, swelling will occur until equalization of pore pressure and surcharge pressure is achieved. Available water molecules will continue to be attracted to the clay particles until the charge equilibrates. The condition where the charge equilibrates and water molecules are no longer attracted to the clay particles is known as the stability value of water content for the clay. When this stability value is reached, further increases in water content do not result in continued swell (McCarthy 2007). Figure 30 shows how increasing water contents affect the size of the double diffuse layer and the total volume of the clay.

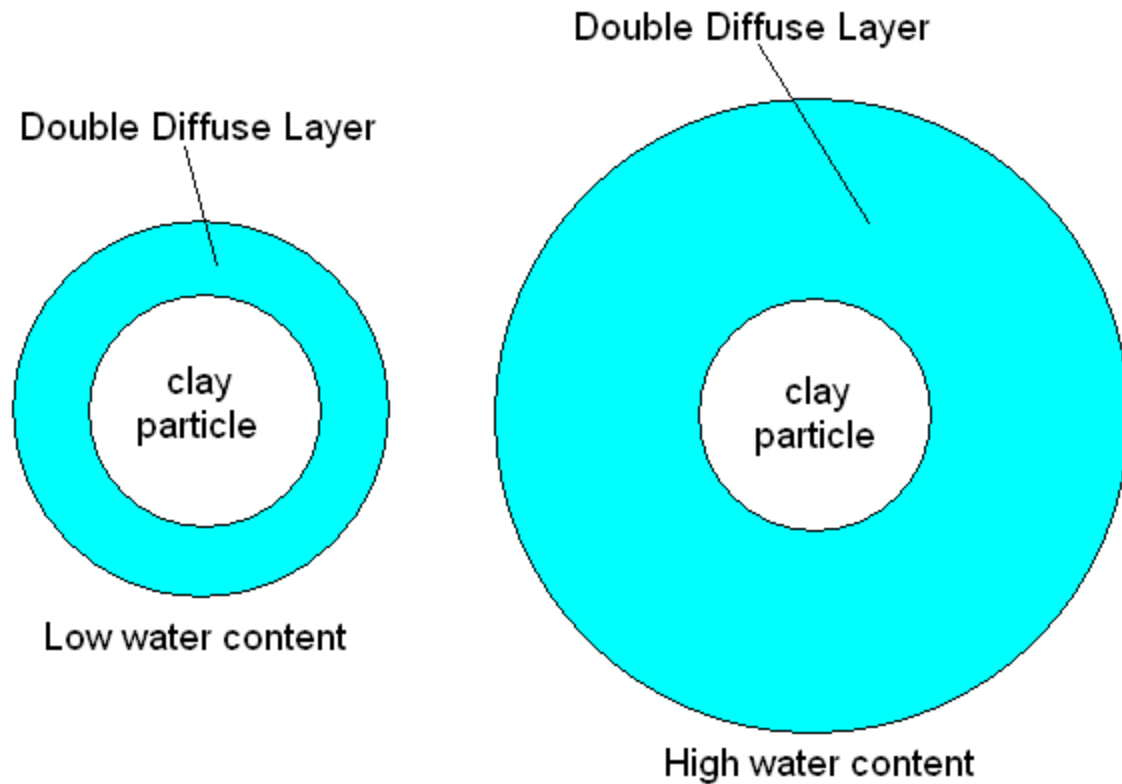


Figure 30: Schematic of double diffuse layer size as it varies with water content.

ii. Ettringite Formation and Sulfates

1. Introduction

This section provides information regarding sulfate swell and the formation of ettringite. The problems associated with ettringite formation and sulfate swell, detection and remediation of sulfate rich soils, critical sulfate concentrations, and the sources of sulfate are discussed.

2. Problems Associated with Ettringite Formation

Ettringite formation in soils causes heave that can lead to localized bumpy sections of pavement. Often, this distress can lead to total destruction of the pavement requiring expensive remediation measures. Ettringite formation often exists in the subgrade layers of the roadway and may require the entire pavement section to be removed to remediate the problem (Little 2009). Roadways in Texas have experienced tens of millions of dollars in damage due to

distresses caused by sulfate bearing soils (Harris 2004). Figure 31 shows vertical heaves caused by ettringite formation during construction of U.S. 67 near Midlothian, TX. The pavement was initially at the elevation of the bottom of the white box but the portion of pavement to the right of the picture has heaved to the elevation of the top of the white box.



Figure 31: Heave caused by ettringite formation (Harris 2004).

3. Soil Conditions conducive to ettringite formation

Sulfate rich soils, water, calcium, and a high pH environment are required for the formation of ettringite and sulfate induced heave. Typically, sulfate levels in excess of 3000 ppm are thought to be problematic (Little 2009). The level of risk associated with sulfate induced heave increases with increasing sulfate content. The level of risk with respect to sulfate concentration is shown in Table 1.

Table 1: Risk associated with sulfate concentration in sulfate-bearing clays (Little 2009).

Risk Involved	Soluble Sulfate Concentrations	
	Parts Per Million (ppm)	Percent Dry Weight
Low Risk	Below 3,000	Below 0.3%
Moderate Risk	Between 3,000 and 5,000	Between 0.3% and 0.5%
Moderate to High Risk	Between 5,000 and 8,000	Between 0.5% and 0.8%
High to Unacceptable Risk	Greater than 8,000	Greater than 0.8%
Unacceptable Risk	Greater than 10,000	Greater than 1.0%

Although Table 1 provides general guidance regarding sulfate concentration, it should be noted that sulfate induced heave has been observed in soil with sulfate concentrations as low as 320 ppm (Puppala 2005). Since sulfate induced heave is caused by the formation of ettringite and thaumasite minerals, it can be experienced in any soil containing the reactants needed for the formation of these minerals. However, the volume change experienced in clays is typically higher than the volume change experienced in sandy soils (Little 2009). Also, mixed and clayey soils are typically more susceptible to ettringite formation than sandy soils (Puppala 2005). Table 2 shows results of swell tests run by Puppala on three different soil types at three different lime contents and five different sulfate concentrations. At 10,000 ppm sulfate concentration, this test shows that the percent swell decreases as percent clay decreases and percent swell increases as percent lime increases, inferring swell due to ettringite formation.

Table 2: Percent swell of three soil types in differing lime and soluble sulfate conditions (Puppala 2005).

Lime	Soil type	Soluble sulfate (mg/kg)				
		0	1,000	2,500	5,000	10,000
0% lime	Kaolinite clay	24.9	23.4	24.1	22.9	24.2
	Mixed soil	3.5	NT	NT	3.2	4.3
	Sand	0.00	NT	NT	NT	0.00
4% lime	Kaolinite clay	22.9	25.1	28.7	29.7	32.3
	Mixed soil	2.7	NT	NT	5.55	7.3
	Sand	0.0	NT	NT	NT	0.7
8% lime	Kaolinite clay	19.9	23.7	27.4	31.1	39.2
	Mixed soil	2.3	NT	NT	4.9	9.4
	Sand	0.0	NT	NT	NT	1.2

Note: NT=Not tested.

Since one of the reactants necessary for ettringite formation is calcium, sulfate induced heave is most commonly experienced in clayey soils that have been stabilized with a calcium based stabilizer such as lime. In addition to the presence of sulfates and calcium, ettringite forms more readily in basic environments (pH between 11 and 13) (Puppala 2005). Since the addition of lime to soil increases the pH, the basic environment is formed allowing ettringite to form more readily.

4. Sources of Sulfate

There are multiple sources in soil that provide sulfate ions. The most common source of sulfate is gypsum, as it provides sulfate ions when dissolved (Harris 2004). Other sources of sulfate include atmospheric sulfate as well as sulfate produced by the decomposition of organic matter (Schulte and Kelling 1992). If organic matter is allowed into the base and sub-base materials, decomposition will increase the sulfate content and increase the possibility of ettringite formation.

5. Distribution of Sulfates

Sulfates are commonly found in the western and southern United States. In the western United States, sulfates are present in the form of naturally occurring gypsum. In areas laden with sulfate rich soils, sulfates commonly exist in isolated pockets and seams. The uneven distribution of sulfates often leads to randomly isolated areas of distress along a section of pavement (National Lime Association 2004). Volcanic ash can be a major source of sulfates in soil (Bao 2004). The uneven ash fall distribution explains the uneven distribution of sulfates.

6. Testing for Sulfate-Rich Soils

To determine the proper plan of action for dealing with sulfate rich soils, it is necessary to determine the sulfate content. The sulfate level can be determined through Inductively Coupled Argon Plasma (ICAP) testing. However, the unpredictable distribution of sulfates would require a large amount of soil sampling and lab testing which can be costly and inefficient. A more practical and feasible method for determining the sulfate content is a geophysical method that relates the sulfate content to the electrical conductivity of the soil. The electrical conductivity of the soil can be measured rapidly and accurately using a magnetometer (Natarajan 2004). A magnetometer has a transmitter coil and a receiver coil. The transmitter coil produces a primary magnetic field, which in induces small currents in the soil and creates a secondary magnetic field. The receiver coil senses the primary and secondary magnetic fields and relates their strength to soil electrical conductivity (McNeill 1980). The electromagnetometer can either be handheld or pulled behind a vehicle on a cart made of nonconductive material. A magnetometer, the EM 38, manufactured by Geonics, is shown in Figure 32.



Figure 32: The EM 38 Magnetometer (Natarajan 2004).

7. Ettringite Formation Mechanism

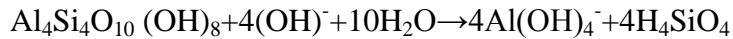
The formation of ettringite requires sulfate, a source of calcium ions, a source of water, and a high pH environment. Chemically, the formation of ettringite can be described through four reactions (Reaction) shown below.

The first reaction is the dissolution of lime into ions:



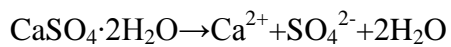
This reaction produces the required calcium ions necessary for ettringite formation. Also, the introduction of hydroxide ions increases the pH to a level required to form ettringite.

Assuming Reaction 1 caused the pH to increase to at least 10.5, the dissolution of kaolinite also occurs as shown in Reaction 2.



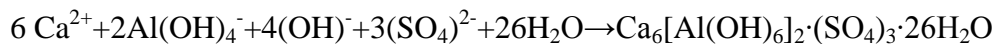
Reaction 2

Reaction 3 describes the dissolution of gypsum to provide sulfate ions. Gypsum is a common source for sulfate ions but is not the only source. Reaction 3 is shown below because gypsum is the most commonly found source for sulfate ions.



Reaction 3

When all of the necessary ions are present in a high pH environment, the formation of ettringite can occur as shown in Reaction 4, below.



Reaction 4

(Ettringite)

The formation of the ettringite crystal described in Rxns. 1-4 is responsible for the volume change that causes distress (Harris 2004).

d. Soil Stabilization Techniques

i. Treatment of Expansive Clays

1. Introduction

This section provides an overview of techniques used to stabilize swelling soils. The techniques include lime stabilization, mechanical stabilization and cement stabilization. It is important to have a thorough understanding of stabilization techniques so that the proper technique can be utilized for unique situations.

2. Lime Stabilization

Lime stabilization is a common method used to reduce volume change potential in clays when it is determined that compaction is not adequate. Generally, soils with more than 25% of the particles smaller than 0.002 mm and a plasticity index greater than 10 require further stabilization efforts beyond compaction. It is common for the strength of clay stabilized with lime to double (Lytton 1994).

a. Lime Stabilization Mechanism

The stabilization of clay soils with lime occurs through a chemical reaction involving the cation exchange between the calcium ions present in lime and the exchangeable cations present in the clay particles. This reaction causes a decrease in the thickness of the bound water layer surrounding the clay particles allowing them to move closer together. Flocculation occurs as the particles move closer together. The addition of lime to the soil causes an increase in pH, allowing flocculation to occur more readily. Flocculation results in an increase in internal friction, shear strength, and workability (Lytton 1994). Although all clay soils react with lime, the most prominent effects are seen in soils containing montmorillonite with lesser effects in

kaolinite (Bell 1996). Through lime stabilization, the plasticity index of the soil is reduced and the soil behaves like a granular material rather than plastic clay (Lytton 1994).

b. Lime-Soil Interactions

The interaction of lime with soil is dependent on a number of factors including degree of weathering, soil-water pH, base cation concentrations, silica-alumina concentrations, organic content, and soluble sulfate content (Little 1995).

Organic carbon inhibits the reaction of lime with soil by either adsorbing the lime's calcium ions or reacting with the soil and preventing the cation exchange between the lime and the soil. Typically, organic contents greater than one percent are believed to interfere with the pozzolanic reaction, but this varies as different soils and different types of organic matter react differently (Little 1995).

Soluble sulfates present in the soil will react with the calcium ions from lime to produce a calcium-sulfate-aluminate-hydrate known as ettringite. Not only does this formation of ettringite inhibit the pozzolanic reaction, but the ettringite mineral swells during formation and defeats the purpose of stabilizing the clay (Little 1995). Ettringite can expand 227% of the volume of the reactant solids. However, the ettringite mineral does not experience shrinkage and swell with changing moisture conditions (Lytton 1994). This means that if the soil is compacted after the ettringite mineral forms, problems related to lime sulfate-induced heave are diminished. Construction techniques to minimize the problems related to sulfate-induced heave include ensuring enough water is available to solubilize the sulfates, homogenous mixing prior to compaction, proper drainage of the pavement structure, and ensuring that enough calcium ions are present. These construction methods focus on allowing a majority of the ettringite mineral to form prior to compaction and preventing high sulfate water from penetrating the stabilized layer

and causing ettringite formation deeper in the soil structure (Little 1995). Alternative stabilizers in the form of low calcium fly-ashes have also been considered to reduce sulfate-induced swell in high sulfate content soils. These low calcium stabilizers reduce the amount of calcium ions present to react with the sulfates which reduces the amount of ettringite that can be formed (Lytton 1994). Sulfate induced ettringite formation is reviewed in section ii.

Enough silica and alumina must be present in the soil to react with the lime. Clay minerals are the most abundant source of silica and alumina, so the clay content must be high enough to support the pozzolanic reaction (Little 1995).

Weathering of the soil causes changes in the base cation concentrations as well as the pH of the soil. As pH increases, the clay minerals are more readily dissolved allowing increased interaction between the calcium ions from the lime and the minerals from the soil. These calcium ions are replaced by hydrogen ions resulting in a decrease in pH and a reduced potential for the pozzolanic reaction to occur. A good indicator of the degree of weathering of a soil is the Ca/Mg ratio. As weathering takes place, the Ca ions are leached resulting in a lower Ca/Mg ratio. A low Ca/Mg ratio typically means an increased amount of weathering and a reduction in the pH has occurred, resulting in reduced soil-lime reactivity (Little 1995).

c. Curing Conditions

For an effective lime-soil reaction to take place, moisture and temperature must be controlled. Since the reaction occurs through cation exchange, it is necessary for the lime as well as the reacting soil minerals to be dissolved in water to form ions. Maximum effectiveness of the lime is only achieved when enough water is present to fully dissolve the reactants. Increasing the temperature during curing accelerates the pozzolanic reaction (Little 1995). If the temperature is below freezing, the water is no longer in liquid form and cannot dissolve the

reactants. If the reactants cannot be dissolved, no cation exchange, and therefore no pozzolanic reaction can occur. Pozzolanic reactions are retarded at around 4 degrees Celsius and may remain dormant until temperatures increase (Bell 1996).

d. Swell Potential vs. Plasticity Index

The plasticity index of a soil is the difference in the water contents of the soil acting as a plastic and the soil acting as a liquid. A proper pozzolanic reaction between lime and clay often results in a decrease in the plasticity index and therefore a decrease in the swell potential of the soil (Little 1995). Figure 33 demonstrates the typical relationship between plasticity index and swell potential.

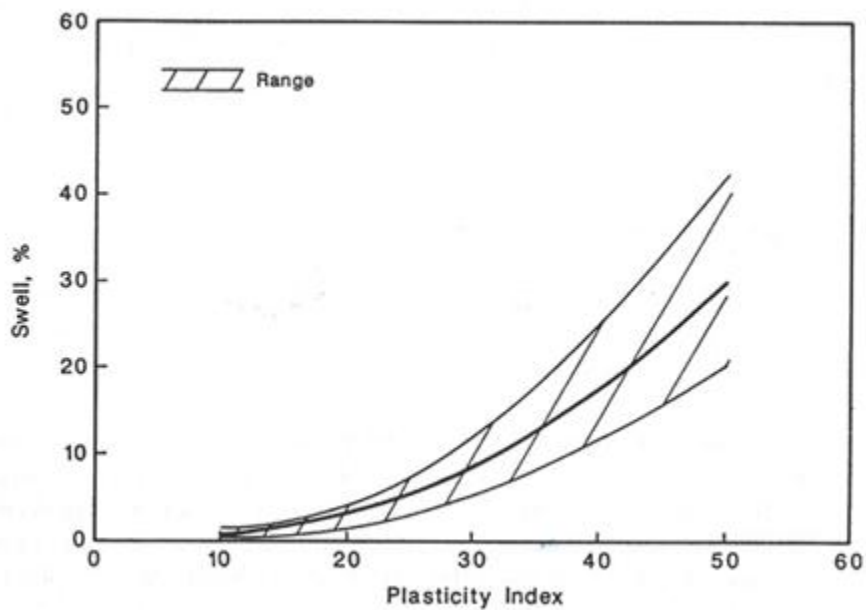


Figure 33: Typical relationship between swell and plasticity index (Little 1995).

e. Lime Stabilization Techniques

The three prominent methods used to stabilize a soil with lime are lime slurry, dry hydrated lime, and lime injection.

i. Lime Slurry

Lime slurry refers to a slurry solution of hydrated lime and water. This slurry solution is mixed before its application to the soil.

The first step in applying lime slurry is to scarify the roadbed. After scarifying, a tank truck equipped with a spray bar makes passes over the scarified roadbed until the desired amount of lime slurry has been applied to the soil (Little 1995). After the lime application, it is common to mix the lime in the soil with a rotary mixer and compact to the specified density (Lytton 1994).

The three methods of mixing the lime slurry are central mixing tanks, jet mixers, or tank trucks. Central mixing tanks use compressed air and recirculating pumps to mix the slurry. The slurry is then transferred to the truck used to apply the mixture. Jet mixers employ a 70 psi water jet to mix lime at a continuous 65% water to 35% lime ratio to instantaneously produce lime slurry. This type of mixer is advantageous because it is easily transported to a jobsite and does not require off-site mixing. Tank trucks are only capable of making one batch of slurry at a time by mixing measured amounts of water and lime with compressed air. After the correct water and lime portions are put in the tank, the truck mixes the slurry solution on the way to the jobsite by using a recirculating pump (Little 1995). A jet mixer is shown in Figure 34.



Figure 34: Lime slurry mixed with a jet mixer (Little 1995).

ii. Dry Hydrated Lime

Dry hydrated lime is often applied to roadways in a powder or pelletized form. Small projects often use bags of lime and smaller equipment for soil mixing. Larger projects such as roadways utilized larger machinery and apply the lime in bulk form. For bulk application of lime, the lime is transported to the jobsite using self unloading transport trucks employing one of numerous discharge systems including screw conveyors, pneumatic blowers, or pipe spreader bars. Often the pneumatic blowers apply the lime in windrows which are later mixed with soil to provide a uniform lime treatment (Little 1995).

Pelletized lime consists of larger particles than powdered lime and therefore avoids the dusting problem associated with powdered lime. After the proper amount of water is applied, it is common to further mix the lime using a rotary mixer and compact to the specified density (Lytton 1994). Figure 35 shows a pipe spreader bar used for dispersing powdered lime. As soon as powdered lime is placed, it is necessary to sprinkle it with water to prevent it from blowing away and dusting (Little 1995).

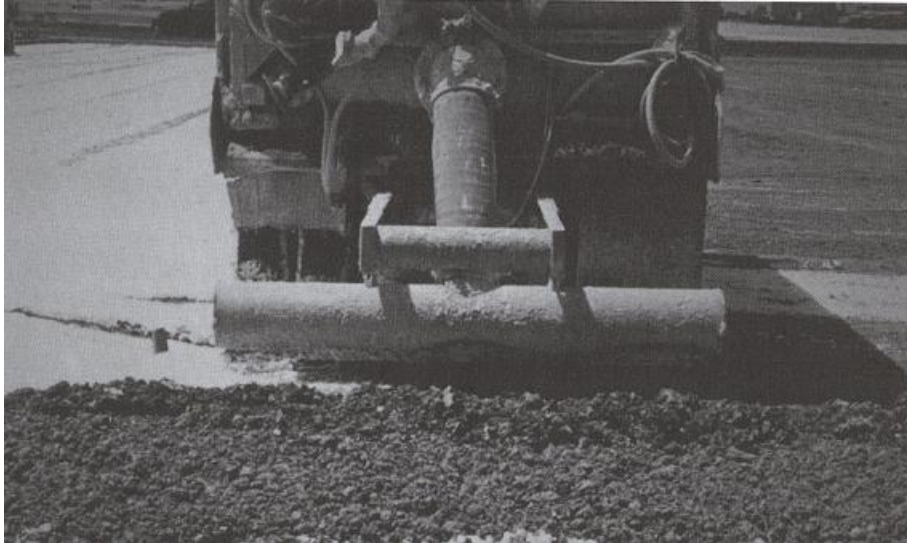


Figure 35: Pipe spreader bar used for spreading dry hydrated lime (Little 1995)

iii. Lime slurry Pressure Injection

While lime slurry, pelletized lime, and powdered lime are all surface applications of lime stabilization, lime injection is used to stabilize deeper clay layers. Lime injection requires a lime slurry solution be produced. After this lime slurry is made, it is injected into the soil under pressure through pipes that are pushed into the soil to the application depth. The lime slurry then travels through the soil mass taking the path of least resistance through cracks and other voids. The slurry then reacts with the soil, resulting in an increase in strength and a reduction of moisture migration. The shrink-swell cycling of clay soils creates tension cracks in the soil structure. Since the lime slurry penetrates through cracks, more tension cracks in the soil leads to increased success of a lime injection treatment (Little 1995). The typical device used to perform lime slurry pressure injection is shown in Figure 36.

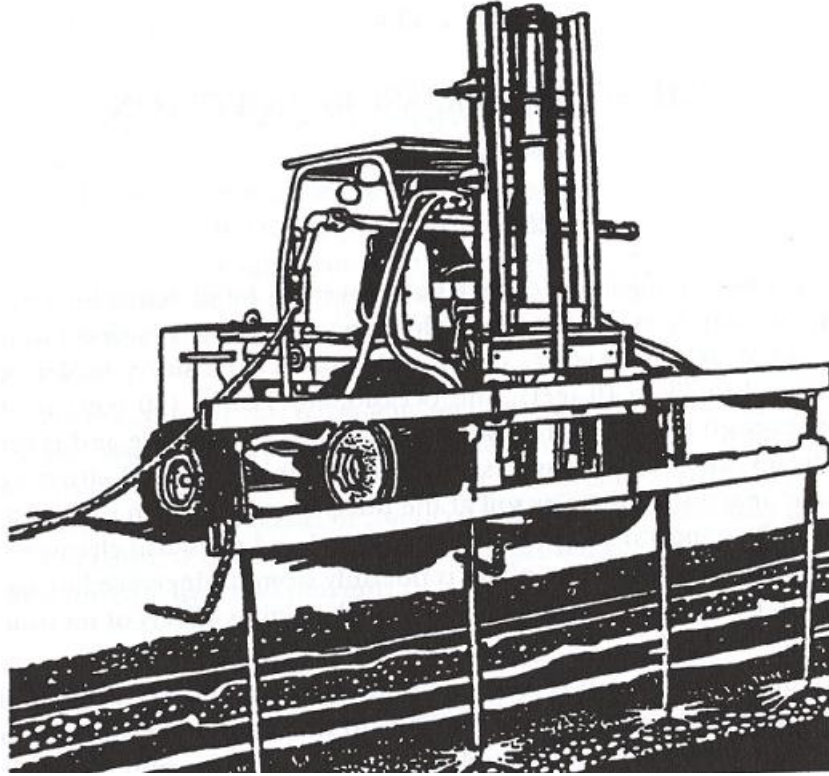


Figure 36: Typical machinery used for lime slurry pressure injection (Little 1995)

The typical lime slurry injection process consists of injecting lime slurry containing between 22 and 36 percent lime solids into the subgrade on a 5 foot grid pattern. If more lime treatment is desired, secondary and tertiary injections may be made in between the initial injections. The slurry is first injected at the deepest point of desired treatment and subsequent injections are made frequently as the pipes are extracted from the ground until the lime treatment is complete. Typical injection pressures range from 50 to 200 psi. Figure 37 shows typical lime injection patterns.

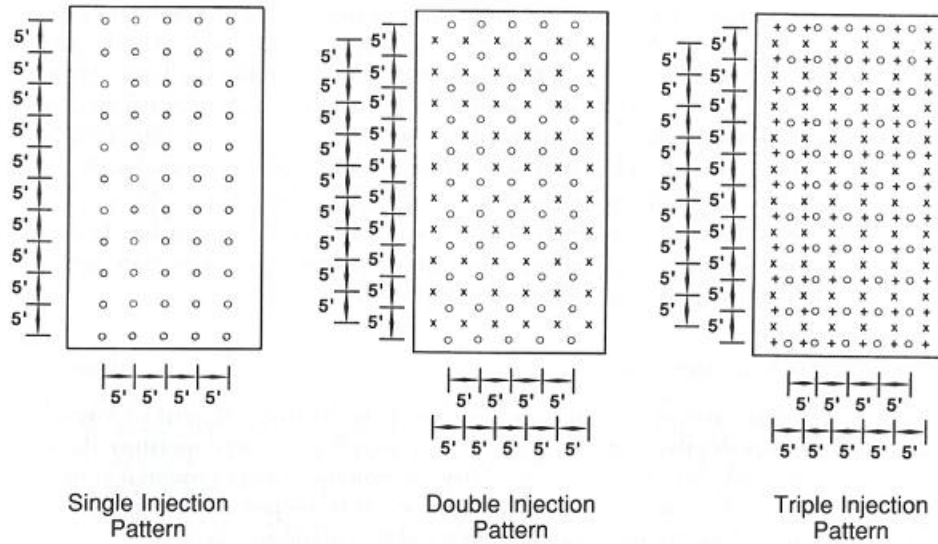


Figure 37: Typical grid patterns for single, double, and triple injection (Little 1995)

Surfactants and fly ash are often added to the lime slurry. Surfactants provide a reduction in surface tension allowing the slurry to penetrate the soil easier. Fly ash is a pozzolan that can increase the amount of available silica and alumina to react with the lime resulting in higher soil strengths (Little 1995).

3. Mechanical Stabilization

Mechanical stabilization methods improve the properties of the soil mass, but do not change the chemical composition. Methods of mechanical stabilization include the most common soil improvement method, compaction, as well as the use of geosynthetics.

a. Compaction

Compaction is the most common form of soil improvement. Proper compaction leads to an increase in strength, reduction in permeability, reduction in compressibility, decrease in susceptibility to volume change, and increased durability (McCarthy 2007).

The typical compaction procedure involves placing soil in thin lifts and compacting each lift before the next is placed. Compaction is achieved by vibration for cohesionless soils and

kneading for cohesive soils. Although compaction using rollers is the most common, other methods such as dynamic deep compaction, vibrocompaction, and compaction grouting exist for specialized applications (McCarthy 2007).

b. Geosynthetics

Geosynthetics are a relatively new, but increasingly popular choice for stabilizing soils. Geotextiles and geogrids are the most common geosynthetics used for stabilization. Geogrids and geotextiles can be placed over weak subgrades to cause an immediate strength increase. Geofibers may also be mixed with the soil to provide an increase in strength (McCarthy 2007).

Unlike other soil stabilization methods, geosynthetics add a manmade item to a soil structure. Also unique to geosynthetics is their ability to withstand much higher tensile forces than soils subjected to other stabilization methods. Although geosynthetics provide soil stabilization, there are multiple types of geosynthetics that can provide separation, filtration drainage, and containment in addition to the reinforcement aspect (Koerner 2005).

4. Cement Stabilization

Although lime stabilization is considered a form of cement stabilization, this section will focus on fly ash and Portland cement. While Portland cement is a manufactured product, fly ash is a byproduct of burning coal causing it to be a more variable material (Little et al. 2000).

Stabilization by coal fly ash can be achieved by using either a non-self-cementing or a self-cementing coal fly ash. A non-self-cementing coal fly ash requires the use of an activator such as Portland cement or lime. The resulting pozzolanic reaction causes an increase in strength of the soil (Little et al. 2000).

A self-cementing coal fly ash does not require an activator such as Portland cement or lime for a pozzolanic reaction to occur. However, self-cementing fly ash may not be suitable for

stabilizing plastic clay soils. Performing stabilization by self-cementing coal fly ash results in increased stiffness, strength, and freeze thaw resistance as well as a decrease in permeability, plasticity, and swelling (Little et al. 2000).

Portland cement stabilization consists of soil, Portland cement, and water. When correct proportions of each ingredient are maintained, proper stabilization can occur (Portland Cement Association 2001). Portland cement stabilization has been in use for nearly 100 years. Portland cement stabilization is suitable for use in fine-grained soils, granular soils, and aggregates. Portland cement stabilization utilizes a pozzolanic reaction between the calcium hydroxide and alumina and silica from fine grained clay soils to improve soil properties. The result of a Portland cement stabilized material is increased moisture resistance, durability, and leaching resistance (Little et al. 2000).

ii. Treatment of Sulfate Rich Soil

Typical lime treatment of sulfate laden clayey soils poses a dilemma due to the swelling mechanism related to the formation of ettringite. However, there are a number of construction procedures that can be implemented to mitigate the effect of sulfate swell while still allowing the required stabilization benefits of lime. The two most widely used methods for mitigating sulfate swell involve controlling the sulfate-lime reaction.

The first method retards the sulfate-lime reaction by limiting at least one of the reagents required for ettringite formation (AASHTO 2008). This can be achieved by limiting the availability of calcium ions by implementing the use of a low calcium stabilizer such as low calcium fly ash. Since water is also required to ionize the reagents needed for ettringite formation, proper drainage can limit the amount of water available to solubilize reagents required for ettringite formation (Little 2009).

The second method uses a dual lime treatment with a mellowing period between the two treatments. The mellowing period allows the sulfate and lime to react and form ettringite. The rate of sulfate-lime reaction is increased so that the reaction occurs before subsequent pavement layers are placed. The reaction speed is increased by creating conditions that favor the dissolution of sulfates and calcium ions so more are available to react. It is common to add additional 3 to 5 percent moisture during the mellowing period (Little 2009).

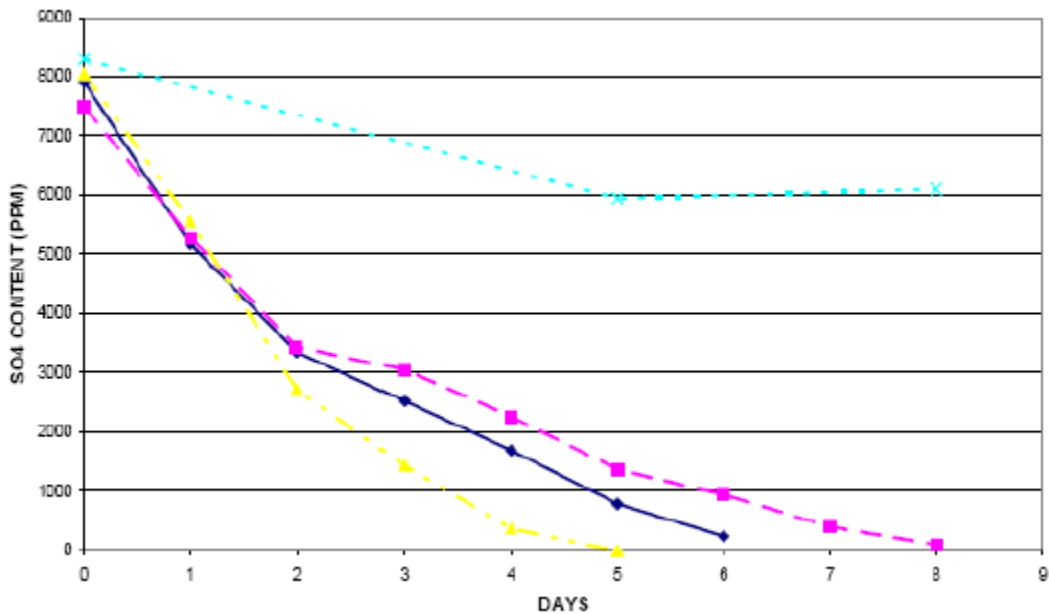


Figure 38: Effect of mellowing period on sulfate content (Little 2009).

After this mellowing period the second treatment is applied and allowed to mellow (Little 2009). The irreversible formation of ettringite before compaction and paving keeps pavement distresses from occurring due to sulfate swell.

Although there are construction procedures to mitigate the effect of sulfate swell, it is widely accepted that soils with sulfate levels greater than about 10,000 ppm are considered an unacceptable risk and stabilization with lime should not be performed (Little 2009).

e. Clay Chemistry

i. Introduction

This section provides an overview of the chemistry involved with clay minerals. The topics covered in this section include the mineral types, chemical structures, and characteristics exhibited by these minerals. It is important to have a thorough understanding of clay chemistry because of the variety of minerals that each exhibit unique properties that affects the performance of the clay material.

ii. Significance of Clay Chemistry

Unlike cohesionless soils, clays may experience large volume changes with the addition or removal of water. Such volume changes can damage overlying structures and pavements (Ranjan 1991). Since the clay mineral type is the key factor regarding the activity of the clay, it is necessary to study these minerals to understand why this volume change occurs and how to remediate it.

iii. Mineral Structure

Clay minerals are comprised of a combination of silica tetrahedral and aluminum octahedral sheets. A silica tetrahedron consists of four oxygen ions bonded with a single silicon ion to form the four sided tetrahedron shown in Figure 39 (Ranjan 1991). Multiple silica tetrahedrons bonded together form a silica tetrahedral sheet shown in Figure 39.

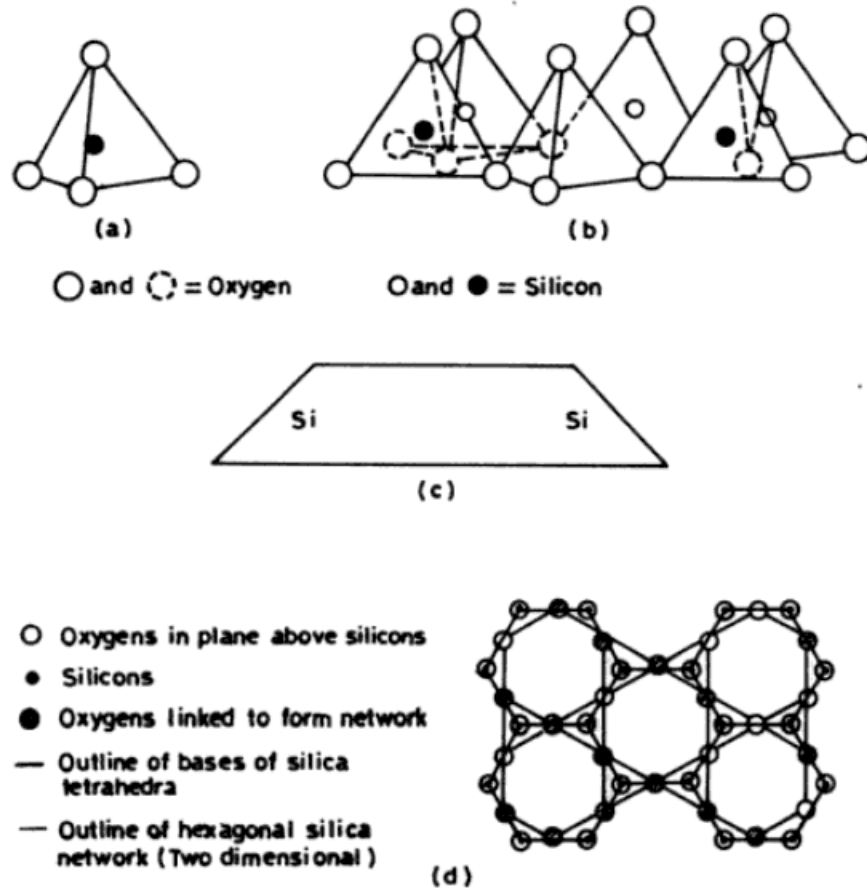


Figure 39: (a) Single silica tetrahedron. (b) Isometric representation of silica tetrahedral sheet. (c) Symbolic representation of silica tetrahedral sheet. (d) Top view of silica tetrahedral sheet (Ranjan 1991).

An aluminum octahedron consists of six oxygen or hydroxyl molecules bonded with a single aluminum molecule to form the eight sided octahedron shown in Figure 40. In an aluminum octahedron, it is common for the aluminum ion to be replaced by magnesium, iron, or another neutral ion. Multiple aluminum octahedrons bonded together form an aluminum octahedral sheet shown in Figure 40.

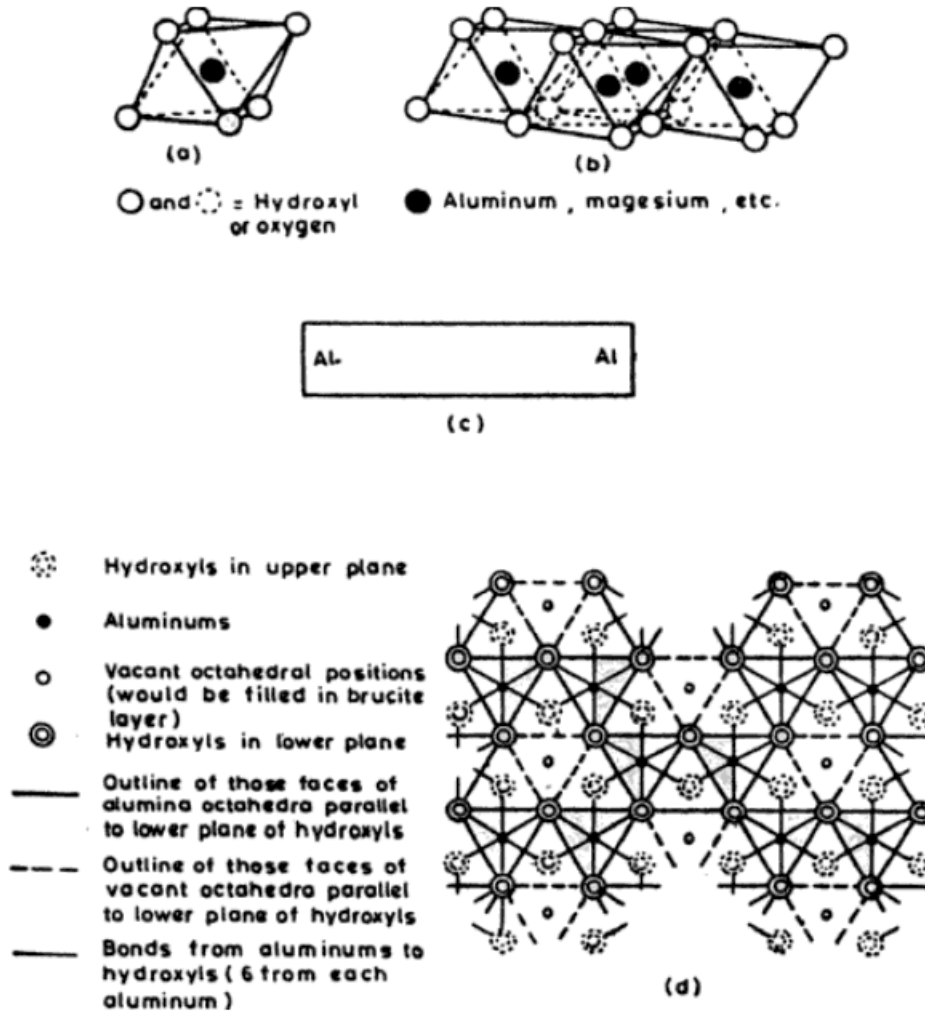


Figure 40: (a) Single aluminum octahedron. (b) Isometric representation of the aluminum octahedral sheet. (c) Symbolic representation of the aluminum octahedral sheet. (d) Top view of the aluminum octahedral sheet (Ranjan 1991).

Both silica tetrahedral and aluminum octahedral sheets are approximately five Angstroms thick. Different combinations of these sheets form a variety of clay minerals with highly variable properties (McCarthy 2007).

iv. Mineral Types

The five most common clay minerals formed by alternating aluminum octahedral and silica tetrahedral sheets are kaolinite, halloysite, illite, montmorillonite, and chlorite. The sheet like structure of these minerals allows them to develop cohesion and plasticity. The clay

particles formed by these minerals are typically less than 0.002 mm in diameter (McCarthy 2007).

1. Kaolinite

Kaolinite is the most abundant clay mineral and forms in humid climates from crystalline rocks. The kaolinite mineral layer consists of one aluminum octahedral and one silica tetrahedral sheet, layers are bonded together very strongly. The thickness of a kaolinite mineral layer is 7.5 Angstroms (McCarthy 2007). A kaolinite crystal consists of approximately 70-100 of these mineral layers stacked together resulting in a crystal thickness of approximately 500-1000 Angstroms. The layers are held together by hydrogen bonding which increases the strength and reduces the activity of the clay (Ranjan 1991). Figure 41 shows a representation of the kaolinite mineral.

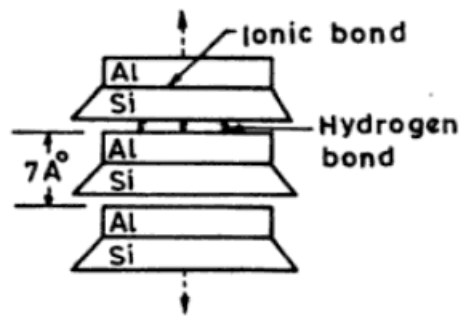


Figure 41: Schematic of the kaolinite structure (Ranjan 1991).

The thick, plate-shaped particles formed from kaolinite are resistant to volume change caused by water (McCarthy 2007).

2. Halloysite

Halloysite is a tubular mineral similar to kaolinite in the sense that it consists of a single silica tetrahedral sheet bonded to a single aluminum octahedral sheet. However, halloysite differs because a sheet of water molecules is sandwiched between the silica tetrahedral sheet and

the aluminum octahedral sheet. This layer of water molecules causes the strength and plasticity of halloysite to be significantly affected by drying the clay. Upon drying, the water layer between the silica and aluminum sheets is removed. Subsequent wetting of the clay will not form another water layer and the clay will exhibit characteristics very similar to kaolinite. Halloysite samples that have been dried and rewetted exhibit increased strength and decreased plasticity when compared to naturally wetted halloysite. The thickness of a halloysite mineral layer is ten Angstroms (McCarthy 2007).

3. Illite

Illite is formed when a single aluminum octahedral sheet is bonded between two silica tetrahedral sheets. The illite layers are bonded together with potassium (McCarthy 2007). Although similar in structure to montmorillonite, the potassium bond is stronger than the bonds in montmorillonite. The increased bond strength reduces the activity of the illite (Ranjan 1991). A diagram of illite's structure is shown in Figure 42.

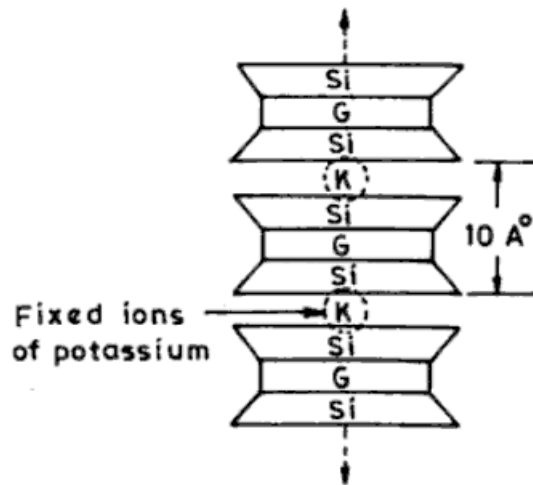


Figure 42: Representation of the illite structure (Ranjan 1991)

The thickness of an illite mineral layer is ten Angstroms. Illite clays are often found in marine deposits and soil formed from micaceous rock. Illite is typically more plastic than

kaolinite, but does not expand when exposed to water unless a deficiency of potassium causes a weakened bond between the silica and aluminum sheets (McCarthy 2007).

4. Montmorillonite (Smectite)

Montmorillonite is formed from ferromagnesium rock in semi-arid and temperate climates as well as from the decomposition of volcanic ash. Montmorillonite consists of a single aluminum octahedral sheet bonded between two silica tetrahedral sheets. The montmorillonite layers are weakly bonded together. It is common for iron or magnesium ions to replace the aluminum ions in the aluminum octahedral sheet. Some silicon ions in the silica tetrahedral sheet may be replaced by aluminum ions. The thickness of a montmorillonite layer is approximately 9.5 Angstroms, but varies due to the variable mineral shape. Montmorillonite is formed in irregular plate shapes or as a fibrous mineral (McCarthy 2007). The bond between the silica and aluminum sheets is a result of van der Waals forces which are much weaker than hydrogen bonds or other types of bonding. The weak bonds allow this mineral to absorb water readily between the layers (Ranjan 1991). A schematic of the montmorillonite structure is shown in Figure 43.

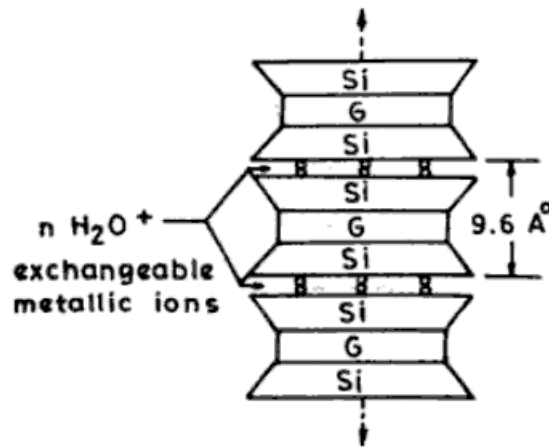


Figure 43: Diagram of the montmorillonite structure (Ranjan 1991).

The tendency of this clay to absorb water results in a high tendency for volume change with changing water contents (McCarthy 2007).

5. Chlorite

Chlorite consists of an aluminum octahedral sheet sandwiched between two silica tetrahedral sheets. The chlorite layers are approximately 14.1 Angstroms thick. Chlorite layers are bonded together with an aluminum octahedral sheet, creating a mineral that has alternating aluminum and silica sheets. Chlorite typically forms from well draining soils as well as micaceous rocks in humid climates. Chlorite typically forms as irregular plate shapes that do not experience volume change with varying water contents (McCarthy 2007).

f. X-Ray Diffraction

i. Introduction

X-Ray Diffraction is a method of identifying crystalline materials by bouncing an X-Ray beam off of a substance and recording and analyzing the diffraction pattern of the X-Ray beam caused by the substance. The two basic types of diffraction methods are single crystal diffraction and powder/polycrystalline diffraction. The single crystal diffraction method is mainly used to determine the molecular structure of crystalline compounds. Single crystal samples consist of a single crystalline compound with all the unit cells aligned in a perfect extended pattern. The powder/polycrystalline diffraction method is typically used for characterizing and identifying polycrystalline phases. Samples used for powder/polycrystalline diffraction may include multiple crystalline phases (Scintag 1999).

X-ray diffraction samples must have a smooth plane surface. To achieve this surface, the particles are typically ground down to particles having a diameter of 0.00008-0.0002 in. using a shatter box (Scintag 1999).

ii. Instrumentation

The apparatus used to perform X-ray diffraction consists of an X-ray tube, X-ray detector, and a goniometer. The X-ray tube produces an X-ray beam. This X-ray beam is reflected by the sample and the diffracted X-ray beam is received by the X-ray detector. The goniometer consists of the sample holder, the detector arm, and the gearing required to produce various diffraction angles. The two setups for the X-ray diffractometer are the Theta : 2-Theta goniometer and the Theta : Theta goniometer (Scintag 1999). The Theta : 2-Theta goniometer is shown in Figure 44.

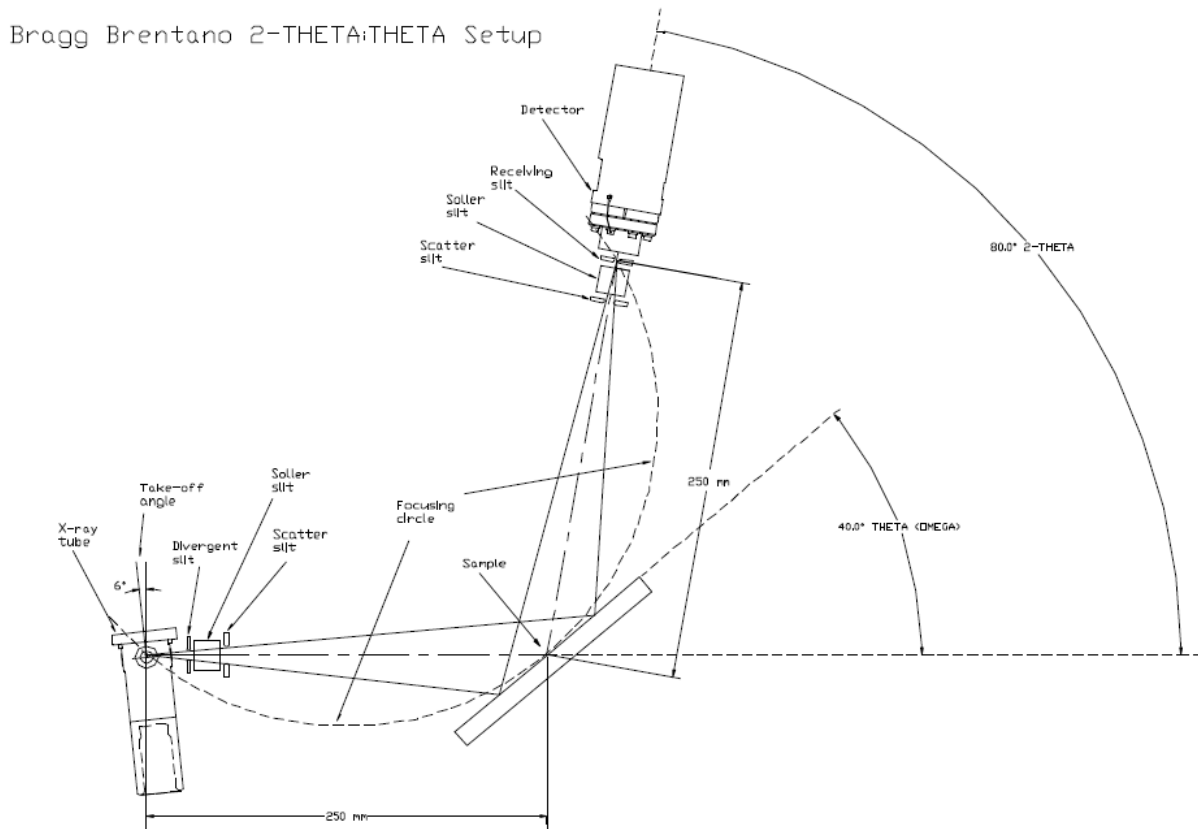


Figure 44: Bragg Brentano 2-Theta : Theta goniometer setup (Scintag 1999).

In the 2-Theta : Theta goniometer, the X-ray tube is held stationary while the sample is rotated through angle theta and the X-ray detector is simultaneously rotated through angle 2-

theta. In this setup, the sample is tilted, which increases the possibility of loose or small samples falling off of the sample holder (Scintag 1999). Figure 45 shows the Theta : Theta goniometer setup.

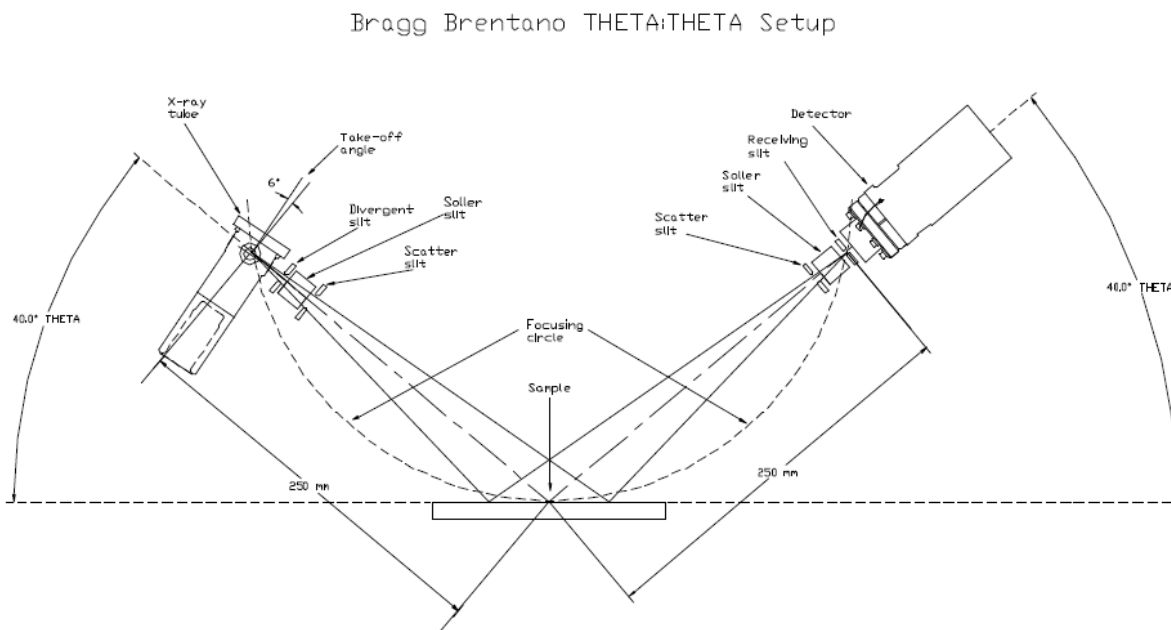


Figure 45: Bragg Brentano Theta : Theta goniometer setup (Scintag 1999).

In the Theta : Theta goniometer setup, the sample is held stationary while the X-ray tube and X-ray detector are each rotated through angle theta simultaneously. The stationary horizontal sample position makes the Theta : Theta goniometer more suitable for loose or small samples than the aforementioned Theta : 2-Theta goniometer (Scintag 1999).

iii. Identification of ettringite mineral

Like other crystalline substances, ettringite has a unique X-ray diffraction pattern and can be identified using an X-ray diffractometer. Although other substances will be present in the X-ray diffraction, each substance produces its own pattern independently of the others and can be positively identified using a search/match procedure. The search/match procedure compares the results of the X-ray diffraction with the database created by International Center Diffraction

Database (ICDD) which contains diffraction data for approximately 50,000 inorganic compounds and 25,000 organic compounds (Scintag 1999).

g. Electromagnetometer

i. Introduction

Electromagnetometers measure the apparent conductivity of soils (Geonics 2004). Electrical conductivity in soils is directly related to water content, pore size, and electrolyte concentration in soils. Electrolyte concentration is the primary contributor to electrical conductivity of a soil. Dissolved salts are the primary source of electrolytes in soils. If the electrical conductivity of a soil is known, an estimation of soil salinity can be made (Bredenkamp and Lytton 1995).

Portable electromagnetometer units, such as the EM 38 by Geonics, allow conductivity measurements to be measured very rapidly (Geonics 2004).

ii. Explanation of how Electromagnetometers work

The electromagnetometer operates by inducing a secondary magnetic field in the soil as well as applying an alternating current through the soil. The alternating current creates a time dependent magnetic field. These two magnetic fields create eddy currents in the soil. The dipole receiver senses the time dependent magnetic field as well as the secondary magnetic field. The ratio of the relative strengths of these magnetic fields represents the bulk electrical conductivity of the soil. The EM 38 model determines the bulk electrical conductivity of the soil for an area of 3.3 ft. in width and 5 ft. in depth (Natarajan 2004).

An electromagnetometer can either be used as a handheld device or mounted to a nonconductive cart for rapid surveys. The device displays the electrical conductivity in mS/m.

If desired, the EM 38 can be attached to a data logger along with a GPS to simultaneously collect electrical conductivity readings and GPS readings (Geonics 2004).

iii. Instrumentation used in this study

The Geonics EM 38 electromagnetometer was used in this investigation. The EM 38 consists of a dipole transmitter, dipole receiver and a power source. The EM 38 is a compact and portable unit weighing approximately 6.5 lb. with a length of approximately 3.3 ft. (Geonics 2004). The EM 38 magnetometer is shown in Figure 32.

iv. Sulfate determination

Since soluble salts are a major contributor to the electrical conductivity of soils, the sulfate content of soils can be correlated to the electrical conductivity (Bredenkamp and Lytton 1995). Soils exhibiting electrical conductivity of approximately 300 mS/m or greater often contain 3,000-5,000 ppm of soluble sulfates. Sulfate levels in this range often correspond to sulfate induced distress (Natarajan 2004).

Chapter III: Field Study of US 331

a. Introduction

A field study was conducted to identify the cause of distress along northbound US 331 between mile markers 88.480 and 91.070 south of Montgomery, AL. Several causes of the distress were investigated: swelling clay, drainage, construction practice, and formation of ettringite, a swelling mineral. Ettringite is the most likely cause, and is discussed below.

b. Possible causes of distress

Throughout the investigation, seven possible causes of distress were identified. Each possible cause is identified below along with the reasons that the possible cause was discarded or researched further.

i. Sulfate induced swell

Sulfate induced swell is caused by the interaction of lime and sulfates. This possible cause of distress was researched further because of the presence of sulfates and lime. The relationship found between electrical conductivity and distress makes this the likely cause of distress.

ii. Swelling clays

Swelling clays experience volume change with respect to moisture content. Swelling clay was discounted as a possible cause of distress because the roadway was limed, mitigating this type of swell. Also, swelling clays typically produce much longer wavelength bumps than what was observed on U.S. 331.

iii. Logging truck traffic

Empty logging trucks utilize the southbound roadway and full logging trucks utilize the distressed northbound roadway. Logging truck traffic was discounted as a possible cause of

distress because the distress was localized to short sections of roadway instead of experiencing distress along the entire roadway. Also, the asphalt was not cracked or rutted, which would be expected with traffic induced distress, which typically occurs rapidly, compared to the much slower occurring distress due to swelling soils. The longer time allows the asphalt concrete to deform (creep), instead of crack.

iv. Poor drainage

Poor drainage augments swelling problems associated with both clays and sulfates. Poor drainage was observed in the medians and side ditches as standing water was present. Poor drainage is considered a contributor to the problems associated with sulfate swell.

v. Poor compaction

Poor compaction causes distress because loose soil settles as it becomes denser under roadway loads. Poor compaction was admitted by ALDOT at the culverts and is believed to have caused distress at those locations. However, compaction throughout the rest of the project could not be verified because of construction records that reported inappropriate values for compaction. The short length of distress suggests poor compaction was not the cause of the distress. Poor compaction would have typically extend over longer distances.

vi. Lime Reactivity Issues

Poor lime reactivity would not mitigate the swelling clay problem. No method was found to determine the reactivity of the lime that was placed on the roadbed so no correlation could be made between reactivity and distress.

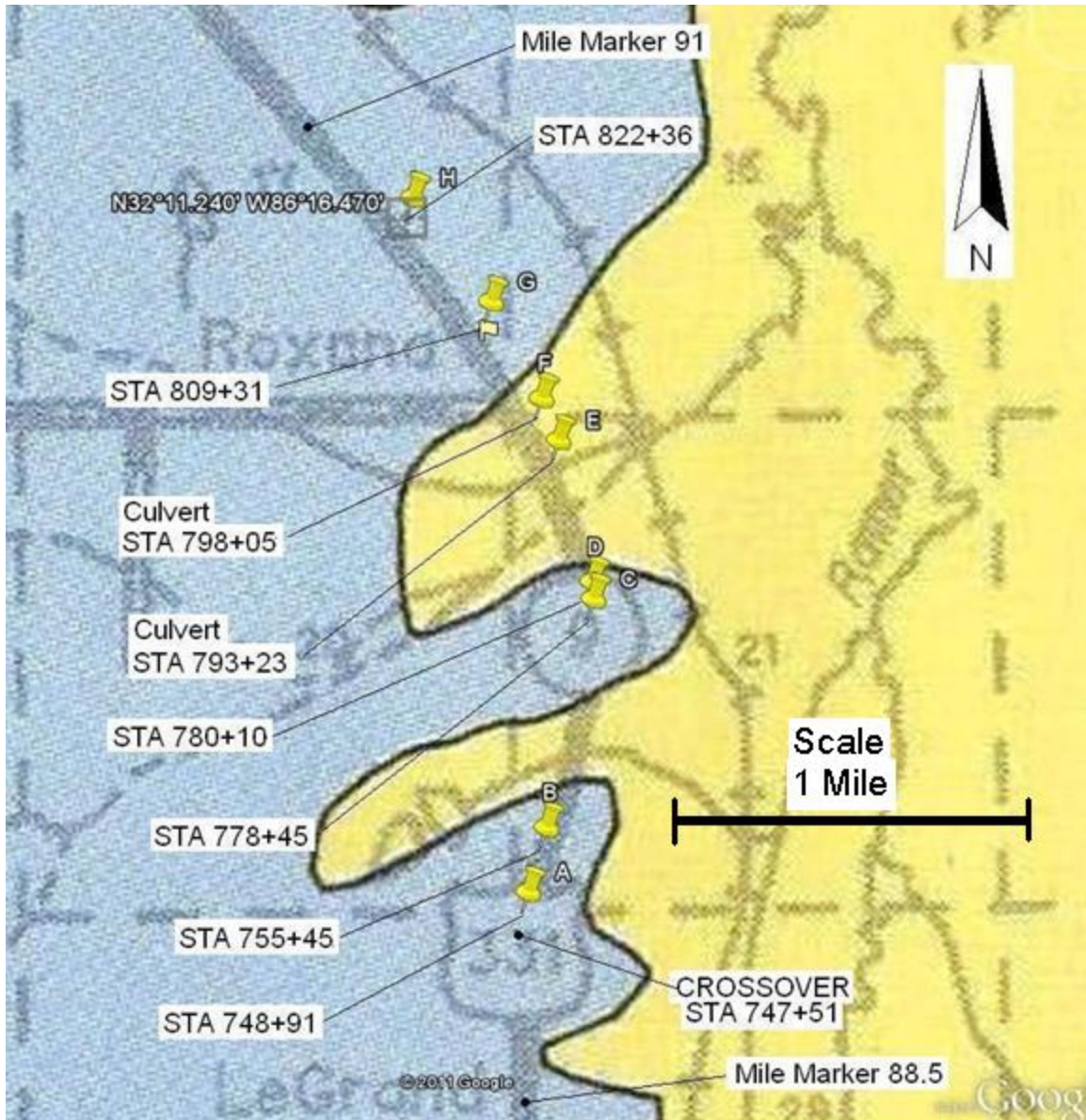
vii. Construction procedures

Construction procedures, particularly those performed at the beginning and end of a day's work, were considered areas where distress may occur. This possible cause of distress was

discounted because the distressed locations did not always correspond to daily construction interfaces.

c. Locations of distressed areas

The distressed areas are on northbound US 331 between mile markers 88.480 and 91.070 shown as points A-H in Figure 46. They were identified by visual inspection, driving the roadway, and International Roughness Index (IRI) testing.





EXPLANATION	
	Low stream alluvial deposits of sand, silt, and sandy clay with low to no gravel content
	Chalk and calcareous clay (Selma Group)

Figure 46: Areas of Distress along U.S. 331 (USDA 1926) and (Google, U.S. Geological Survey 2012).

d. Description of Problem

Distress along this section of U.S. 331 occurs as intermittent bumpy sections that are approximately 150 ft in length and occur about every 0.5 miles. The bumps that do not occur at the culverts occur in a wave-like fashion with the wavelength being approximately 20 – 30 ft. This wavelength is long enough that it does not cause corrugation-type distress that causes vehicles to shake, but causes a gentler, yet undesirable vertical displacement of the vehicle. The distress that is present at the buried culvert locations occurs as violent, shorter wavelength dips in the roadway that causes rapid vertical displacement of a vehicle. The distress is greatest at the beginning and end of each culvert but is present for the entire length of the culvert. No distress to the asphalt concrete is evident anywhere along the roadway except for some patching at the culvert locations. According to ALDOT, the non-culvert location distress occurred very rapidly as the roadway has degraded in just a few years.

e. Data from ALDOT

i. Introduction

ALDOT provided a variety of resources including construction records, soil testing data, and plan and profile drawings.

ii. Background

While most of the ALDOT data were helpful for the investigation, some of the construction records were incomplete which made it unrealistic to make inferences based solely on the records. However, these records provided important chronological information.

iii. Resources

1. Construction Records

Lime treatment records were obtained showing how much lime was placed, when it was placed and when it was mixed with the soil.

Paving records were obtained to determine the duration that the lime treated roadbed was exposed to weather before paving.

Nuclear gauge records for unit weight of the soil were also obtained from ALDOT to ensure proper compaction had occurred.

Weather records were obtained from ALDOT including temperature and precipitation.

2. Soil Testing Data

Various soil testing data including particle size distribution and Atterberg limits were obtained from ALDOT. This information provided a general feel for the type of soils present in the area as well as providing information on the potential for swell.

3. Plan and Profile drawings

ALDOT provided complete plan and profile drawings for the section of U.S. 331 between mile marker 88.480 and 91.070. These drawings showed the slopes of drainage ditches, elevations, and identified drainage structures and streams.

f. Experimental Approach

i. Overview

The experimental approach included soil sampling, soil testing, and roadway testing.

ii. Soil Sampling

1. Introduction

To investigate the causes of distress along U.S. 331, it was necessary to employ a sampling program to obtain soil for testing. The sampling program was successful in obtaining samples from various distressed and nondistressed stations. International Roughness Index (IRI) testing was performed to determine the level of distress along U.S. 331 between mile marker 88 and 92, to identify locations for sampling.

2. Sampling Strategy

Sampling locations were chosen based on visual observation, IRI testing, and identifying roughness by driving the roadway. Three sets of samples were taken:

1. Surface samples
2. Two foot borings
3. Twelve foot borings.

Both the surface samples and the two foot deep samples were taken at six locations identified as distressed sections by driving the roadway, visual inspection, and IRI testing. The borings were taken at four locations with two taken at particularly distressed areas as identified by IRI testing. The other two were taken at particularly nondistressed areas as identified by IRI testing.

3. Surface Samples

Disturbed surface samples were taken using a shovel at an approximate depth of 1 ft. Six samples were taken at each of the eight cross sections that were the most distressed between mile markers 88.5 and 91. Figure 47 shows the six locations where 1 ft samples were taken at each of

the eight cross sections: Sta 748+91, Sta 755+45, Sta 778+45, Sta 780+10, Sta 793+23, Sta 798+05, Sta 809+31, and Sta 822+36.

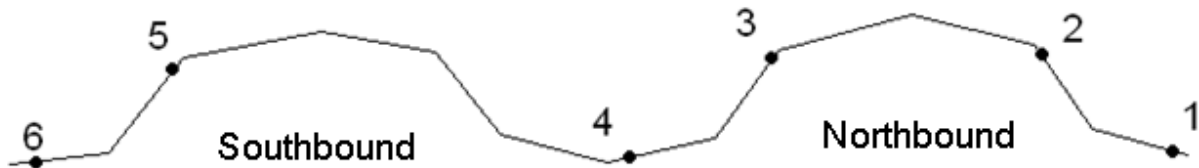


Figure 47: Key for soil samples taken at each of the six U.S. 331 cross-sectional locations shown above (1-6) at each of the eight distressed locations.

a. Map of Sample Locations

Figure 46 shows a map of the eight distressed locations (A-H) with corresponding stations numbers where sampling occurred. Additional maps of the area are presented in Appendix A.

b. Sample Identification key

Each sample was assigned an alphanumeric label. The letter refers to the station at which the sample was taken and the number refers to the location in the cross section that the sample was taken from. A sample taken from station C at location 3 in the cross section is labeled C-3.

4. Subsurface Sampling

a. Two foot deep samples

i. Sampling procedure and locations

Samples were taken at an approximate depth of 2 ft using a hand auger. Samples were taken at similar locations to the one foot samples except stations E and F were excluded from

this stage of sampling because the distress at these locations is thought to be caused by poor compaction around the culverts, confirmed by ALDOT interviews.

ii. Sample Identification Key

The labeling scheme for these samples includes a letter, number, and depth. A sample taken from a depth of 2 ft from station C at location 3 within the cross section is labeled C-3-2' with the 2' referring to the sample depth.

b. Borings

i. Location of borings

Eight borings were taken at four stations at two transverse locations per station. The objective of the boring samples was to obtain samples from both distressed and nondistressed locations so that correlations could be made between the findings and distress. Table 3 shows the location and depth of the eight borings.

Table 3: Boring Locations

Longitudinal Location	Boring Number	Transverse Location	Depth
Sta 748+66	1-A	Centerline of right lane	12' or Bedrock
Distressed	1-B	Centerline of right shoulder	12' or Bedrock
Sta 742+86	2-A	Centerline of right lane	12' or Bedrock
Non-distressed	2-B	Centerline of right shoulder	12' or Bedrock
Sta 807+52	3-A	Centerline of right lane	12' or Bedrock
Distressed	3-B	Centerline of right shoulder	12' or Bedrock
Sta 806+61	4-A	Centerline of right lane	12' or Bedrock
Non-distressed	4-B	Centerline of right shoulder	12' or Bedrock

ii. Sampling Method used

The borings were taken using the continuous drilling technique that allows a continuous sample to be taken in clear plastic tubes. The clear plastic tubes have an inside diameter of 3.25 in. and an outside diameter of 3.5 in. A sample taken using this technique is shown in Figure 48. The samples were taken with the CME drill rig shown in Figure 49.



Figure 48: A continuous drilling sample in the plastic tube.



Figure 49: Drill rig used for sampling.

The samples were taken in clear plastic tubes that are inserted into a hollow stem auger. As the auger is drilled into the earth, it rotates around the plastic tube, forcing the sample into the tube. It is common for the plastic tube to rotate along with the auger causing sample disturbance. Every five feet that the auger penetrates, two sample tubes are removed from the auger and two new ones are inserted. Sample tubes are then capped, taped, and labeled. Figure 50 shows the plastic tubes being inserted into the hollow stem auger.



Figure 50: Inserting tubes into hollow stem auger.

iii. Soil Testing

1. Introduction

Testing was performed to determine properties of the soil. Standard Proctor tests, loss on ignition tests, clay mineral determination, X-ray diffraction, swell tests, Atterberg limits,

inductively coupled argon plasma tests, and electrical conductivity tests were performed. International roughness index testing was performed to relate soil properties to distress.

2. Lab Study

a. Visual Inspection

Upon visual inspection of boring samples, large gypsum crystals were identified in the soil. The crystals were identified as gypsum by Dr. James Saunders of the Auburn University Geology department (Saunders 2012). The gypsum crystals are shown in Figure 51. Visual inspection also showed the presence of organics.

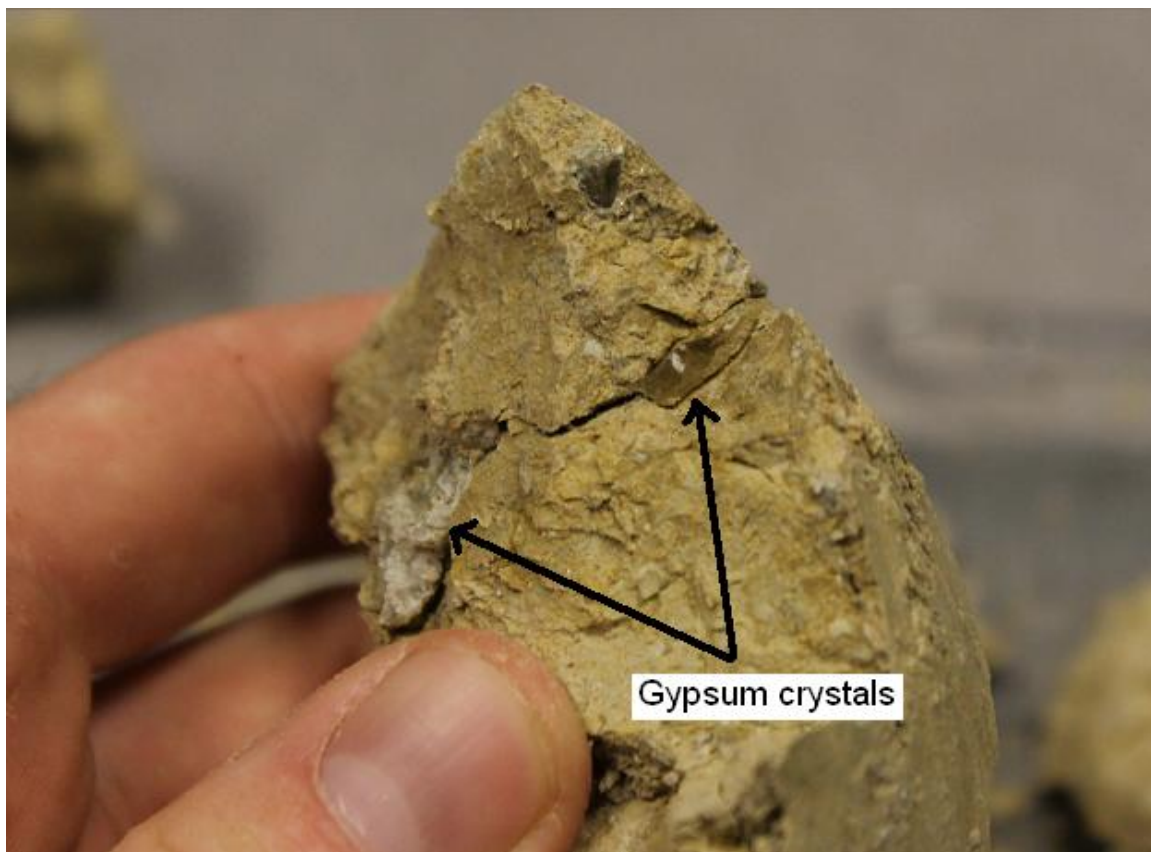


Figure 51: Gypsum crystals found in Boring 4-A.

b. Standard Proctor Tests (ASTM 2005)

Seven Standard Proctor tests were run to determine the optimum moisture content that is necessary to perform a swell test. The optimum moisture contents ranged from 16% to 25%.

Proctor curves for the seven samples are shown in Appendix C. The Standard Proctor curve for sample A-2-2 is shown in Figure 52.

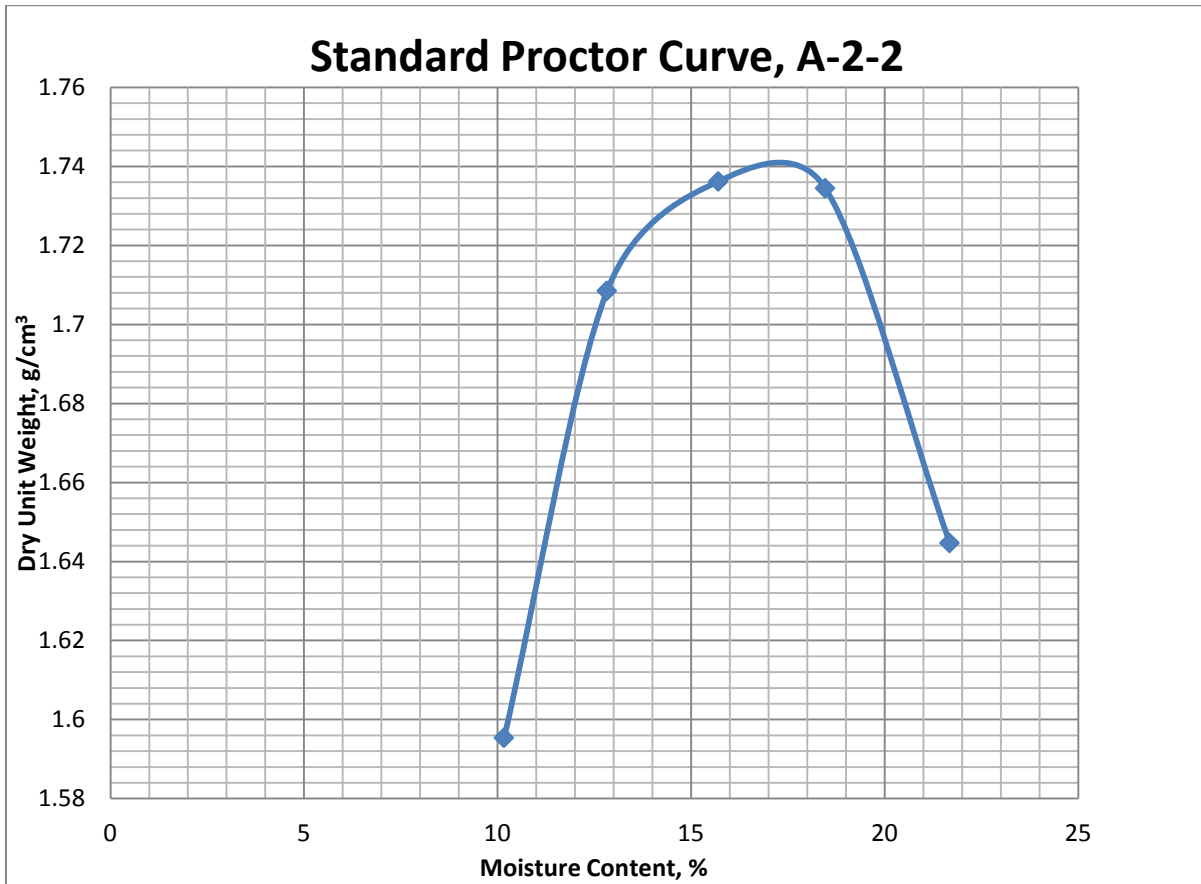


Figure 52: Standard Proctor Curve for sample A-2-2.

c. Loss on Ignition (AASHTO 1986)

Four loss on ignition tests were performed on boring samples to determine the percent by weight of organic matter. The percent by weight of organic matter in the four tests ranged from 4.2 to 6.2 and are shown in Table 4.

Table 4: Percent loss of boring samples

Longitudinal Location	Transverse Location	Percent Loss (by weight)
Sta 748+66	Centerline of right shoulder	6.20
Sta 742+86	Centerline of right shoulder	4.23
Sta 807+52	Centerline of right lane of NBR	4.52
Sta 806+61	Centerline of right shoulder	5.21

d. Clay Mineral Type

The clay mineral type can be estimated by relating the liquid limit and the plastic limit using Figure 53.

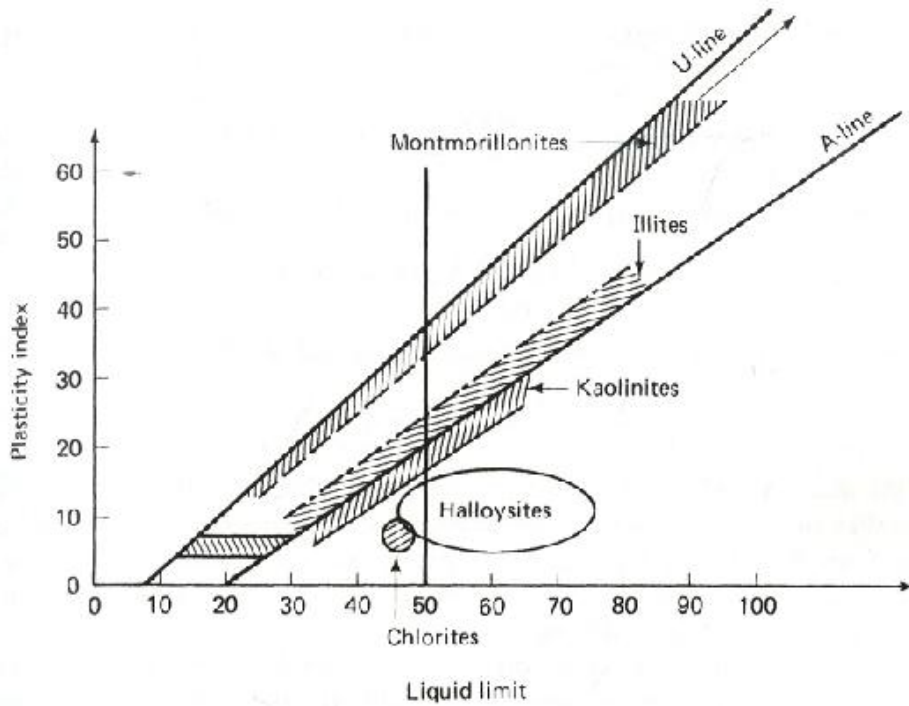


Figure 53: Relationship between Atterberg limits and mineral type (Casagrande 1948, Mitchell 1976).

The clay mineral types were estimated for the one foot and two foot deep samples. The estimated mineral types are shown in Tables 5 and 6. USCS soil classification is presented in Appendix B.

Table 5: Clay Mineral types for one foot deep samples

Key: I-illite, M-montmorillonite, K-kaolinite.

	6	5	4	3	2	1	
H	K	K	K	I	K	K	North
G	K	I	K	I	K	K	
F	I	K	K	M	M	K	
E	K	M	M	I	I	M	
D	I	I	I	M	K	I	
C	M	I	I	I	I	K	
B	M	I	K	I	I	M	
A	I	I	I	M	I	I	South
	West			East			

Table 6: Clay Mineral types for two foot deep samples, n/a – not available.

Key: I-illite, M-montmorillonite, K-kaolinite.

	6	5	4	3	2	1	
H	n/a	n/a	K	K	K	K	North
G	I	M	M	K	I	I	
F	n/a	n/a	n/a	I	I	n/a	
E	n/a	n/a	n/a	I	M	n/a	
D	I	I	M	I	I	K	
C	I	M	I	I	I	M	
B	I	I	I	I	I	K	
A	M	I	I	M	M	I	South
	West			East			

e. X-Ray Diffraction

Samples from two distressed areas under the pavement, borings 1-A and 1-B, were analyzed using X-Ray diffraction. Both samples contained ettringite and gypsum. Figure 54 shows the presence of ettringite and gypsum for sample 1-A.

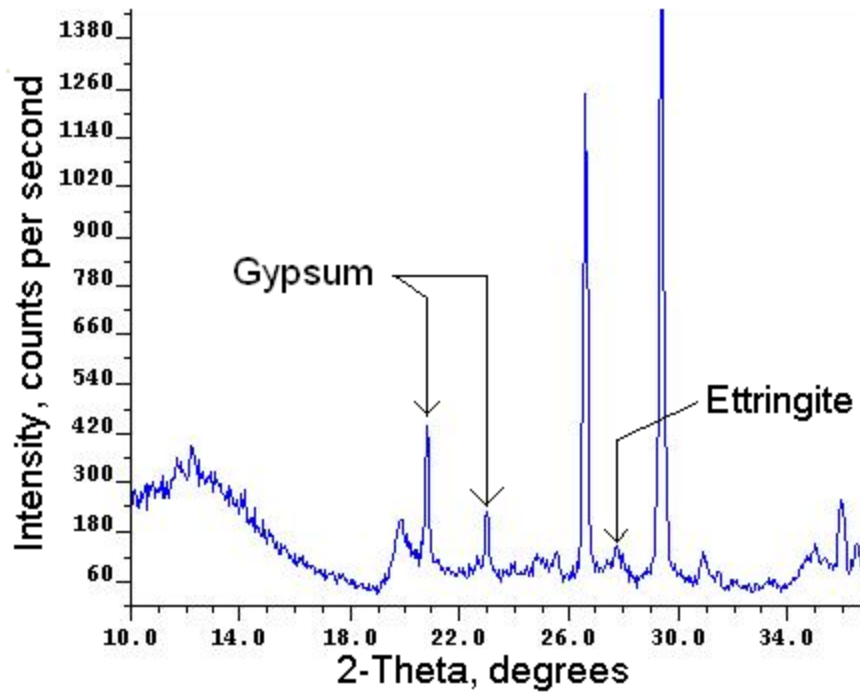


Figure 54: X-Ray diffraction results from sample 1-A, showing presence of ettringite and gypsum.

f. Swell Tests (ASTM 2008)

Six swell tests were performed. The volumetric swell ranged from 2.4% to 10.2%. Swell test results for the six samples are shown in Appendix D. The swell test for sample B-6 is shown in Figure 55.

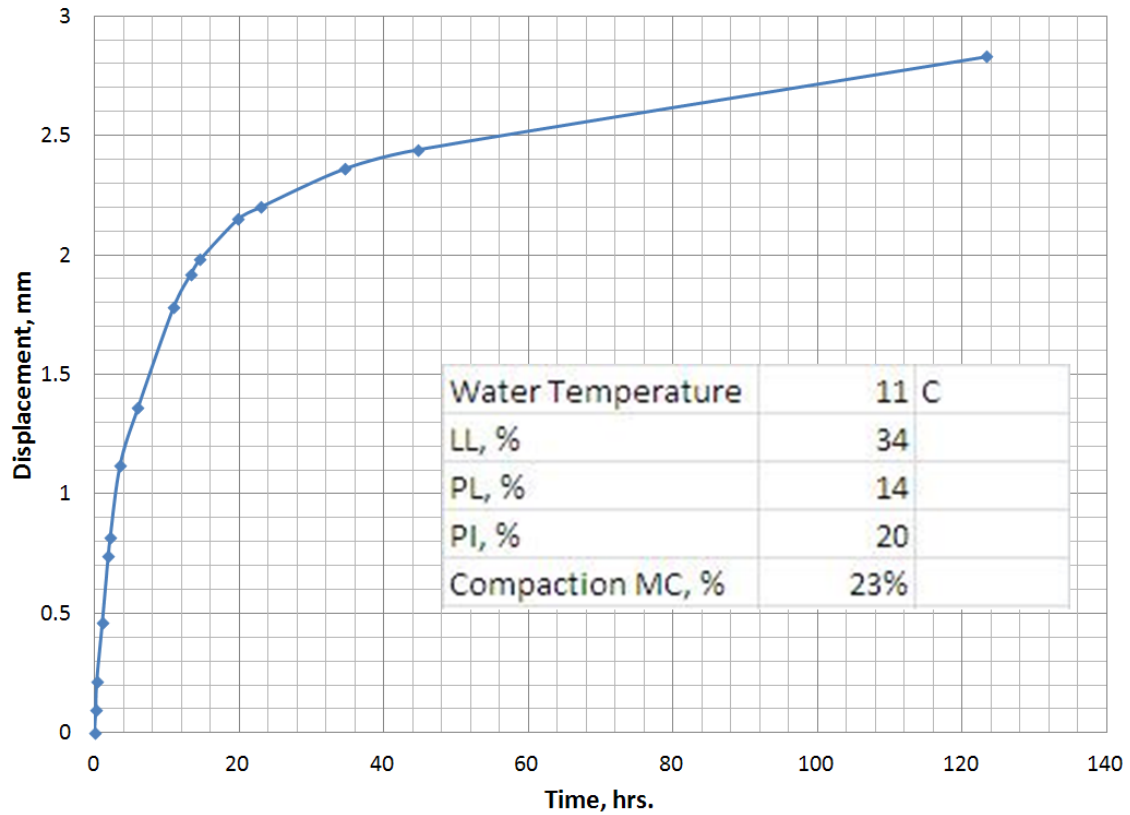


Figure 55: Swell test, Sample B-6. Peak swell =2.4%

g. Atterberg Limits

Atterberg limits were performed on one foot and two foot deep samples to determine the swell potential. The Atterberg limits for one foot and two foot deep samples are shown in Tables 7 and 8.

Table 7: Atterberg limits for one foot deep samples.

	6	5	4	3	2	1	
Key	PI, LL, PL	PI, LL, PL	PI, LL, PL	PI, LL, PL	PI, LL, PL	PI, LL, PL	
H	5, 32, 27	6, 31, 25	6, 30, 24	11, 34, 23	10, 41, 31	18, 49, 31	North
G	2, 31, 29	17, 45, 28	15, 51, 36	27, 50, 23	1, 35, 34	15, 50, 35	
F	24, 46, 22	4, 31, 27	11, 40, 29	55, 84, 28	33, 54, 21	5, 29, 24	
E	27, 63, 36	18, 36, 18	25, 43, 18	32, 55, 23	26, 49, 23	46, 65, 19	
D	19, 43, 24	10, 33, 23	15, 35, 20	47, 68, 21	13, 41, 28	8, 27, 19	
C	95, 127, 32	28, 51, 23	32, 60, 28	23, 44, 21	15, 38, 23	10, 27, 16	
B	20, 33, 14	12, 26, 15	14, 47, 34	30, 54, 24	34, 57, 23	21, 36, 15	
A	17, 40, 23	12, 36, 24	25, 45, 20	18, 35, 17	32, 60, 28	29, 55, 25	South
	West					East	

Table 8: Atterberg limits for two foot deep samples, n/a – not available.

	6	5	4	3	2	1	
Key	PI, LL, PL	PI, LL, PL	PI, LL, PL	PI, LL, PL	PI, LL, PL	PI, LL, PL	
H	n/a	n/a	12, 38, 27	22, 48, 26	27, 55, 34	28, 50, 30	North
G	41, 68, 27	30, 46, 16	30, 50, 20	16, 44, 28	33, 61, 28	33, 61, 28	
F	n/a	n/a	n/a	46, 75, 29	27, 55, 28	n/a	
E	n/a	n/a	n/a	53, 82, 29	48, 76, 28	n/a	
D	60, 97, 37	60, 97, 37	31, 52, 21	37, 65, 28	42, 76, 34	1, 26, 25	
C	31, 61, 29	38, 58, 20	10, 29, 19	26, 54, 28	37, 74, 37	50, 74, 24	
B	15, 38, 23	12, 31, 19	13, 36, 23	46, 77, 31	30, 55, 25	12, 65, 53	
A	22, 39, 17	16, 36, 20	23, 44, 21	45, 66, 21	49, 74, 25	44, 71, 27	South
	West					East	

h. Inductively Coupled Argon Plasma (ICAP)

Inductively coupled argon plasma (ICAP) analysis was performed on one foot and two foot deep samples to determine the calcium content of the soils. Other ICAP tests were performed on boring samples to determine the sulfate content of the soils. The calcium content was determined to ensure that lime was placed. The sulfate content was determined to establish the susceptibility of the soil to sulfate swell.

Calcium content values for the one foot and two foot samples ranged from 3458 parts per million (ppm) to 10460 ppm, with most samples having about 10000 ppm.

Calcium content values for the boring samples ranged from 974 ppm to 11150 ppm, with most samples having about 10000 ppm. Sulfate concentrations were random and ranged from 111 ppm to 13610 ppm.

3. Field Study

a. International Roughness Index (IRI) Testing

Three IRI tests were performed using the National Center for Asphalt Technology's automatic road analyzer (ARAN) van. The ARAN van was used to see how the pavement roughness varied with changing moisture conditions and to identify rough areas as a function of distance. Results of the IRI testing for the right lane of northbound U.S. 331 are shown in Figure 56.

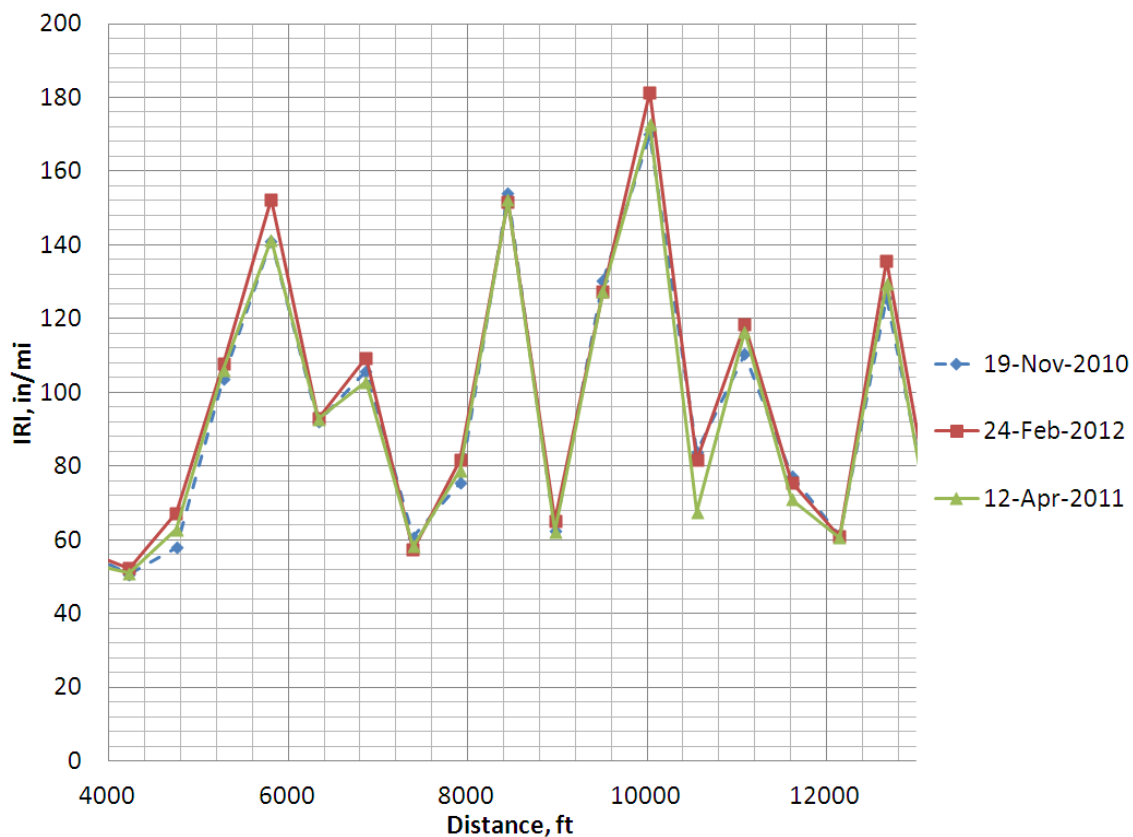


Figure 56: IRI data from northbound U.S. 331, right lane.

b. Electromagnetic Survey

An electromagnetic survey was conducted to measure the electrical conductivity of the soil as a function of distance, using a Geonics EM 38 conductivity meter (Geonics 2004). Electrical conductivity indicates presence of sulfates, which react with lime, swell, and cause pavement distress. The electrical conductivity readings, taken along the shoulder every 20 ft. from mile marker 88.758 to mile marker 90.463 are in Figure 57. The threshold value of 100 mS/m is shown as a dashed line. The survey identified many soils with electrical conductivity greater than the threshold value of 100 mS/m, indicating susceptibility to sulfate swell. These are indicated by the spikes in Figure 57.

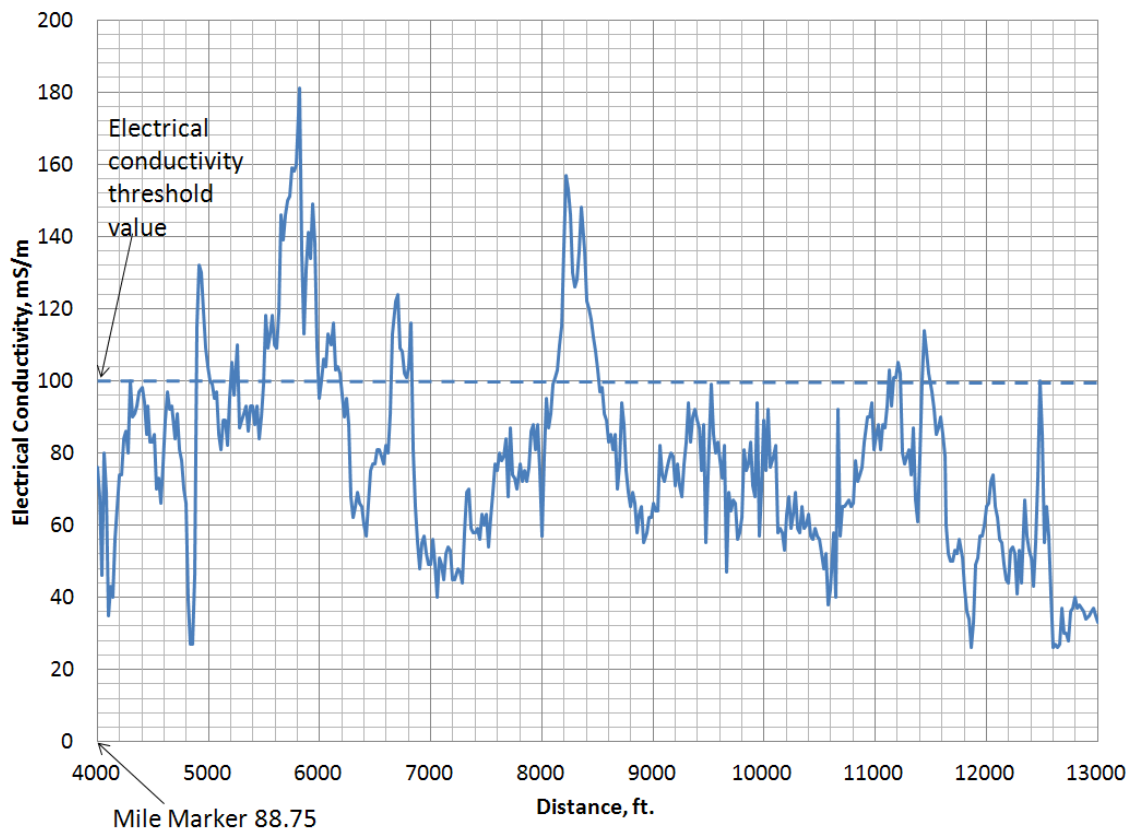


Figure 57: Electrical Conductivity vs. Linear Distance

c. Drainage Observations

Standing water is often present in many ditches along the roadway. This standing water indicates inadequate drainage which causes soil moisture to increase.

d. Visual Inspection

A visual inspection was conducted to determine locations of distressed areas. The distressed areas determined by visual inspection are shown in Table 9 and were confirmed by IRI testing.

Table 9: Distressed locations determined by visual inspection

Location Designation	Longitudinal Location, ft.
A	Sta 748+91
B	Sta 755+45
C	Sta 778+45
D	Sta 780+10
E	Sta 793+23
F	Sta 798+05
G	Sta 809+31
H	Sta 822+36

iv. Analysis of Soil Testing Data

1. Lab Study

a. Visual Inspection

The gypsum crystals that were found during the visual inspection of the soil samples provide a source of sulfate which could lead to swelling due to ettringite formation. Visual inspection also revealed showed organic matter.

b. Loss on Ignition

Results of the loss on ignition testing indicate that large amounts of organic matter, up to 6.2% by weight, is present in the soil. When the organic material decomposes, settlement of the roadway occurs. Also, decomposition of organic matter causes an increase in soil sulfate concentration which could lead to swelling caused by ettringite formation (Schulte and Kelling 1992).

c. X-Ray Diffraction

X-Ray diffraction testing shows the presence of both ettringite and gypsum in the soil. The presence of gypsum indicates a source of sulfates for ettringite formation.

d. Swell Tests

Swell testing indicates that the soils experience volume change, up to 10.2%, with varying moisture contents.

e. Atterberg Limits

The plasticity indices of many of the soils that were tested were above 25, indicating the potential for swell. Swell potential was confirmed through swell testing.

2. Field Study

a. Inductively Coupled Argon Plasma (ICAP)

ICAP testing shows that the high levels of calcium and sulfate necessary for ettringite formation are present in the soils.

b. International Roughness Index (IRI) Testing

IRI testing indicates distressed locations and allows the level of roughness to be quantified.

c. Electromagnetic Survey

Elevated electrical conductivity values indicate high sulfate levels in soil. Electrical conductivity values higher than 100 mS/m are susceptible to distress caused by ettringite formation due to interactions between sulfate and lime. Several distressed locations along U.S. 331 displayed electrical conductivity values higher than 100 mS/m.

d. IRI and Electrical Conductivity vs. Distance

Figure 58 shows IRI vs. distance, and electrical conductivity vs. distance. There is a good visual correlation between IRI vs. distance and electrical conductivity vs. distance, suggesting sulfates are related to the cause of pavement distress. A Pearson product moment correlation of 0.72 shows a good correlation between IRI and electrical conductivity values. Appendix E explains this correlation in more detail.

ditch slopes did not occur at the locations of distress so no correlation was made between distress and areas that have flat ditch slopes. However, it should be noted that flat ditch slopes do not provide adequate drainage and the excess water may augment a swelling problem.

2. Construction Records

The construction records gave the liming schedule. The delay between the 2% and 3% lime treatments was determined for each roadway section and the delay between placement of the lime and mixing the lime was also determined. The interface locations between one day's work and the next day's work were also determined.

The records showed that the delay between the 2% and 3% treatments varied between 4 and 197 days. Approximately half of the roadway had a delay less than ten days while the other half had a delay greater than 181 days. However, the construction records provided by ALDOT were incomplete and, according to the records, multiple locations never received a 2% lime treatment. The areas that lacked lime treatments as indicated by the construction records did not necessarily occur at the areas of distress so no correlation was found between distress and delay between treatments or distress and locations that did not have a record of 2% lime treatment.

According to the records, the delay between placing lime and mixing lime varied between 0 and 27 days. In most locations, lime was mixed within 15 days of placement. The mixing records were also incomplete. The distressed locations did not correspond to a particular mixing delay so no correlation was found between distress and mixing delay.

3. Soil Testing Data

Atterberg limits and compacted dry unit weight of roadway soils were provided by ALDOT.

The Atterberg limits provided by ALDOT were comparable to the Atterberg limits determined in this study. No correlation was found between Atterberg limits and distress.

The compacted unit weight records often contained the unattainable value of 150 pcf. If the nuclear gauge reads values that are too high, compaction cannot be verified. No correlation was found between the unit weight values in the construction records and distress.

4. Borings

Nearly all of the borings provided by ALDOT showed at least a 10 ft. thick clay layer directly underlying the roadway. The vast majority of this clay is classified as highly plastic. Highly plastic clays have a high swell potential which may cause heave. The volume change experienced in clays due to ettringite formation is typically higher than the volume change experienced in sandy soils (Little 2009). Due to this, the thick clay layer may experience a high volume change due to ettringite formation.

g. Evaluation of Causes of Pavement Distress in US 331

i. Drainage Issues

Inadequate roadway drainage allows excess water to enter underlying soil strata. Excess water allows volume change associated with the swelling clays present in the area to occur. Additional water also aids in ettringite formation which causes swelling. Proper drainage can reduce volume change associated with swelling clays and ettringite formation.

ii. Swelling Soils

Swelling soils experience volume change with changes in moisture content. Swelling soils are often characterized by high plasticity indices and can be tested for swell with swell testing.

1. Surface soils

The plasticity indices of the surface soils were determined. A majority of the soils were found to be highly plastic clays. Swell tests were run on five surface soil samples. The amount of free swell ranged from 2.4% to 6.7%.

2. Deeper soils

The two foot deep soils exhibited similar plasticity indices as the surface soils and were found to be highly plastic clays. A swell test that was run on a 2' deep sample showed a 10.2% volume change.

iii. Ettringite Formation

Ettringite is formed when excess calcium ions react with sulfate ions. The formation of ettringite causes a positive volume change associated with pavement distress.

Chapter IV: Conclusion

This section of U.S. 331 was constructed by adding lime to high sulfate bearing soils. The relationship between distress, electrical conductivity, and the presence of ettringite at distressed sections indicates that the cause of distress along U.S. 331 may be swelling due to ettringite formation induced by adding lime to soil that contains elevated levels of sulfates, and paving before the ettringite reaction was complete.

Chapter V: Recommendations

a. Introduction

During the investigation, several recommendations were devised that may improve the quality of lime treated roadways. Not all of these recommendations are based on our testing data, but are based on observations and research of literature.

b. Site preparation considerations

i. Check for sulfate rich soils

1. Recommendation

Run an electromagnetic survey to determine soil conductivity. If the conductivity of the soil is above the threshold level of approximately 100 mS/m, detrimental sulfate levels may be present. Sample every 50 ft. in areas exceeding 100 mS/m and perform ICAP to determine actual sulfate level. If the sulfate levels exceed 100 ppm, techniques to mitigate sulfate swell should be employed.

2. Importance

Identification of sulfate rich soils is necessary to determine whether special construction procedures to mitigate the effects of ettringite formation due to lime addition should be taken. If untreated, limed sulfate rich soils cause roadway distress.

ii. Treat sulfate rich soils

1. Recommendation

To mitigate formation of ettringite, treat soil with a low calcium stabilizer such as fly ash. If lime is the desired stabilizer, a split lime treatment with a mellowing period of approximately two weeks between the treatments should be used. During this mellowing period, three to five percent additional moisture should be added to increase the sulfate-lime reaction.

2. Importance

Low calcium stabilizers limit the amount of ettringite by reducing the amount of calcium ions available to react with sulfate and form ettringite.

Since the sulfate-lime reaction produces one time swelling, allowing ettringite to form before the pavement is placed will mitigate detrimental effects due to ettringite formation.

iii. Remove organic matter from roadbed.

1. Recommendation

Remove organic matter from the pavement structure.

2. Importance

Organic matter decomposes and leaves voids in the soil mass which lead to settlement of the roadway. Moreover, decomposition of organic matter increases the sulfate content of the soil which increases the probability of sulfate swell due to ettringite formation.

Chapter VI: Suggestions for Further Research

- a. Methods of controlling the speed of ettringite formation should be researched.
- b. The effectiveness of low-calcium methods for stabilizing sulfate laden high plasticity soils should be researched.
- c. The use of electromagnetometers to identify areas that are susceptible to sulfate swell should be further investigated.
- d. The susceptibility of different types of soil to ettringite formation should be researched.
- e. Laboratory methods for synthesizing ettringite should be further investigated.

Chapter VII: References

- AASHTO (2008). "Standard Recommended Practice for Stabilization of Sulfate-Bearing Subgrade Soils." American Association of State Highway and Transportation Officials, Washington, DC.
- AASHTO (1986). "T 267 Standard Method of Test for Determination of Organic Content in Soils by Loss on Ignition." Standard Specifications for Transportation Materials and Methods of Sampling and Testing. 28th ed. Washington, DC.
- ASTM. (2007). "D698-07e1 Standard Test Methods for Laboratory Compaction Characteristics of Soil Using Standard Effort (12 400 ft-lbf/ft³ (600 kN-m/m³))." Annual Book of ASTM Standards, ASTM International, West Conshohocken, Pennsylvania.
- ASTM. (2008). "D4546-08 Standard Test Methods for One-Dimensional Swell or Collapse of Cohesive Soils." Annual Book of ASTM Standards, ASTM International, West Conshohocken, Pennsylvania.
- Bao, Huiming (2004). "Different Sulfate Sources and Their Post-Depositional Migration in Atacama Soils." *Earth and Planetary Science Letters* Vol. 224. Elsevier.
- Bell, F.G. (1996). *Lime Stabilization of Clay Minerals and Soils*. Engineering Geology, Vol. 42, Pages 223-237.
- Bredenkamp, S. and Lytton, R. (1995). "Reduction of Sulfate Swell in Expansive Clay Subgrades in the Dallas District." Texas Transportation Institute, Texas A&M University, College Station, TX.
- Casagrande, A. (1948). Classification and identification of soils: Transactions of the American Society of Civil Engineers, v. 113, p. 901-930.
- Federal Highway Administration (FHWA). (2003). "Distress Identification Manual for the Long Term Pavement Performance Program." McLean, VA
- Geological Survey of Alabama (1988). Geologic Map of Alabama, Southeast Sheet. Williams and Heintz Map Corporation. Capitol Heights, MD.
- Geonics (2004). "Geophysical Instrumentation for Exploration and the Environment." Geonics Limited, 1745 Meyerside Drive, Unit 8, Mississauga, Ontario, Canada.
- Google, U.S. Geological Survey (2012). Google Earth. Image Date: Jan 31, 2008.
- Halifax Regional Municipality (2012). "HRM's Asphalt Distortion Guide." Halifax Regional Municipality, Nova Scotia, Canada.

- Hankins, K. (1985). *The Slometer*, Texas State Department of Highways and Public Transportation, Austin, TX.
- Harris, P. (2004). “Hydrated Lime Stabilization of Sulfate-Bearing Soils in Texas.” Texas Transportation Institute, Texas A&M University, College Station, TX.
- Hoffman, Celeste and Muench, Steve (2011). “Pavement Interactive Core.” *General Guidance/Pavement Distress*, <http://www.pavementinteractive.org/index.php?title=General_Guidance/Pavement_Distress> (Oct. 1, 2010).
- Huang, Y. (2004). *Pavement Analysis and Design*, 2nd Ed., Pearson Prentice Hall, Upper Saddle River, NJ.
- Koerner, R.M. (2005). *Designing With Geosynthetics*. 5th ed. Pearson Prentice Hall, Upper Saddle River, NJ.
- Little, D. (2009). “Recommended Practice for Stabilization of Sulfate Rich Subgrade Soils.” Texas Transportation Institute, Texas A&M University, College Station, TX.
- Little, D.N., E.H. Males, J.R. Prusinski, B. Stewart (2000). Cementitious Stabilization. Transportation in the New Millennium: Perspectives from TRB Standing Committees. Committee A2J01, Committee on Cementitious Stabilization. TRB.National Research Council. Washington, D.C.
- Little, Dallas (1995). *Handbook for Stabilization of Pavement Subgrades and Base Courses with Lime*, National Lime Association.
- Lytton, Robert (1994). *Reduction of Sulfate Swell in Expansive Clay Subgrades in the Dallas District*, Texas Transportation Institute, The Texas A&M University System, College Station, TX.
- McCarthy, D. (2007). *Essentials of Soil Mechanics and Foundations, Basic Geotechnics*. 7th ed. Pearson Prentice Hall, Upper Saddle River, NJ.
- McNeill, J. D. (1980). *Electromagnetic Terrain Conductivity Measurement at Low Induction Numbers*, Technical Note TN-6, Geonics Limited, Mississauga, Ontario, pp 5.
- Mitchell, J.K. (1976) *Fundamentals of Soil Behavior*, John Wiley & Sons, Inc., New York, 422 pp.
- Nair, S., Hudson, W., and Lee, C. (1985). *Realistic Pavement Serviceability Equations Using The 690D Surface Dynamics Profilometer*, Center for Transportation Research, The University of Texas at Austin, Austin, TX.

- Natarajan, S. (2004). "An Integrated Approach to Predict Ettringite Formation in Sulfate Soils and Identifying Sulfate Damage Along SH 130." Texas A&M University, College Station, TX.
- National Lime Association (2004). "Lime-Treated Soil Construction manual/Lime Stabilization & Modification." National Lime Association, Arlington, VA.
- Parker, F., and Brown, R. (1993). *A study of rutting of Alabama asphalt pavements : final report / by Frazier Parker, E. Ray Brown.*, Alabama Department of Transportation, Montgomery.
- Portland Cement Association (2001). Suggested Specifications for Soil-Cement Base Course Construction.
- Puppala, A. (2005). "Experimental Studies on Ettringite-Induced Heaving in Soils." *Journal of Geotechnical and Geoenvironmental Engineering*, ASCE.
- Ranjan, Gopal (1991). *Basic and Applied Soil Mechanics*, 2nd Ed., New Age International, Daryaganj, New Delhi.
- Saunders, James (2012). Personal Communication. Saundja@auburn.edu. 210 Petrie Hall, Auburn University, AL 36849.
- Sayers, M., and Karamihas, S. (1998). *The Little Book of Profiling*, The Regent of the University of Michigan.
- Schulte, E. and Kelling, K (1992). "Understanding Plant Nutrients/Soil and Applied Sulfur." University of Wisconsin Extension, Madison, WI.
- Scintag, Inc. (1999). "Chapter 7: Basics of X-ray Diffraction" Cupertino, CA 95014.
- U.S. Geological Survey (1958). Montgomery South, AL, SE/4 Montgomery 15' Quadrangle. Washington, DC.
- United States Department of Agriculture (1926). Soil Survey of Montgomery County, Alabama. Washington, DC.
- Wersin, P., Curti, E., Appelo, C.A.J. (2004). "Modeling bentonite–water interactions at high solid/liquid ratios: swelling and diffuse double layer effects". *Appl Clay Sci*, 26, pp. 249–257
- Yoder, E.J., and Witczak, M. W. (1975). *Principles of Pavement Design*, 2nd Ed., John Wiley and Sons, New York.

**Appendix A: GEOLOGIC, SOILS, AND TOPOGRAPHIC MAPS OF
DISTRESSED AREAS**

A.1 Geologic map of U.S. 331

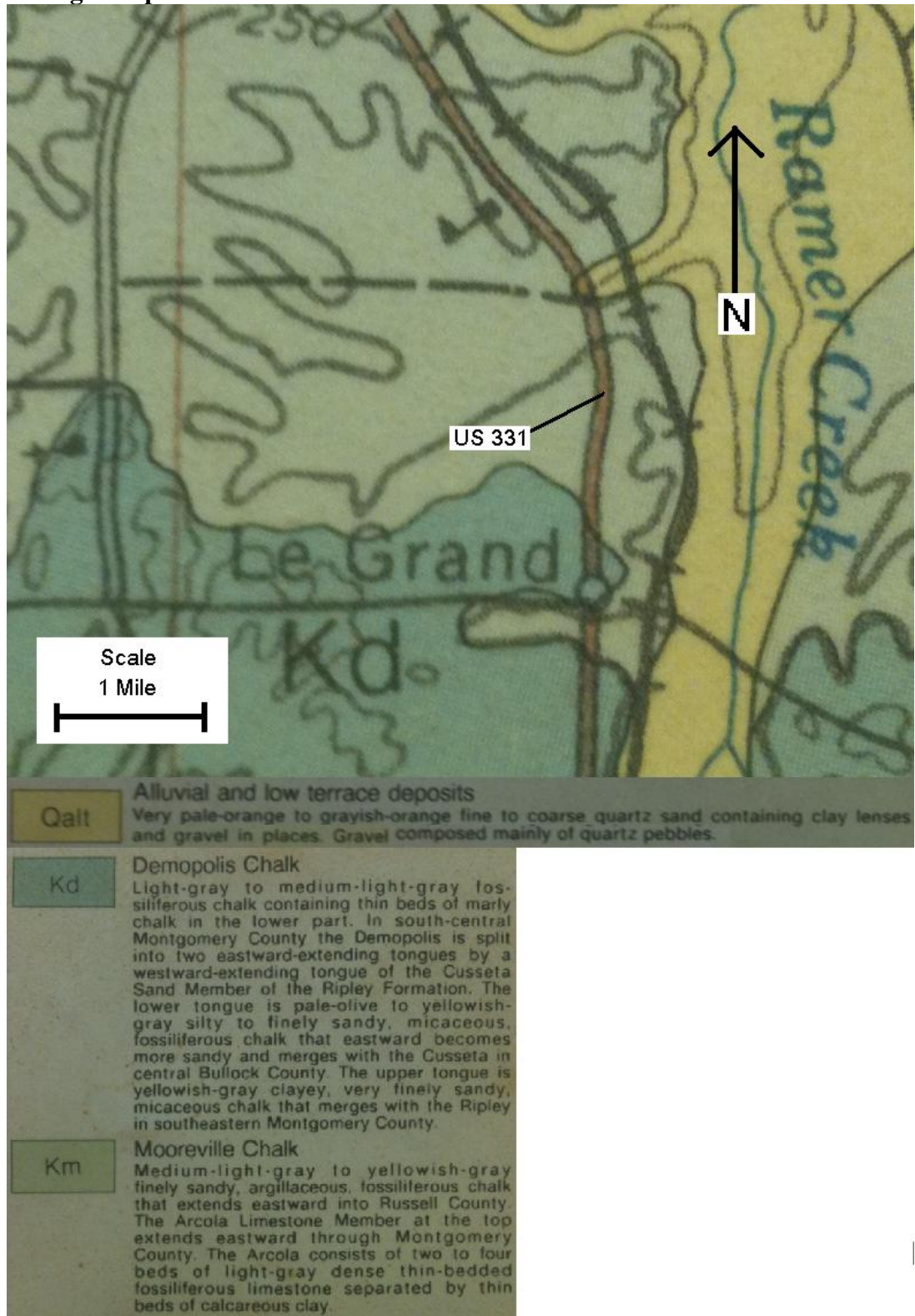


Figure 59: Geologic Map of U.S. 331 (Geological Survey of Alabama 1988)

A.2 Soils Map Of U.S. 331 Showing Distressed Areas A-H

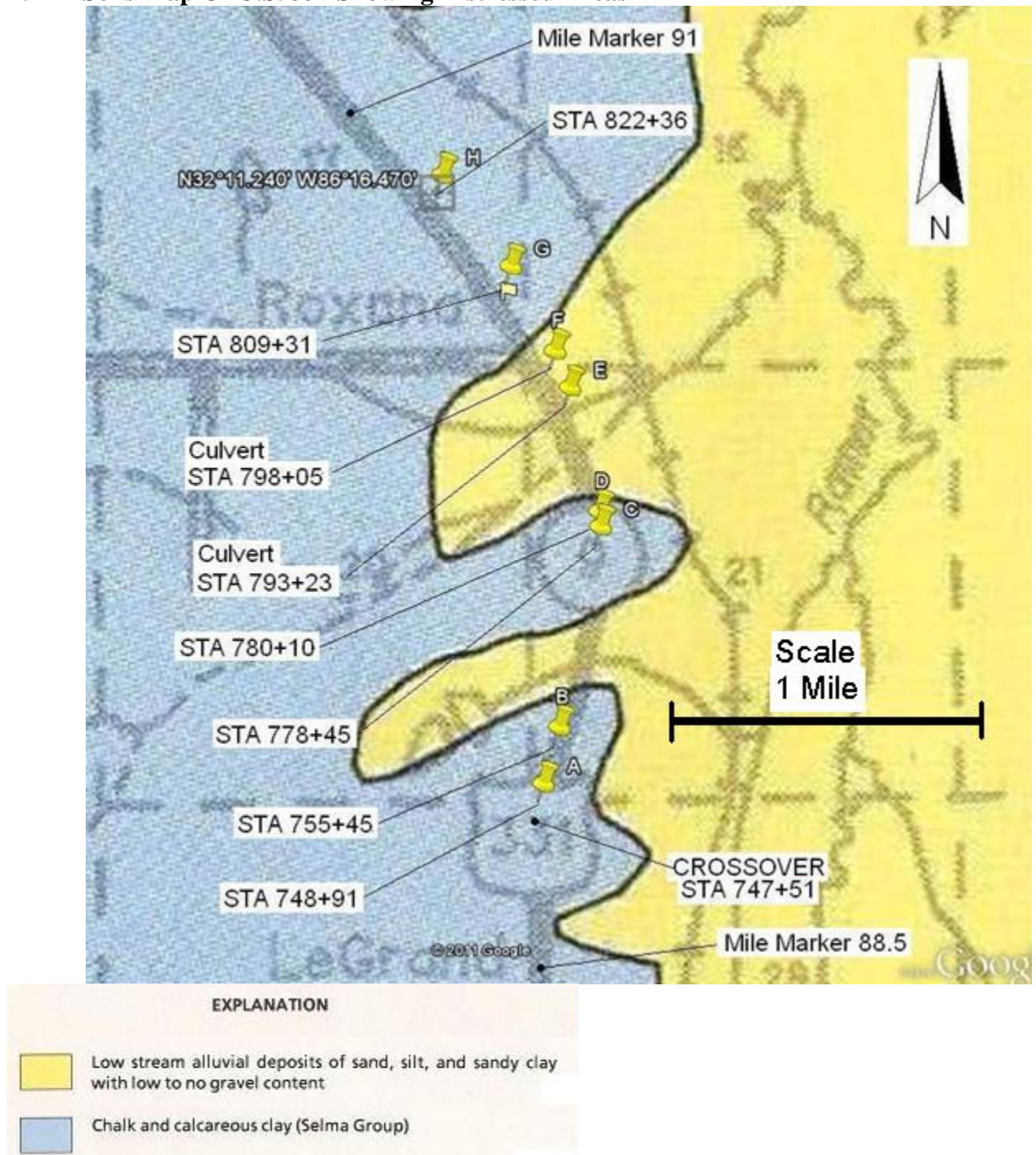


Figure 60: Soils map of U.S. 331 distressed areas, A-H (USDA 1926); (Google, U.S. Geological Survey 2012).

A.3 Topographic Map of U.S. 331 between mile markers 88.5 and 91

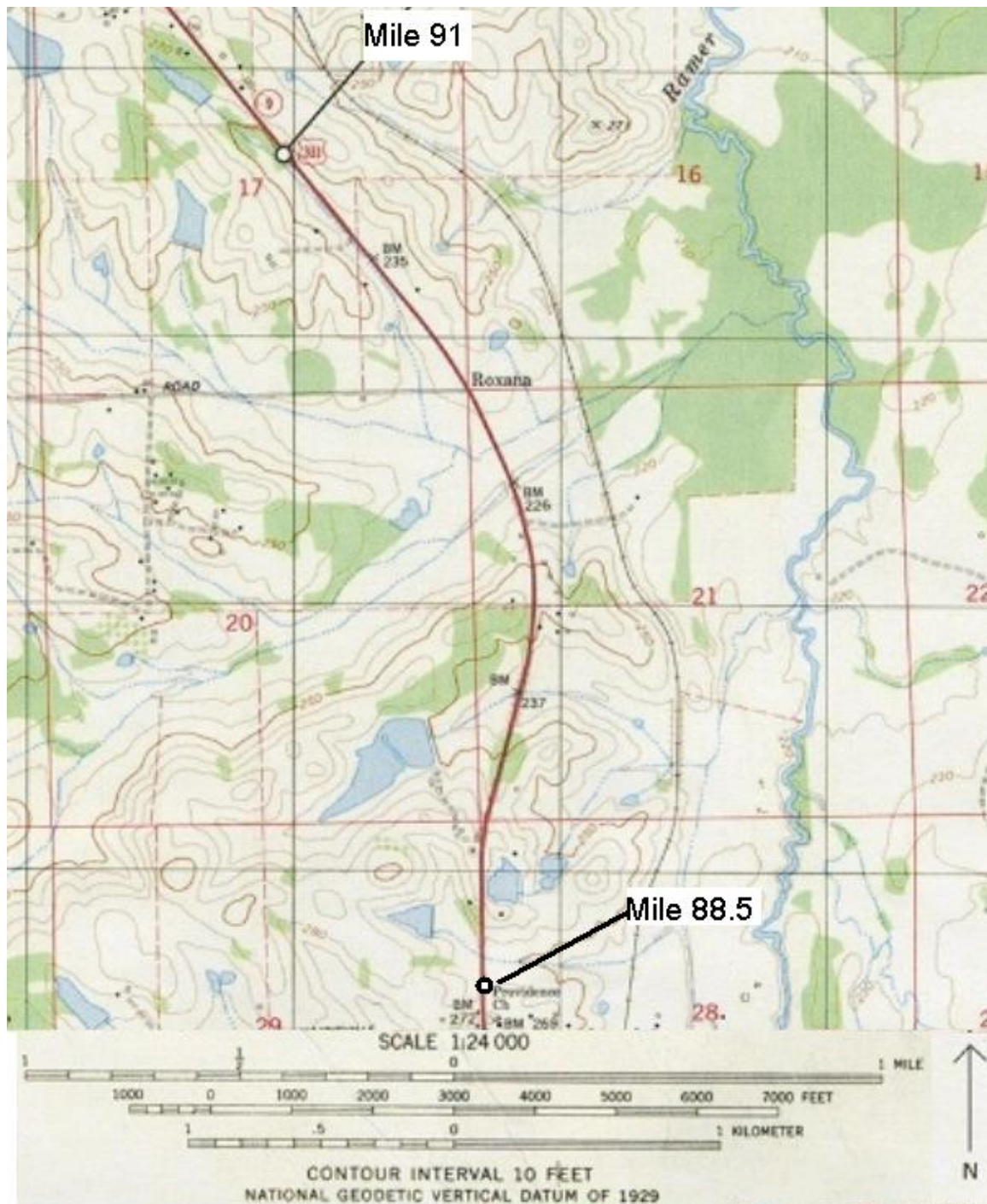


Figure 61: Topographic map of U.S.331 between mile markers 88.5 and 91 (U.S. Geological Survey 1958).

Appendix B: SOIL CHARACTERIZATION AND CLASSIFICATION

B.1 Atterberg Limits

Atterberg limits were performed on one foot and two foot deep grab samples to determine the swell potential. The Atterberg limits for one foot and two foot deep samples are shown in Tables 10 and 11, respectively.

Table 10: Atterberg limits for one foot deep samples, n/a – not available.

	6	5	4	3	2	1	
Key	PI, LL, PL	PI, LL, PL	PI, LL, PL	PI, LL, PL	PI, LL, PL	PI, LL, PL	
H	5, 32, 27	6, 31, 25	6, 30, 24	11, 34, 23	10, 41, 31	18, 49, 31	North
G	2, 31, 29	17, 45, 28	15, 51, 36	27, 50, 23	1, 35, 34	15, 50, 35	
F	24, 46, 22	4, 31, 27	11, 40, 29	55, 84, 28	33, 54, 21	5, 29, 24	
E	27, 63, 36	18, 36, 18	25, 43, 18	32, 55, 23	26, 49, 23	46, 65, 19	
D	19, 43, 24	10, 33, 23	15, 35, 20	47, 68, 21	13, 41, 28	8, 27, 19	
C	95, 127, 32	28, 51, 23	32, 60, 28	23, 44, 21	15, 38, 23	10, 27, 16	
B	20, 33, 14	12, 26, 15	14, 47, 34	30, 54, 24	34, 57, 23	21, 36, 15	
A	17, 40, 23	12, 36, 24	25, 45, 20	18, 35, 17	32, 60, 28	29, 55, 25	South
	West					East	

Table 11: Atterberg limits for two foot deep samples, n/a – not available.

	6	5	4	3	2	1	
Key	PI, LL, PL	PI, LL, PL	PI, LL, PL	PI, LL, PL	PI, LL, PL	PI, LL, PL	
H	n/a	n/a	12, 38, 27	22, 48, 26	27, 55, 34	28, 50, 30	North
G	41, 68, 27	30, 46, 16	30, 50, 20	16, 44, 28	33, 61, 28	33, 61, 28	
F	n/a	n/a	n/a	46, 75, 29	27, 55, 28	n/a	
E	n/a	n/a	n/a	53, 82, 29	48, 76, 28	n/a	
D	60, 97, 37	60, 97, 37	31, 52, 21	37, 65, 28	42, 76, 34	1, 26, 25	
C	31, 61, 29	38, 58, 20	10, 29, 19	26, 54, 28	37, 74, 37	50, 74, 24	
B	15, 38, 23	12, 31, 19	13, 36, 23	46, 77, 31	30, 55, 25	12, 65, 53	
A	22, 39, 17	16, 36, 20	23, 44, 21	45, 66, 21	49, 74, 25	44, 71, 27	South
	West					East	

B.2 Clay Mineral Type

The clay mineral type can be estimated by relating the liquid limit and the plastic limit using figure 62.

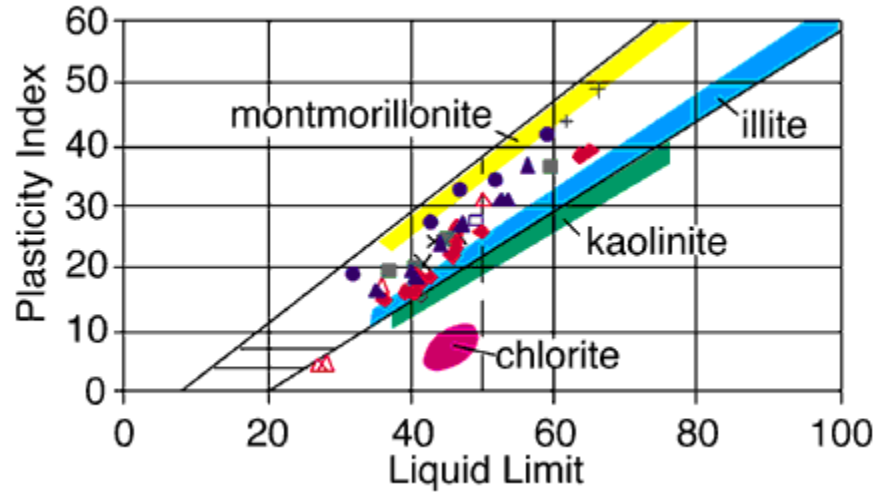


Figure 62: Relationship between Atterberg limits and mineral type (Casagrande 1948).

The clay mineral types were estimated for the one foot and two foot deep samples. The estimated mineral types are shown in Tables 12 and 13.

Table 12: Clay Mineral types for one foot deep samples, n/a – not available.

Key: I-illite, M-montmorillonite, K-kaolinite.

	6	5	4	3	2	1	
H	K	K	K	I	K	K	North
G	K	I	K	I	K	K	
F	I	K	K	M	M	K	
E	K	M	M	I	I	M	
D	I	I	I	M	K	I	
C	M	I	I	I	I	K	
B	M	I	K	I	I	M	
A	I	I	I	M	I	I	South
	West					East	

Table 13: Clay Mineral types for two foot deep samples, n/a – not available.

Key: I-illite, M-montmorillonite, K-kaolinite.

	6	5	4	3	2	1	
H	n/a	n/a	K	K	K	K	North
G	I	M	M	K	I	I	
F	n/a	n/a	n/a	I	I	n/a	
E	n/a	n/a	n/a	I	M	n/a	
D	I	I	M	I	I	K	
C	I	M	I	I	I	M	
B	I	I	I	I	I	K	
A	M	I	I	M	M	I	South
	West					East	

B.3 Soil Classification

Tables 14 and 15 are the USCS soil classifications for the one foot deep and two foot deep grab samples.

Table 14: USCS soil classification for one foot deep samples, n/a – not available.

Key: C-Clay, M-Silt, L- Low Plasticity, H-High Plasticity.

	6	5	4	3	2	1	
H	ML	ML	ML	CL	ML	ML	North
G	ML	ML	MH	CL	ML	ML	
F	CL	ML	ML	CH	CH	ML	
E	MH	CL	CL	CH	CL	CH	
D	CL	CL	CL	CH	ML	CL	
C	CH	CH	CH	CL	CL	CL	
B	CL	CL	ML	CH	CH	CL	
A	CL	CL	CL	CL	CH	CH	South
	West					East	

Table 15: USCS soil classification for two foot deep samples, n/a – not available.

Key: C-Clay, M-Silt, L- Low Plasticity, H- High Plasticity

	6	5	4	3	2	1	
H	n/a	n/a	ML	CL	CL	CH	North
G	CH	CH	CL	ML	CH	CH	
F	n/a	n/a	n/a	CH	CL	n/a	
E	n/a	n/a	n/a	CH	CH	n/a	
D	CH	CH	CL	CH	MH	ML	
C	CH	CH	CL	MH	MH	CH	
B	CL	CL	CL	CH	CL	MH	
A	CL	CL	CL	CH	CH	CH	South
	West					East	

Appendix C: STANDARD PROCTOR TESTING

C.1 Introduction

Six Standard Proctor tests were performed on samples A-2-2, B-1, B-4, B-6, E-6, and G-3 according to ASTM D-698 to determine optimum moisture content (ASTM 2007).

C.1.1 Standard Proctor Curve, Sample A-2-2

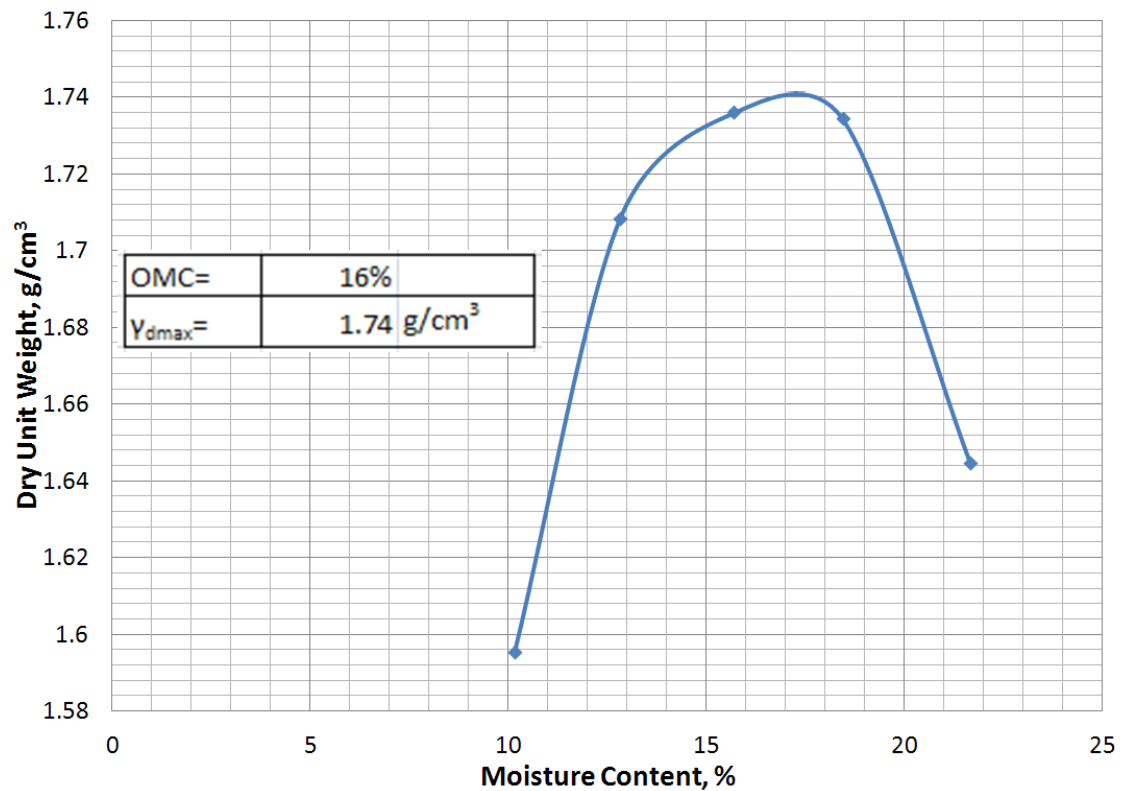


Figure 63: Standard Proctor curve, Sample A-2-2

C.1.2 Standard Proctor curve, Sample B-1

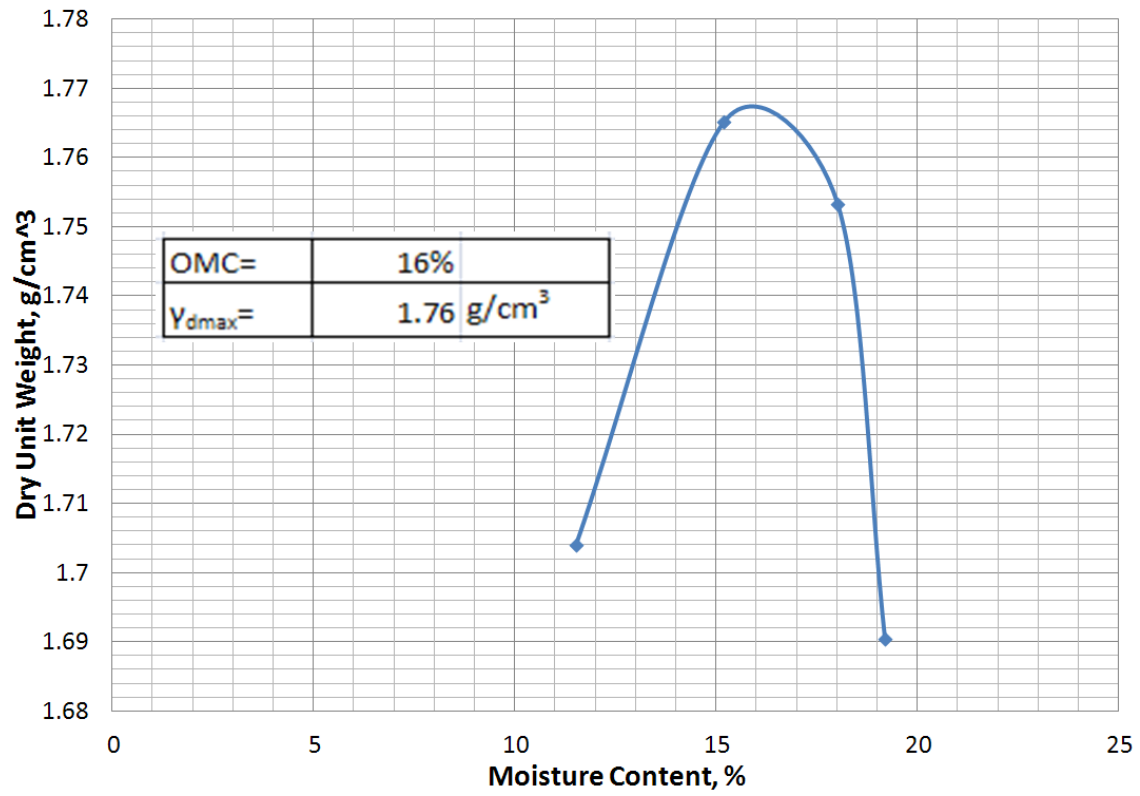


Figure 64: Standard Proctor curve, sample B-1

C.1.3 Standard Proctor Curve, Sample B-4

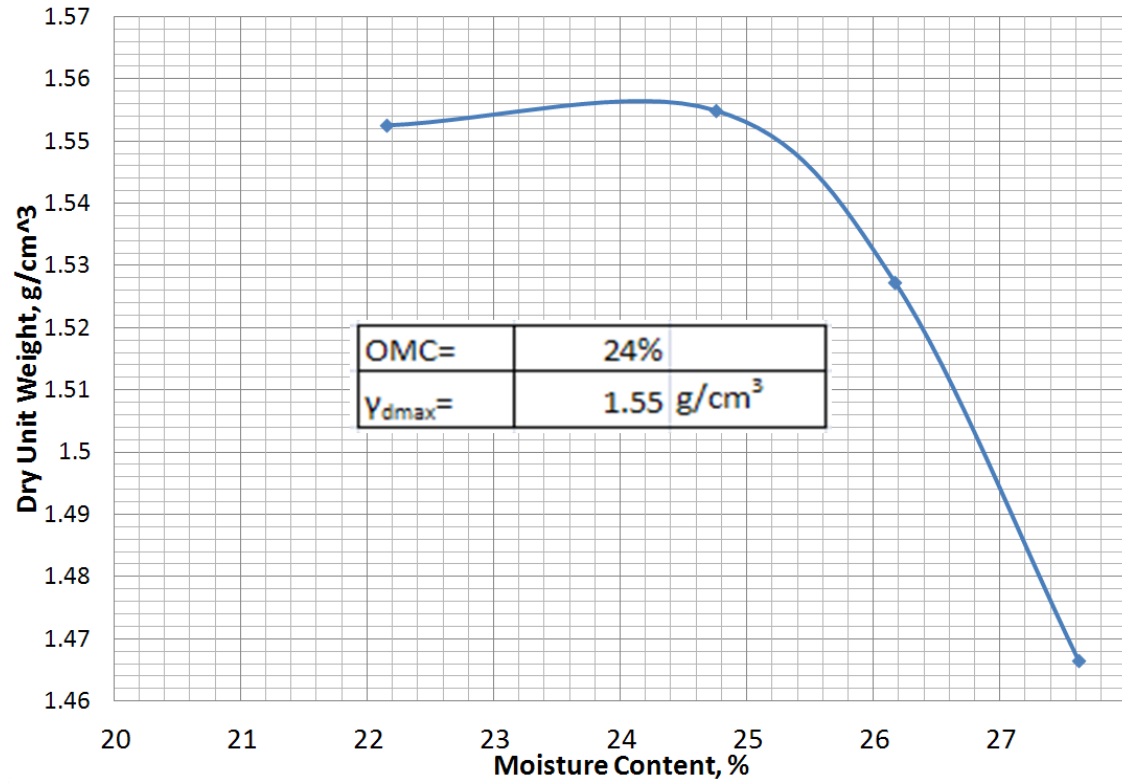


Figure 65: Standard Proctor curve, sample B-4

C.1.4 Standard Proctor Curve, Sample B-6

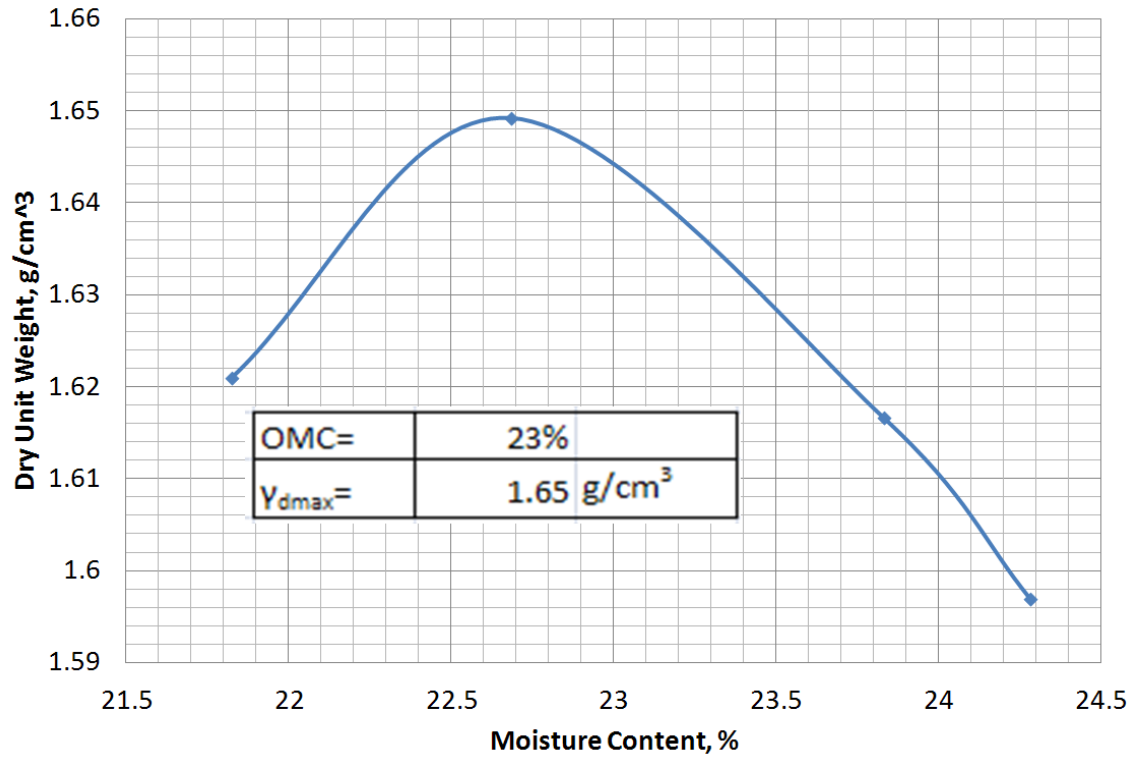


Figure 66: Standard Proctor curve, sample B-6

C.1.5 Standard Proctor Curve, Sample E-6

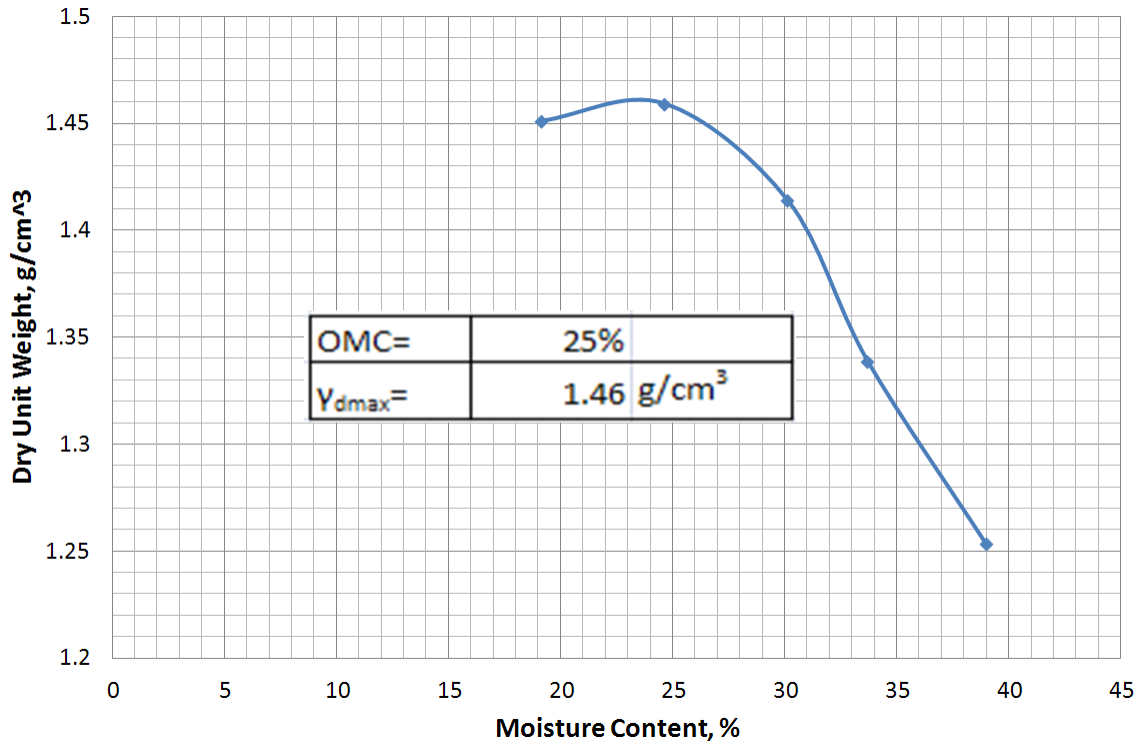


Figure 67: Standard Proctor curve, sample E-6

C.1.6 Standard Proctor Curve, Sample G-3

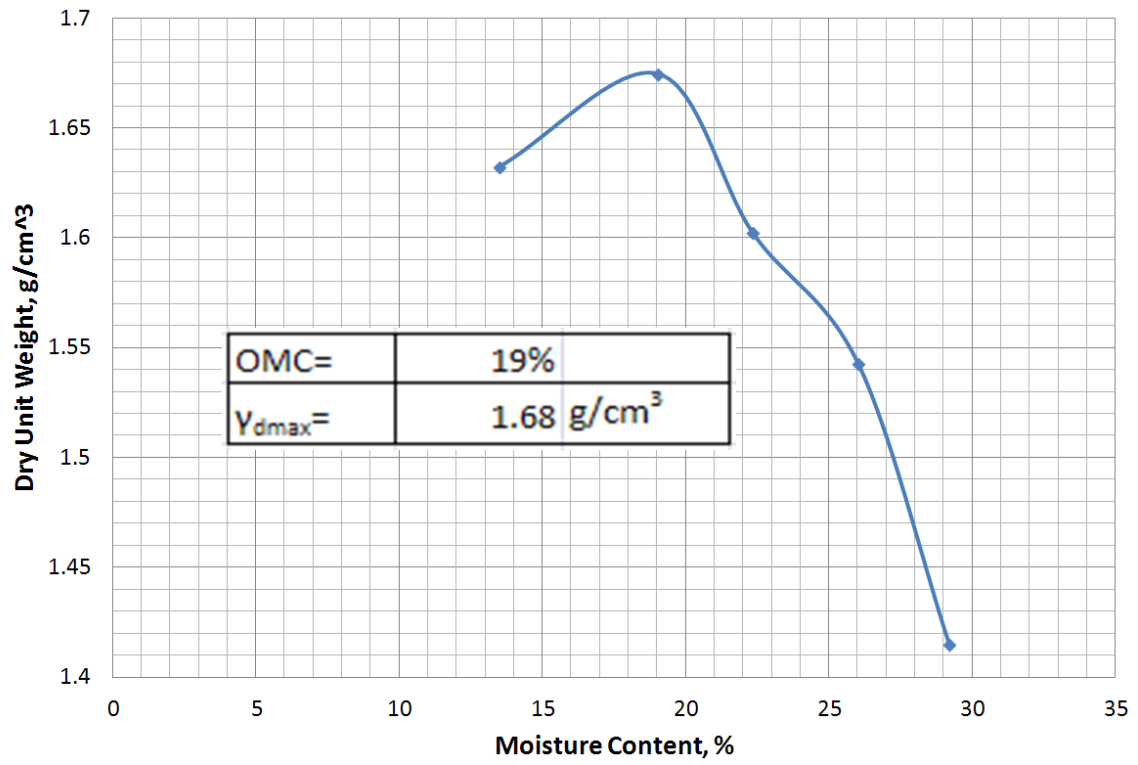


Figure 68: Standard Proctor curve, sample G-3

Appendix D: SWELL TESTING

D.1 Introduction

Swell tests were performed on samples A-2-2, B-1, B-4, B-6, E-6, and G-3 according to ASTM D-4546 (ASTM 2008). The volumetric swell ranged from 2.4% to 10.2%.

D.1.1 Sample A-2-2, swell = 10.2%

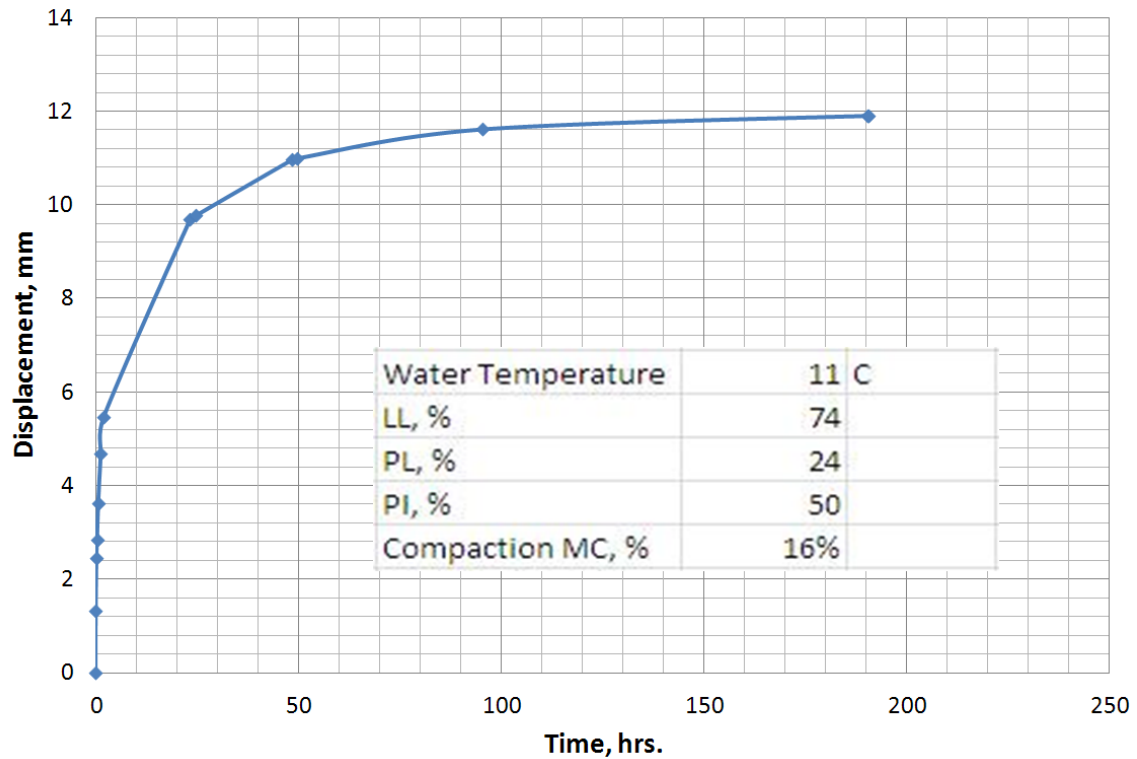


Figure 69: Swell test, Sample A-2-2. Peak swell =10.2%

D.1.2 Sample B-1, swell = 3.3%

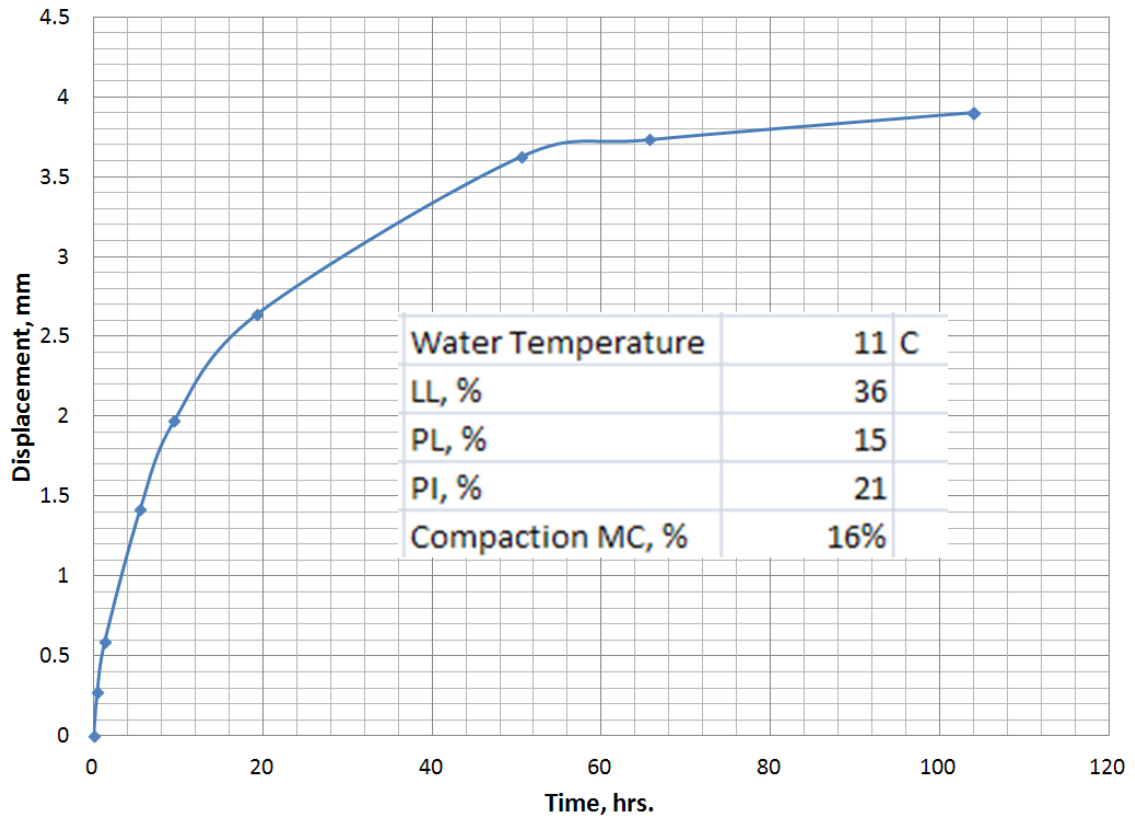


Figure 70: Swell test, Sample B-1. Peak swell =3.3%

D.1.3 Sample B-4, swell = 3.7%

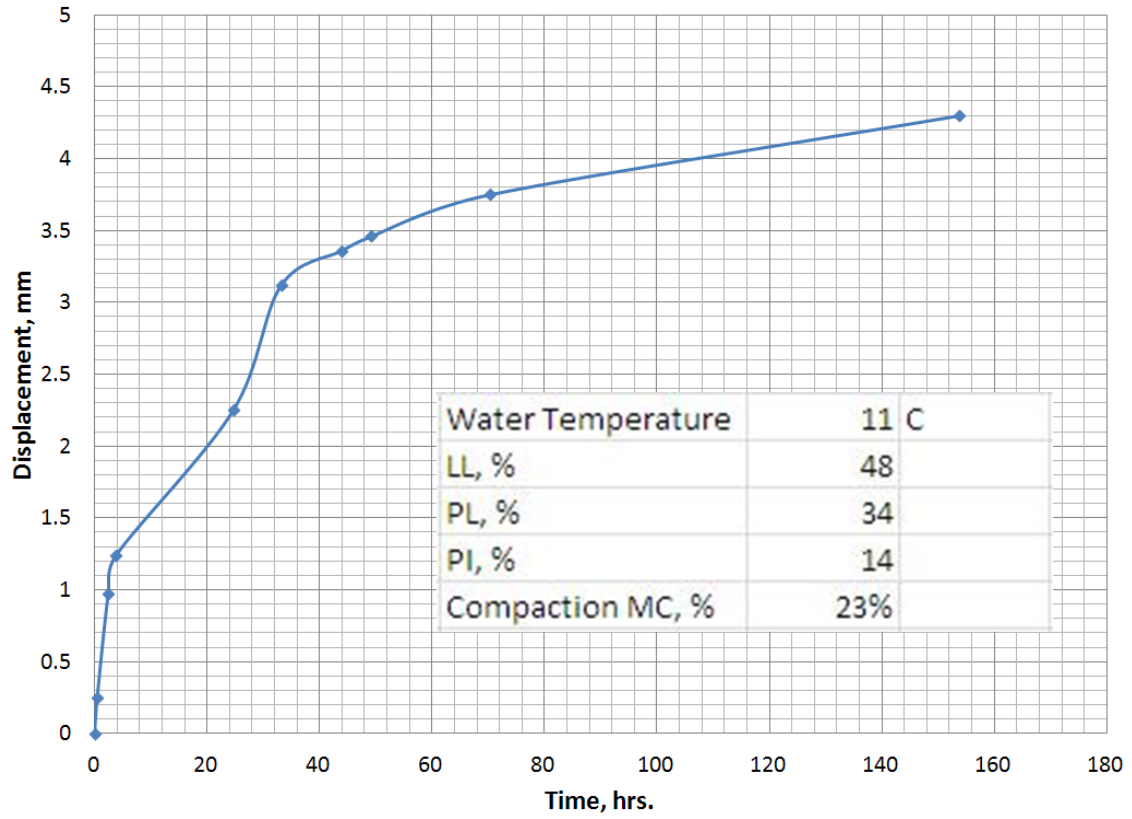


Figure 71: Swell test, Sample B-4. Peak swell =3.7%

D.1.4 Sample B-6, swell = 2.4%

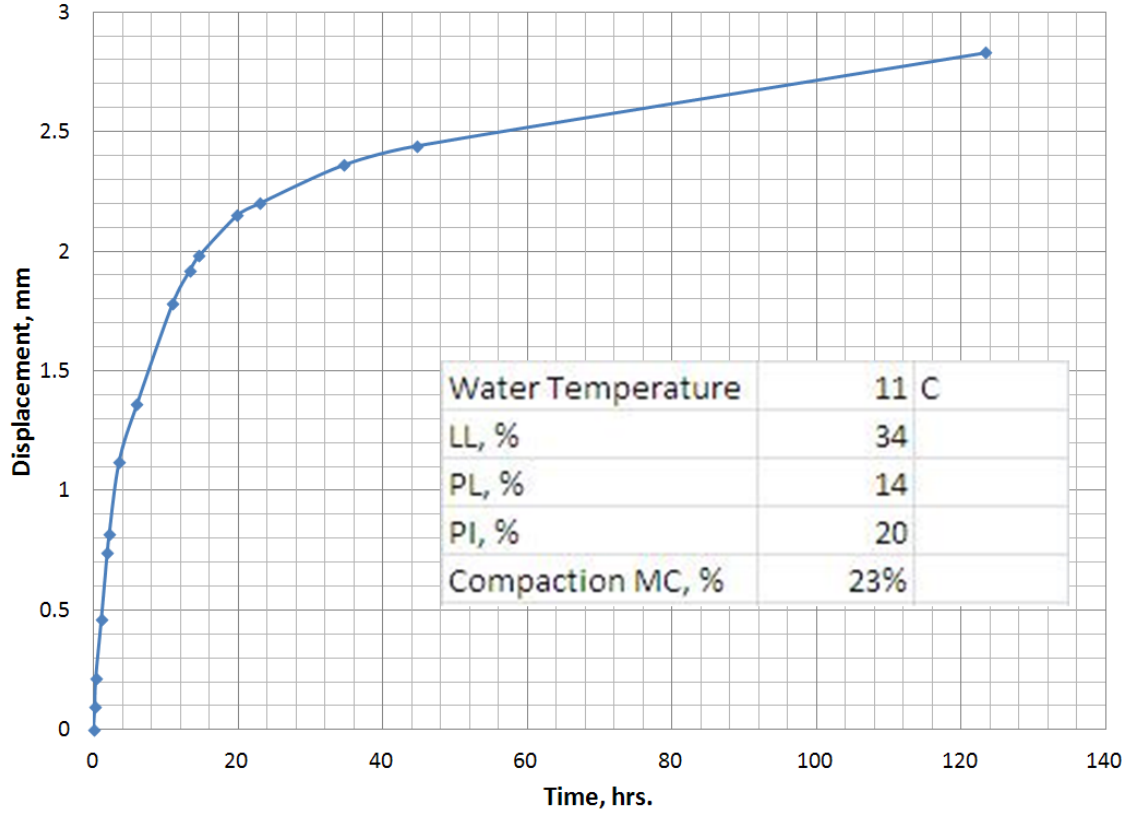


Figure 72: Swell test, Sample B-6. Peak swell =2.4%

D.1.5 Sample E-6, swell = 6.7%

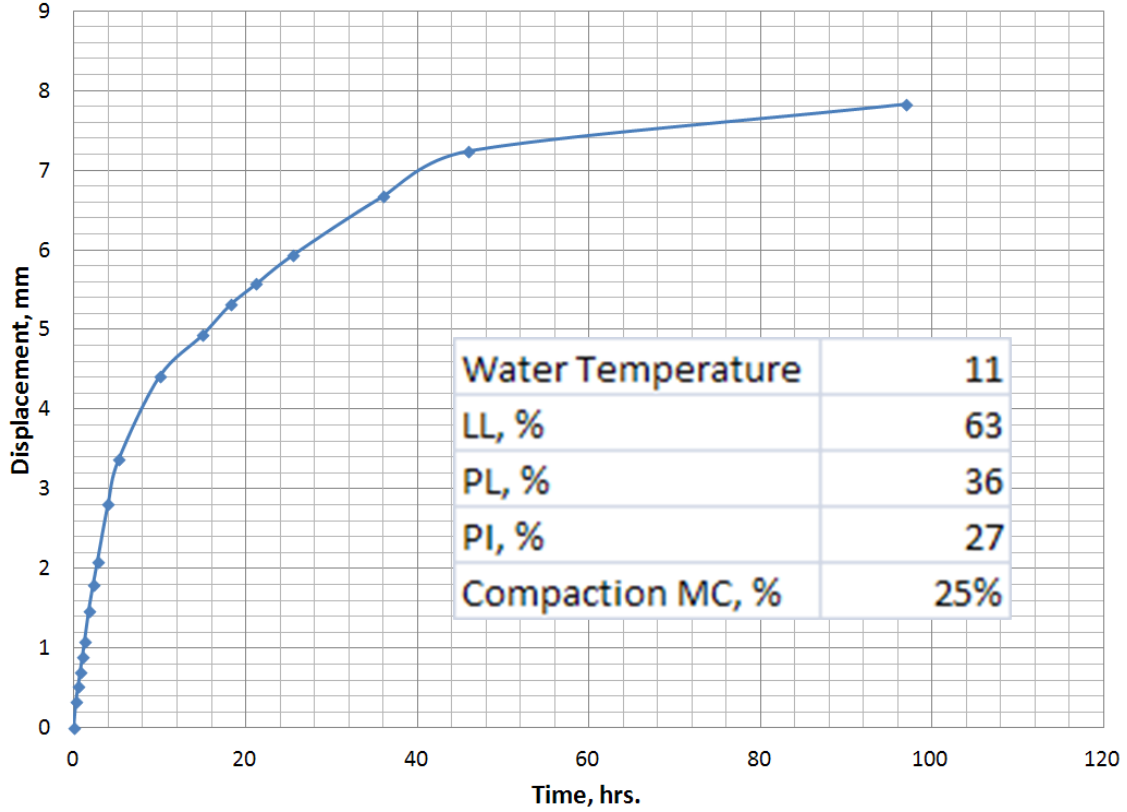


Figure 73: Swell test, Sample E-6. Peak swell =6.7%

D.1.6 Sample G-3, swell = 3.0%

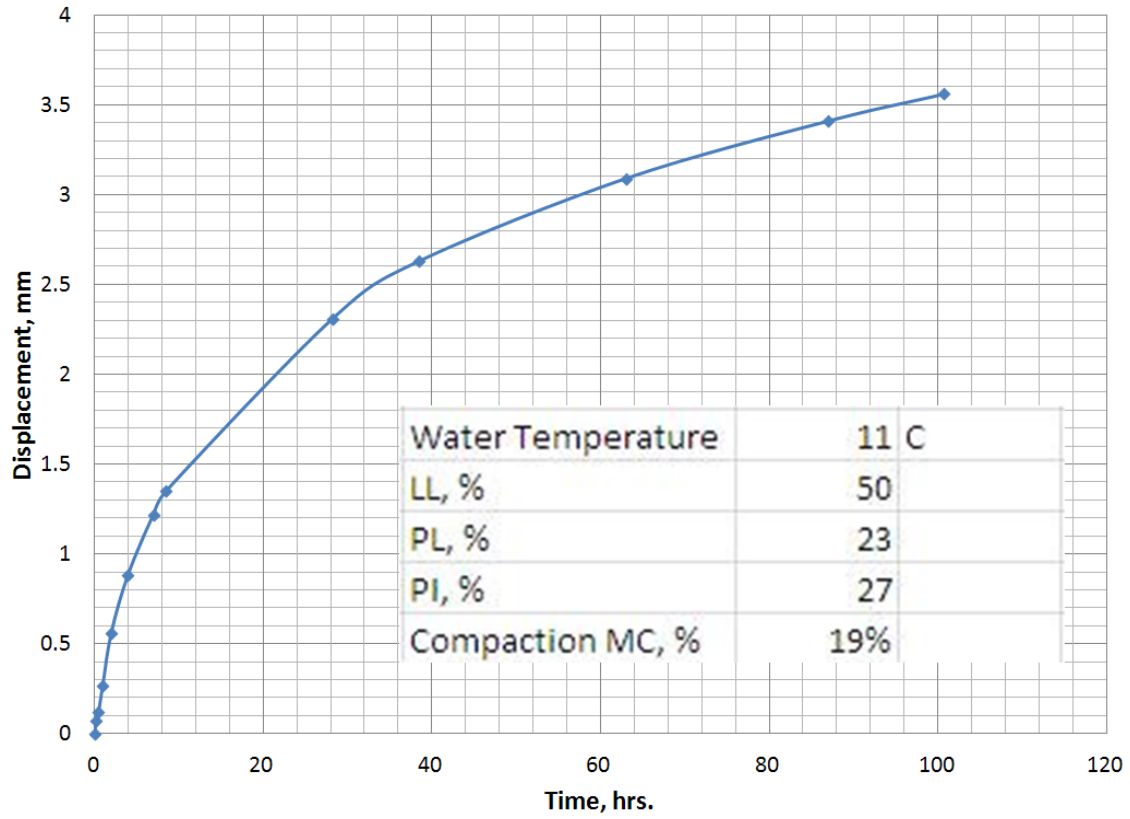


Figure 74: Swell test, Sample G-3. Peak swell =3.0%

Appendix E: STATISTICAL COMPARISON OF PROFILOGRAPH AND ELECTRICAL CONDUCTIVITY DATA

A statistical analysis was performed to determine how well the profilograph and electrical conductivity data correlate. The first step in this analysis is to plot the electrical conductivity values vs. IRI values to ensure a trend exists. This trend is shown in figure 75.

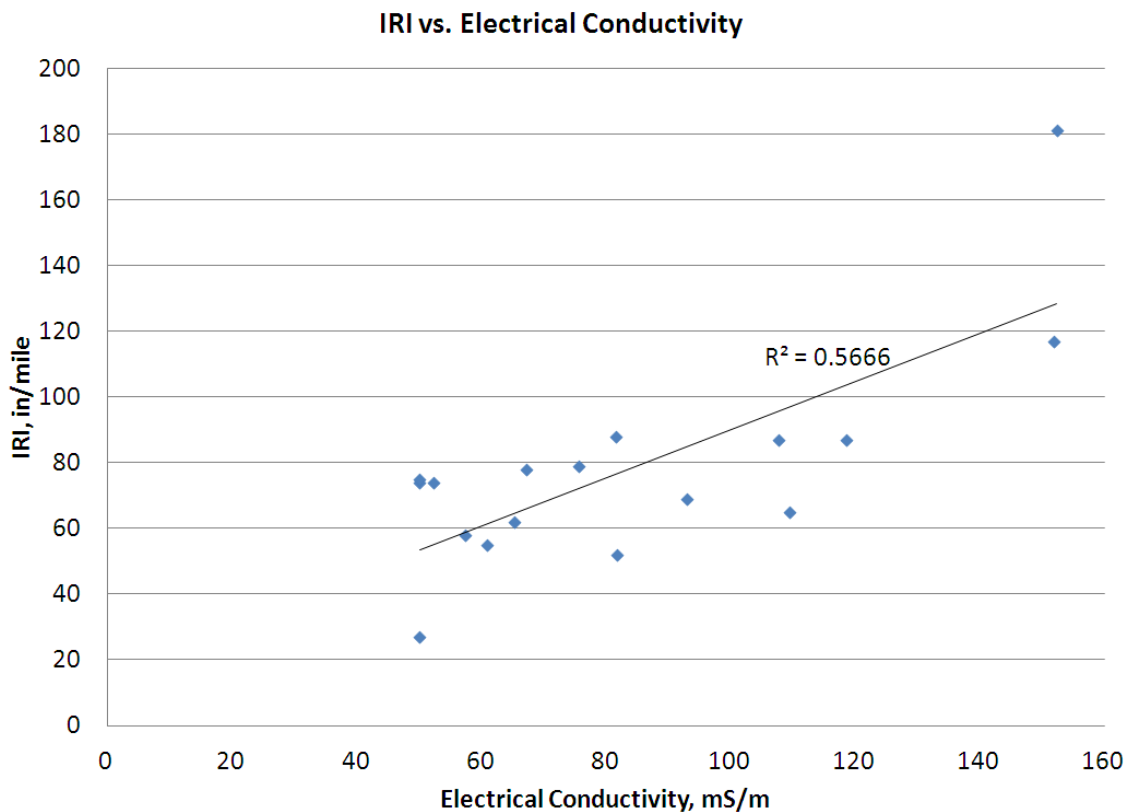


Figure 75: IRI vs. Electrical Conductivity

The empirical data presented in Figure 75 has scatter resulting in an R^2 value of 0.566. However, the upward trend is shown that as electrical conductivity increases that IRI also increases.

The electrical conductivity data and the IRI values at the locations that the IRI values were collected are plotted in Figure 76 and a Pearson product moment correlation

was performed on the data. Neither the IRI data nor the electrical conductivity data at the culvert locations was used in the Pearson product moment correlation.

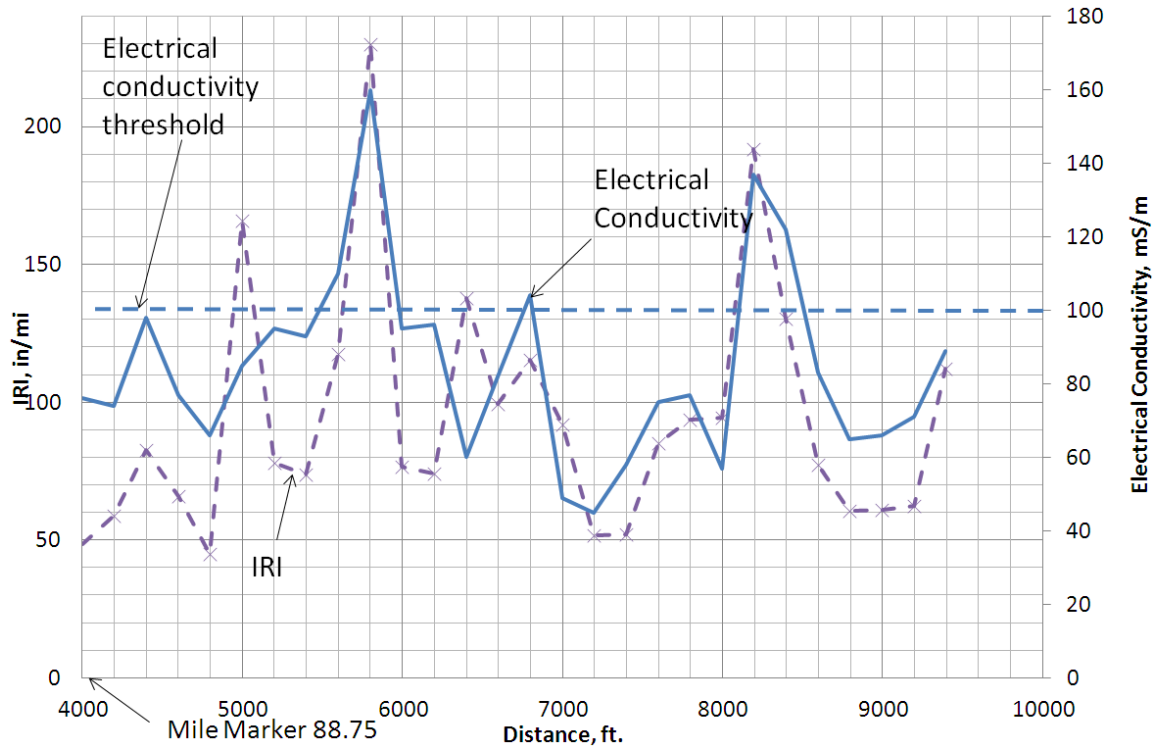


Figure 76: IRI and electrical conductivity vs. distance. The February 10, 2012 electrical conductivity test is represented by the solid line and the February 24, 2012 IRI test is represented by the dashed line.

Pearson product moment correlations assign a numerical value to how well two variables correlate. A Pearson product moment correlation of 1 means that the two variables have a perfect correlation.

The Pearson product moment correlation between the profilograph data and the electrical conductivity is 0.72. This relatively high value indicates that these two variables have a high correlation, especially when considering the multitude of other factors that can affect the profilograph reading.